Fine-Scale Habitat Zonation of Fringing Reef Flats in the Solomon Islands; A Geospatial Analysis

By

Grace Martin 2024

A thesis submitted to Auckland University of Technology in partial fulfilment of the requirements for the degree of Master of Science (Research)

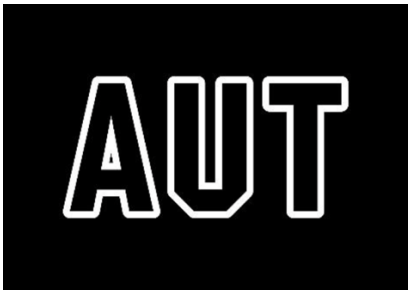

Auckland University of Technology

Department of Health and Environmental Science

School of Science

Abstract

Coral reefs are highly productive, biologically diverse ecosystems, that support an assortment of marine organisms and provide many ecological goods and services to local and surrounding coastal populations. The reef flat is a delicate coastal habitat that faces vulnerability to influences such as coastal runoff and development, sedimentation, overharvesting, increased temperatures, and other effects of climate change. Precise, effective, and repeatable assessments of reef flat habitat dynamics are pivotal for the mapping, monitoring, and conservation efforts aimed at preserving these distinctive environments.

The overall aim of this research was to investigate the ability of Unoccupied Aerial Vehicle (UAV) Full Motion Video (FMV) techniques to effectively quantify the dynamics of habitat zonation across the Vavanga reef flat on Kolombangara Island, Solomon Islands. This study combined UAV footage with synchronous underwater video within ArcGIS Pro, to map the distribution of substrata and biota across the reef flat at multiple classification levels.

Many patterns in the distribution of substrata and biota were illustrated in this study, through a combination of summary statistics, simple linear regressions, and classification and regression trees. Additionally, the classifying ability of the image recognition software ReefCloud.AI was found to be moderately successful when applied to a subset of the collected data. An Object-Based Image Classification (OBIA) was also performed across a section of the high-resolution photo orthomosaic and resulted in variable classification accuracies across the selected classes.

The combination of synchronous UAV FMV and underwater imagery successfully achieved the anticipated outcomes of the project, yielding precise images, maps, and statistical models of the subtidal area. This innovative approach has a broad range of potential applications and has contributed to the development of effective subtidal surveying and mapping techniques. These advancements will enhance our ability to make informed decisions around ecosystem-based management and the conservation of globally threatened coral reef ecosystems.

Contents

List of Figures

List of Tables

Table 1. Abbreviations

Abbreviation	**Definition**
FMV	Full Motion Video
UAV	Unoccupied Aerial Vehicle
GIS	Geographic Information Systems
MISB	Motion Imagery Standards Board
FPS	Frames Per Second
SRSI	Satellite Remote-Sensing Imagery
SfM	Structure from Motion
DEM	Digital Elevation Model
CCA	Crustose Coralline Algae
LIT	Line-Intercept Transect
PIT	Point-Intercept Transect
MAP	Mapped Quadrats
PLIT	Photo Line Intercept Method
PHOTS	Photo Quadrat Method
ROV	Remotely Operated Vehicle

Attestation of Authorship

I hereby declare that this submission is my own work and that, to the best of my knowledge and belief, it contains no material previously published or written by another person (except where explicitly defined in the acknowledgements), nor used artificial intelligence tools or generative artificial intelligence tools (unless it is clearly stated, and referenced, along with the purpose of use), nor material which to a substantial extent has been submitted for the award of any other degree or diploma of a university or other institution of higher learning.

Signed:

Acknowledgements

I would like to thank my lead supervisor Graham Hinchliffe for the endless amount of support, guidance, and patience he has given me throughout this project. Thank you for sharing your expert UAV FMV knowledge and piloting skills, and for your huge assistance with data processing. You helped bring this concept to light and have taught me many valuable geospatial and academic skills along the way.

A massive thank you to Daniel Breen who sat with me through many hours of image classification and generously shared his exceptional coral taxonomic knowledge. Thank you for your in-water assistance during our field trip, and your unwavering guidance through the grueling statistical analysis.

A special thank you to my secondary supervisor Armagan Sabetian, as without him and his generous and welcoming extended family in Vavanga, this research project would have never been possible. Thank you for helping me bring this study to life and for your guidance during the early stages of this research. My first trip to the Solomon Islands with Armagan in 2019, inspired me to continue my postgraduate research in marine biology. Thank you for introducing me to such a diverse and important ecosystem.

Finally, a huge thank you to my friends and family who have been my biggest supporters throughout this whole journey. Without their continuous faith and encouragement, I wouldn't be at this pivotal point, handing in my thesis.

1 Introduction

1.1 Coral reef ecosystems

Coral reefs are one of the most biologically diverse and productive ecosystems on the planet. While covering less than 0.2% of the world's ocean, coral reefs are home to 25% of all marine species (Reaka-Kudla, 1997), making them one of the most biodiverse ecosystems per unit area. The exceptional diversity in these ecosystems can be attributed to the vast number of marine organisms inhabiting the multilayered reef complex created by approximately 1000 species of scleractinian (reef-building) corals (Knowlton et al., 2010). Coral reefs, spanning coastlines in over 100 countries, offer diverse ecosystem goods and services to approximately one-eighth of the global population, sustaining the livelihood and food security of millions, particularly in highly dependent developing countries and island nations (Burke et al., 2011).

Reef fish and invertebrates provide a critical source of protein for tropical countries (Reaka-Kudla, 1997), and are incredibly important for both artisanal and commercial fisheries (Whittingham et al., 2003). In addition, the physical structure of the coral reef plays a crucial role in safeguarding coastal communities and infrastructure against the physical effects of wave action and storm surges (Burke et al., 2011). By dissipating between 75-95% of wave energy, this function leads to a decrease in coastal erosion and a reduction in wave-induced flooding (Brander et al., 2004). Furthermore, nearshore reef flat environments between the reef crest and shore, provide nursery habitats and feeding grounds for many economically and ecologically important reef fish and invertebrate species (Adams et al., 2006; Reaka-Kulda, 1997). Coral reefs also contribute substantially to the economic development of coastal communities through tourism, fishing and recreational activities (Burke et al., 2011; Reaka-Kulda, 1997).

Reef-building hermatypic corals and other calcifying organisms secrete calcium carbonate skeletons or shells in the form of aragonite and calcite, which form the habitat for the remarkable array of marine plant and animal species that live within (Burke et al., 2011). Reef-building corals survive through a photosymbiotic partnership with their algal symbionts, zooxanthellae (Stanley & Swart, 1995). Zooxanthellae inhabit the coral's cellular tissue and contribute up to 95% of the coral's overall energy needs through photosynthesis

(Colombo-Pallotta et al., 2010). In return, this arrangement offers protection and a continuous supply of nutrients to the zooxanthellae (Rahav et al., 1989). This critical relationship is exceptionally delicate and confines the existence of reef-building corals to warm, shallow environments within 30° latitude of the equator (Spalding & Brown, 2015).

Benthic macroalgae play a crucial role within coral reef ecosystems, offering essential ecological functions that include stabilizing reef structure, retaining and recycling nutrients, driving primary productivity, and providing trophic support to highly diverse consumers (Fong & Paul., 2011). For instance, crustose coralline red algae provide significant contributions to calcium carbonate ($CaCO_3$) production, in the form of calcite, to bind the greater quantities of less-dense calcium carbonate produced by corals and other organisms (Littler & Littler, 1988).

Despite their significance, coral reefs are one of the most rapidly declining ecosystems worldwide. Coral reefs are confronted with a substantial array of local and global anthropogenic threats, including unsustainable fishing practices, eutrophication and sedimentation, ocean warming, ocean acidification, sea level rise, and severe weather events due to increased greenhouse gas concentrations, among others (Jackson, 2008; Newton et al., 2007; Riegl et al., 2009; Silverman et al., 2009).

Unsustainable fishing practices currently prevail across a substantial portion of the world's reefs (Newton et al., 2007). Newton et al. (2007) reported over half of the 49 island countries included in their research, were engaged in unsustainable exploitation of their coral reef fisheries. Overfishing has resulted in the collapse and closure of fisheries, the extinction of local fish species, and noticeable ecological transformations (Jackson, 2008; Mumby et al., 2006; Roberts, 1995).

Deforestation, agricultural practices, intensive livestock farming, and increased coastal development have all contributed to increased eutrophication and sedimentation in coastal waters through runoff in freshwater outputs (Fabricius, 2011). This has led to nutrient enrichment, reduced light penetration due to increased turbidity, and alterations to surface properties, which in turn results in trophic structure shifts, an overgrowth of algae, and diminished coral recruitment and diversity (Fabricius, 2011).

Rising levels of greenhouse gas emissions in the atmosphere, primarily through the burning of fossil fuels, have led to an increase in atmospheric and sea surface temperatures, and an increase in concentrations of carbon dioxide (CO_2) (Burke et al., 2011; Silverman et al., 2009). The warming of the ocean has resulted in an unprecedented amount of mass coral bleaching events. When subject to prolonged periods of warming, the delicate relationship between coral and zooxanthellae is disrupted and causes a stress response known as coral bleaching. This phenomenon results in the loss of the corals' photosynthetic symbionts, which turns the coral tissue transparent, revealing its white calcium carbonate skeleton (Ainsworth et al., 2016). When corals are unable to regain their symbionts, they lose a major source of energy and nutrients, causing the coral to be susceptible to damage. If the re-establishment of symbiosis does not occur within several weeks, it frequently results in the mortality of both the coral and the free-living zooxanthellae (Douglas, 2003; Hill & Ralph, 2007).

The ocean absorbs approximately 40% of anthropogenic CO_2 annually, and exports it into its deep interior, making it the largest carbon store on the planet (Reid et al., 2010). As atmospheric concentrations of CO_2 continue to rise exponentially, alterations to the chemical composition of the ocean's surface waters are becoming more severe. An increase in dissolved CO_2 in the ocean causes an increase in the concentration of carbonic acid, bicarbonate ions, and hydrogen ions, and a decrease in carbonate ions (Fabry et al., 2008). The addition of hydrogen ions in seawater lowers the ocean's pH, making it more acidic, and lowers the saturation state of calcium carbonate minerals. This process is referred to as ocean acidification and has a significant impact on calcifying organisms' ability to form their calcium carbonate skeletons or shells (Feely et al., 2010).

The challenges faced by coral reefs have led to a rapid decline in these vital ecosystems across the globe. There is an urgent need to restore and protect coral reef ecosystems and the services they provide. Understanding the responses of reefs to threats and to management is key to developing and assessing effective strategies for conservation and sustainable use.

1.2 Reef flat zonation and ecological significance

Fringing coral reefs in the Indo-Pacific are typically divided into four distinct zones, known as the shoreline, reef flat, crest, and front (Figure 1) (Bellwood et al., 2018). The community composition, structural, and hydrodynamic features of each of these zones have been thoroughly investigated over the last few decades (Fulton & Bellwood, 2005; Wismer et al., 2009). However, the zonation patterns within specific zones are not well understood. In particular, the dynamics of habitat zonation within the reef flat is often overlooked, due to a consensus that this wave-swept coral reef zone provides limited ecological value (Bellwood et al., 2018).

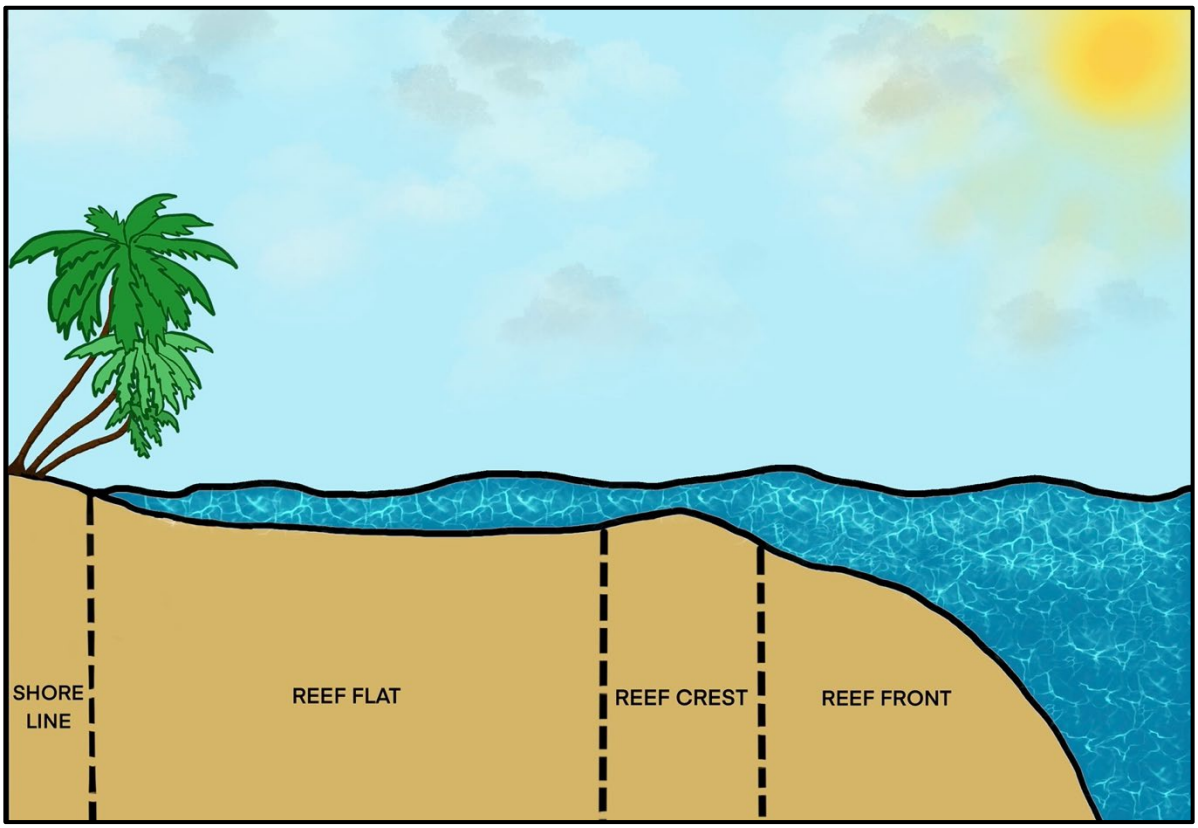

Figure 1. Cross section of a fringing reef flat.

The reef flat is an area situated between the shoreline and the reef crest and is most often the shallowest portion of submerged reef. The reef flat can extend hundreds of metres or kilometres in width and is typically only up to a few metres deep (Bellwood et al., 2018; Harborne, 2013). Due to the shallow nature of reef flats, any change in water depth across tidal cycles can cause significant challenges to organisms (Harborne, 2013). Changes in

water depth can alter environmental parameters such as exposure, water temperature, dissolved oxygen concentration, and ultraviolet radiation (Harborne, 2013).

Due to the reef flat experiencing such a high level of environmental variation, it often supports a more distinct and specialised assemblage of organisms compared to other reef zones (Bellwood et al., 2018; Harborne, 2013). Reef flats are also among the most vulnerable of coastal habitats and are susceptible to impacts from coastal runoff, sedimentation, increased temperatures, overharvesting, coastal development, and climate change (Harborne, 2013).

Reef flats encompass an interlinked assortment of diverse habitat types, which include mangrove forests, seagrass meadows, patch reefs, and a variety of hard-bottom and soft-substrate habitats such as sand, mud, rubble, rocks and consolidated coral rock (Adams et al., 2006). A typical reef flat substrate distribution extends from a sandy beach covered with mangroves or seagrass meadows to a more coral-dominated habitat seaward, culminating at the reef crest (Harborne, 2013).

Shallow reef flats exhibit significantly higher rates of primary productivity in comparison to the adjacent oceanic waters, with most of this productivity attributed to algae (Littler & Littler, 1988). Crustose coralline red algae and algal turfs consisting of a diverse assortment of filamentous algae and juvenile macroalgal species, are typically present across the reef flat (Fong & Paul, 2011). Robust brown algae like *Turbinaria* and *Sargassum*, crustose coralline algae, as well as calcified green algae such as *Halimeda*, are often found closer to the reef crest, as they can withstand the forces of wave action (Littler & Littler, 1988). Klumpp and McKinnon (1992) found epilithic algal communities covered between 50-80% of the reef flats located in the north, central, and southern regions of the Great Barrier Reef.

On fringing reefs, the reef flat and reef crest are incredibly important for shoreline protection as they provide the main break to oncoming wave action for many tropical islands and mainland shores (Sheppard et al., 2005). In 1998, a coral bleaching event resulted in mass coral mortality across the reefs in the Seychelles Islands, with coral mortality on the reef flat near total. This caused significant ecological consequences as the removal of large thickets of staghorn corals and massive boulder corals resulted in increased

water depth over the reef flat, creating a localised ‘pseudo-sea level rise’ (Sheppard et al., 2005). As the coral skeletons on the reef flat slowly deteriorated, the three-dimensional structure of the reef's surface underwent significant changes. This resulted in reduced friction against waves and diminished the reef flat's capacity to attenuate wave energy (Sheppard et al., 2005).

The shallow water of the reef flat offers a place of refuge from predators at low tide, and provides nursery habitat and feeding grounds for high numbers of juvenile fish species (Baker & Sheaves, 2007; Davis et al., 2017). The many different habitat types found in close proximity enable different species to undergo multiple ontogenetic shifts during their life. These ‘ontogenetic shifters’ are species that use specific habitats whilst undergoing changes in diet, morphology, and behaviour before transitioning to their adult habitat (Adams et al., 2006). Many species may also utilize various habitat types within the back-reef system for different purposes during this juvenile stage. For example, McMahon et al. (2011) found juvenile snappers in the Red Sea used seagrass beds as a primary foraging area and found shelter within the mangroves.

Reef flat habitats are highly productive areas important for customary fisheries and food security in the Pacific region. Habitats such as mangroves, seagrass beds, and mud flats support a high diversity of edible invertebrate, seagrass, and seaweed species that contribute substantially to household food and nutrition security in Pacific nations such as the Philippines, Fiji, Micronesia and the Solomon Islands (Kleiber et al., 2014; Takeda, 2001; Thomas et al., 2021; Quinn & Mataki, 1999). Traditional fishing practices such as gleaning on shallow reef flats during low tides, is a customary activity within fishing communities (De Guzman, 2019; Thomas et al., 2021). As the reef flat typically reaches no more than a metre or so in depth, accessing its resources without the use of a boat or specialised fishing gear is common (Takeda, 2001). This practice is often carried out by hand or using minor equipment (e.g., rakes, knives, spoons), making it well-suited for the participation of women, children, and elderly (McManus et al., 1992; Takeda, 2001; Thomas et al., 2021). Common daily catches include crustaceans, sea urchins, sea cucumbers, octopus, some small fish species, *Caulerpa* seaweed, and many species of shellfish such as *Trochus* (McManus et al., 1992; Thomas et al., 2021). The edible invertebrates and seaweeds

obtained through reef gleaning activities offer a cost-effective yet excellent source of high-quality protein for both poor and affluent seafood consumers (De Guzman, 2019).

1.3 Survey methods for benthic biota and substrata on coral reefs

Accurate and precise assessments of benthic communities are essential for marine mapping and monitoring programs (Cresswell et al., 2021). Various quantitative methods have been used to collect information on the distribution and abundance of marine organisms and habitats across reef zones. This has led to ongoing debates among reef researchers regarding the effectiveness of individual methods (Lam et al., 2006; Leujak & Ormond, 2007; Nakajima et al., 2010).

One of the earliest techniques used was the line-intercept transect (LIT). This method involves laying a tape measure across a section of reef and estimating the percentage cover of different benthic organisms and habitats from the proportions of the total length of transect overlying different substrata (Dean et al., 2015; Leujak & Ormond, 2007; Morrissey, 1980). Morrissey (1980) used this method to examine the community structure and zonation patterns of macroalgae and hermatypic corals on the fringing reef flat at Geoffrey Bay, Magnetic Island, and found macroalgae covered 90% of the substratum.

A slightly faster transect method is known as the point-intercept transect (PIT), where the substrate or organism is recorded underneath equally spaced points along the transect. For example, Wismer et al. (2009) recorded macroalgal cover immediately underneath and 1m on either side of their transect lines at 1m intervals across sites within the northern and central regions of the Great Barrier Reef. Comparatively, Dean et al. (2015) decided against using this method as the distribution of crustose coralline algae (CCA) can be patchy, which may have resulted in the under-sampling of rare species. They therefore chose to quantify CCA species distributions using the LIT method.

Another popular reef surveying method is the use of mapped quadrats (MAP). This method typically involves laying out 1m x 1m quadrat frames along a transect line, that is subdivided into a grid of 100 10cm x 10cm squares, using nylon string (Leujak & Ormond, 2007). The surveyor then hand draws a map of the substrate and/or coral communities onto underwater paper. Information such as species present, number of coral colonies, cover

area of live coral species, and other benthic groups are also recorded (Ott & Auclair, 1977; Bouchon, 1981; Weinberg, 1981). The percentage cover of benthic substrate types are then determined by visually assessing the maps, using the grid as a reference (one grid is equal to 1% cover) (Leujak & Ormond, 2007). A variation of this method involves using the same quadrat grid, however, the substrate under each nylon string intersection is recorded. The number of points scored by each substrate type or species is divided by the total number of observed points to determine the percentage cover (Weinberg, 1981).

Transects should ideally be located randomly within the area of interest to meet statistical assumptions but in some studies, transects are permanently marked and the same transects are sampled repeatedly in time (Emslie et al., 2020; English et al., 1998). This can provide more precise estimates of temporal change, especially in highly variable, patchy environments as the repeated measures error terms are based on temporal change rather than spatial differences among transects.

Analysis of these repeated measures data may be as simple as a paired t-test or an analysis of variance (ANOVA) on the differences in percentage cover for each transect between two time periods. However, accurately marking transects is a time-consuming process that involves the introduction of artificial structures such as stakes, pegs, tape, or fishing lines (English et al., 1998). The accuracy achieved is likely limited to a metre at best, and the markers are easily lost due to erosion, storms, herbivorous fish and being overgrown by marine life. Ideally, GPS positions of transects should be recorded, however, there is no GPS reception underwater. Towed surface GPS and diver positions located from sonar have been used in some studies to address this limitation (Parsons et al., 2004).

The introduction of underwater cameras has provided a faster approach to collecting underwater data and provides a permanent visual record that can be used for comparison with other methods (Bohnsack, 1979; Weinberg, 1981). Underwater cameras have been used for both the photo line intercept (PLIT) method and the photo-quadrat method (PHOTS). The PLIT method involves images being taken along a transect line while maintaining a constant vertical distance (Nakajima et al., 2010).

Much like the LIT method, the length of each coral or substrate type is measured against the total transect length, to determine percentage cover, however, this is done on a computer screen or projector (Nakajima et al., 2010). The PHOTS method involves the use of 1m x 1m quadrats that are laid across the reef and photographed using an underwater camera (Carleton & Done, 1995; Leujak & Ormond, 2007; Weinberg, 1981) . Each quadrat image is then overlaid with points, and the substrate underneath is identified and percentage cover is calculated (Leujak & Ormond, 2007), or each colony or substrate type is outlined on the image and the area is calculated (Nakajima et al., 2010).

Placing heavy quadrat frames on top of reef substrate has the potential to cause physical damage to the reef complex. The use of underwater cameras and computer software has allowed reef researchers to create digital quadrats that can be overlaid ontop of underwater images, without causing any disruption to the marine ecosystem (Nakajima et al., 2010).

Nakajima et al. (2010) compared the PLIT method with the PHOTS method, and found that PLIT underestimated coral cover by 8%, a relatively small difference, however, significantly underestimated the number of coral genera present. This suggested the use of PLIT was a convenient and time-efficient approach for estimating coral coverage in management-level monitoring, however, PHOTS is much more appropriate for diversity assessments (Nakajima et al., 2010).

The underwater video transect is another emerging method that has become increasingly popular in the reef surveying community (Cabaitan et al., 2007; Carleton & Done, 1995; Houk & Van Woesik, 2006). Much like the PLIT method, a digital video camera in underwater housing is used to video the substrate along a laid transect line at a relatively consistent distance from the benthos (Carleton & Done, 1995; Leujak & Ormond, 2007). The video data is then imported into computer software, where frames along the transect are extracted at desired intervals, and random or systematic points are overlaid across the images for substrate and species identification (Cabaitan et al., 2007; Houk & Van Woesik, 2006; Leujak & Ormond, 2007).

This method offers many advantages such as reduced data collection time in the field and the permanent historical imagery obtained can be analysed in different ways. Underwater

video cameras are now light and compact, and minimal training is required for data collectors in the field. Observer bias can also be reduced through comparisons between observers post data collection, preferably during pilot studies before full-scale sampling (Cabaitan et al., 2007; Carleton & Done, 1995; Houk & Van Woesik, 2006).

Video transects also have their limitations. Leujak & Orman (2007) found images collected through video or photo methods led to consistent underestimates of encrusting coral cover and an overestimation of massive coral and coral rock cover, due to limited resolution and contrast, compared to *in situ* data collection techniques. They suggested this limitation could be partially overcome if notes were taken on the presence of cryptic coral colonies, during photographic data collection, however this would not be possible during video transects, as the frames to be analysed are unknown at the time of recording.

Lam et al. (2006) found percentage cover was overestimated by the PIT method compared to video transects taken by SCUBA or remotely operated vehicle (ROV). Rare benthic categories such as recently killed coral, rock, rubble, and sponge were detected by the video methods, due to a larger frame of view, however, these categories were missed with the PIT method as only points along a transect line were observed. Additionally, the video method also provides information on coral colony size, which serves as a valuable indicator of coral community stability (Lam et al., 2006).

It has been suggested that reduced data collection time in the field has led to increased post-collection computer analysis (Cabaitan et al., 2007), however, Leujak & Orman (2007) found that post-collection analysis was much greater for MAP and PHOTS, compared to video transects. Video transects have been known to produce lower-resolution frames compared to images taken via the PLIT or PHOTS, which has led to identification limitations (Cabaitan et al., 2007). Nevertheless, recent advances in underwater video camera technology have allowed for higher-resolution underwater footage collection.

In more recent years, image-collection platforms such as ROVs (Lam et al., 2006), automated underwater video (Foster et al., 2014), and towed cameras (Cresswell et al., 2021; Morrison & Carbines, 2006), have been used in coral and temperate reef mapping and monitoring programs, as they offer a safer, more efficient alternative to diver-based data

collection. The effectiveness of obtaining video transects, whether through diver or non-diver methods, is contingent upon various site conditions during each investigation (Lam et al., 2006). Factors such as current patterns, surface conditions, and weather interact to determine the most efficient method. Diver-based methods are often more favored in high wind and high current conditions, as divers can maintain better balance in the water, ensuring the stabilization of the video image and facilitating filming along the necessary transect lines (Lam et al., 2006).

Cresswell et al. (2021) found it more difficult to maneuver the towed camera along a specified GPS track in high wind and swell conditions, which resulted in variable image quality due to uneven distances from the substratum and images not being taken perpendicular to the seafloor. However, a benefit of non-diver image collection, is that the equipment is not constrained by safety considerations that may limit divers, whether in terms of safety of the surveyed environment (e.g. hazardous marine animals, limited visibility, unpredictable weather and current, depth) or limitations on dive time to avoid decompression sickness (Cresswell et al., 2021; Lam et al., 2006).

When deciding on an appropriate method of data collection, the overarching goals of the monitoring program need to be considered, taking into account the scale and desired taxonomic resolution of the required data, the environmental conditions, and the repeatability of the method (Cresswell et al., 2021).

Table 2. Summary table of reef surveying techniques

Method	**Period**	**Technique**	**Benefits/weaknesses**
Line-intercept method	Early 1970s	A tape measure is laid across a section of reef and percentage cover is estimated from the proportion of the total length of the transect overlying different substrata.	- Cost effective, as minimal specialized equipment is used. - Fixed transects for repeated measures introduces artificial structures which may damage the reef complex. - Lengthy time spent in the field.

			- Data collectors need sufficient training on species identification. - Can underestimate number of species present.
Point-intercept method	1980s	The substrate is recorded under equally spaced points along the transect line. Percentage cover of substrate types is determined by the number of points divided by the total number of points along the transect line.	- Slightly faster than LIT, although still a lengthy time spent in the field. - Cost effective as minimal equipment used in the field. - Can result in the under-sampling of rare species. - Data collectors need sufficient training species identification.
Mapped quadrats	1970s	1m x 1m quadrat frames that are subdivided into a grid are laid along a transect line. A map of the substrata can be hand drawn and percentage cover is estimated using visual assessments. Alternatively, substrate is recorded underneath each grid intersection. Percentage cover is determined by the number of points divided by the total number of observed points/intersections.	- Presence/absence data, number and size of colonies, cover area of live/dead coral species is also recorded. - Can physically damage the reef complex. - Can be very time-consuming drawing quadrat maps underwater. - Data collectors need sufficient training species identification.
Photo-line intercept method	1970s	The same technique as the line-intercept method, however, an underwater camera is used to take images along the transect line. Images are then analysed using computer software.	- Underwater cameras are light and compact. - Provides a permanent visual record. - Reduced data collection time in the field. - Resolution and contrast issues can lead to underestimations of cryptic species.

			- Can underestimate coral cover and number of genera present. - Minimal training required for data collectors in the field.
Photo-quadrat method	1970s	An underwater camera is used to photograph quadrat frames along a transect line or digital quadrats are overlaid on underwater images. Images are then analysed using computer software.	- Underwater cameras are light and compact. - Provides a permanent visual record. - Reduced data collection time in the field. - Resolution and contrast issues can lead to underestimations of cryptic species. - Minimal training required for data collectors in the field.
Video transects	1990s	A digital video camera in underwater housing is used to video the substrate along a transect line. Frames are then extracted from the video footage and analysed using computer software.	- Underwater cameras are light and compact. - Provides a permanent visual record. - Reduced data collection time in the field. - Resolution and contrast issues can lead to underestimations of cryptic species. - Minimal training required for data collectors in the field. - Post collection data analysis time can be lengthy. - Equipment and software costs can be high.
ROV's and towed cameras	Late 80s to early 90s	Remotely operated vehicles or towed cameras are used to record video transects. Frames are then extracted and analysed digitally.	- Provides a permanent visual record. - Not limited to dive time constraints. - Reduced data collection time in the field. - Useful in unfavorable diving conditions. - High wind and swell conditions can result in

			variable Image quality due to uneven distances from the substratum. - Equipment costs are substantial.

1.4 Satellite mapping and remote sensing techniques

Remote sensing and geospatial techniques have been used to map and monitor geomorphic and ecological zones, benthic and coral community composition, and assess environmental stress across coral reefs globally (Ahmad & Neil, 1994; Deshmukh et al., 2005; Hoang et al., 2016; Phinn et al., 2012; Roelfsema et al., 2018; Xu et al., 2020). Mapping this data in Geographic Information Systems (GIS) allows for the creation, management, display and analysis of spatial and geographic data collected from many different sources.

Remote sensing techniques encompass a wide range of technologies, including satellites, airborne sensors on planes or helicopters, unoccupied aerial systems, boat-based systems, and autonomous underwater vehicles (Hedley et al., 2016). Satellite remote-sensing imagery (SRSI) combined with GIS software provides a highly cost-effective method of habitat mapping and assessing spatial and temporal patterns across extensive reef areas, compared to field surveying techniques (Green et al., 1996; Mumby et al., 1999).

Mapping reef ecosystems from satellite imagery cannot inherently offer the same level of precision and detail as a field survey conducted at the same location. However, it does have the advantage of providing comprehensive coverage, which enhances its statistical power for deducing large-scale patterns (Hedley et al., 2016). In addition, historical satellite imagery can be used to quantify environmental changes that have occurred across decades (Yang et al., 2019). Mapping of coral reefs has been conducted using remote sensing imagery across the electromagnetic spectrum and can include visible and non-visible wavelengths, either collected as multispectral data (comprising of less than 10 broad wavelength bands) or as hyperspectral data (more than 10 narrow bands) (Mumby et al., 2004).

Remotely sensed imagery ranges from very high resolution (pixels less than 1m) to low resolution (100-1000m), with higher spatial resolution imagery typically covering smaller spatial scales (Hedley et al., 2016). Phinn et al. (2012) used multispectral, high resolution (2.4m x 2.4m pixels) Quickbird 2 satellite imagery to map geomorphic and ecological zones across three western Pacific reefs, using object-based image analysis (OBIA) coupled with field survey data. The use of georeferenced photo-transects, allowed for a robust training and validation of the OBIA, and resulted in accurate (>80%) geomorphic zone maps, and relatively accurate (52%-78%) benthic community maps. Other research has investigated the use of SRSI to map the distribution of *Sargassum* beds (Hoang et al., 2016). With the combination of high-resolution WorldView-2 imagery, field survey data, and specialised image classification techniques (minimum distance, Mahalanobis distance, K-means, and parallel-epiped), Hoang et al. (2016) produced a highly accurate (98.30%) map of *Sargassum* beds around Rottnest Island, Western Australia. Their results show the potential of remote sensing technologies to accurately map and monitor seaweed species in coastal marine environments.

SRSI has also been used to detect coral bleaching events across multiple time periods, as bleaching is indicated by an increase in coral pixel brightness (Xu et al., 2020). Xe et al. (2020) used an approach that involved specialised pre-processing of Planet Dove satellite imagery, a time series analysis for baseline reflectance statistics, and a regional filter based on a live coral map. The time series was divided into baseline and bleaching periods, which allowed for the computation of a coral bleaching probability index – the Standardised Bottom Reflectance (SBR). The SBR enhanced the sensitivity to bleaching detection by transforming weekly bottom reflectance relative to baseline reflectance statistics. The team tested three scales of temporal smoothing (weekly, cumulative average, and three-week moving average), with the cumulative average and three-week moving average correctly identifying 11 and 10 out of 18 bleaching locations, verified through field data. This highlights the potential for high-resolution SRSI techniques to effectively monitor environmental changes in coral reef environments.

SRSI has the capacity to accurately map and monitor geomorphic and ecological zones, and detect and predict changes within coral reef environments, but limitations do exist. Despite significant improvements in the spatial resolution of satellite imagery over the past decade,

the constraints to fine-scale satellite data limit the potential for small-scale reef management and mapping (Ventura et al., 2018). Coral reefs exhibit high heterogeneity at scales of a few metres or less, with distinct benthic types like corals, seagrasses, or macroalgae typically occurring at varying spatial scales (Hedley et al., 2018). Therefore, low pixel resolution can make accurate object-based image classifications difficult due to spectral confusion across multiple habitat types (Knudby & Nordlund, 2011). In addition, meteorological conditions significantly impact satellite imagery, including issues like cloud contamination, aerosol interference, surface glint, and poor synchronization with tides (Hedley et al., 2016; Hedley et al., 2018; Tait et al., 2019). While these limitations are often mitigated by the high frequency of satellite passes in many cases, capturing high-quality images in the intertidal and subtidal zone becomes considerably challenging in turbid coastal waters (Tait et al., 2019).

Furthermore, the high cost per scene derived from commercial imagery makes it undesirable for systematic repeated monitoring or large-scale change detection (Hedley et al., 2018). Thus, alternative finer-scale, cost-effective mapping techniques are required to inform targeted, ecosystem-based management approaches within coral reef monitoring programs.

1.5 Unoccupied aerial vehicle surveys

Advancements in the capabilities and cost-effectiveness of unoccupied aerial vehicles (UAVs – commonly referred to as drones) have sparked a surge in their use in ecological, conservation and agricultural remote sensing applications (Hodgson et al., 2017; Yang et al., 2019; Tait et al., 2019; Ventura et al., 2018). While conventional satellite remote sensing systems provide images with relatively coarse resolutions (10s to 100s of metres), image sensors attached to UAVs, provide finer resolution (centimetre level) and more spatially accurate imagery over localised areas (Colomina & Molina, 2014; Tait et al., 2019).

UAVs also provide a more convenient, on-demand, safer, and cost-effective alternative to manned aircraft, especially in areas that are difficult to access (Tait et al., 2019). Yang et al. (2019) mapped a coastal lagoon from high-resolution (0.25m) multispectral imagery collected by UAVs and compared results with those from analysis of multi-spectral Sentinel-2 satellite imagery. A normalised difference vegetation index (NDVI – a metric used to

quantify the health and density of vegetation using sensor data) and object-oriented classification methods were deployed to compare the two mapping capabilities. The study found the UAV mapping approach offered enhanced insights into the physical conditions of the study area, improved delineation of land features, and a more detailed understanding of mangrove conditions. The spatial resolution and spatial information derived from the multi-spectral UAV imagery was much greater than that of the satellite imagery (Yang et al., 2019).

Tait et al. (2019) investigated the difference between a six band multi-spectral camera and a visible light RGB camera (containing three spectral bands: red, green, and blue) when mapping macroalgae in intertidal and shallow subtidal habitats. The study revealed images taken with a combination of the broad spectral ranges of RGB bands and the narrow multispectral bands, resulted in the most accurate (90% accuracy) classification of the various red, brown, and red algal species. The RGB and multispectral imagery produced remarkably similar accuracies of 79% and 81%, respectively. Despite the slightly lower classification accuracy, the results strongly show RGB imagery collected from drones is capable of accurately classifying macroalgal species across intertidal and subtidal zones.

UAVs provide a low-cost and effective method to obtain high-resolution imagery over coral reefs and other benthic habitats due to their flexibility in flying height, location and timing of surveys (Hodgson et al., 2017; Tait et al., 2019). However, environmental factors such as sun glint, wave action and drifting objects can limit image utility as techniques such as Structure from Motion (SfM) rely on point matching between images (Chirayath & Instrella, 2019). When dealing with open water and the lack of fixed coastal landmarks visible in images, SfM may encounter issues when creating mosaics. This is due to the scarcity of matching points between adjacent photos on a relatively featureless sea surface.

As SfM techniques are negatively affected by water refraction, ideal survey conditions require a calm sea and low sun-glint, which may be rare occurrences during a typical field survey. Casella et al. (2017) utilized a consumer-grade drone and SfM photogrammetry techniques to create an ortho-rectified aerial photomosaic and bathymetric digital elevation model (DEM) of a shallow water reef lagoon environment. The ortho-

photomosaic achieved an exceptionally high resolution (0.78 cm pixel size), enabling the identification of the genera or growth forms of larger corals. These high-resolution drone surveys were able to effectively identify correlations in coral cover and morphology with coral bleaching events (Casella et al., 2017).

The relatively low horizontal accuracy (1.4m) of the ortho-photomosaic was attributed to the use of a handheld GPS when collecting ground control points. The bathymetric DEM had a difference of -0.016m $\pm$ 0.45m compared to the LiDAR data, which itself has an accuracy of 0.25m. These large errors were likely a result of water refraction, and Casella et al. (2017) suggest that the development of fluid lensing correction techniques will likely aid in the reduction of these discrepancies. Their results concluded that conditions of calm water, low wind, and minimal sun glint offer the best chance for consumer-grade drones to collect effective imagery across shallow reef environments.

Chirayath and Earle (2016) successfully produced centimetre scale 3D underwater imagery over two reefs in American Samoa and Western Australia, after removing the effects of surface waves. This was achieved using experimental fluid lensing technology, which passively captures high-resolution imagery of underwater objects using water-transmittable wavelengths, and exploits time-varying optical lensing events caused by refractive wave distortions (Chirayath & Earle, 2016). Chirayath and Instrella (2019) expanded on this research and developed a supervised machine-learning algorithm capable of efficiently distinguishing between living and non-living structures and segmenting the coral reef into four distinct morphological classes from fluid lensing 3D underwater imagery. The algorithm produced 3D maps of reef morphology and living structures for the Ofu Island reef system. Verification through *in situ* mapping, underwater photography and expert knowledge indicated that model accuracies were greater than 90%. While innovative fluid lensing technologies are currently in active development and not widely accessible, these results highlight the extensive capabilities that UAV imagery brings to marine conservation (Chirayath & Earle, 2016; Chirayath & Instrella, 2019).

1.6 Full Motion Video (FMV)

UAVs are increasingly being used to capture Full Motion Video (FMV), commonly known as spatial video data. FMV is a GIS concept that refers to the addition of spatial information into a video stream and allows for the location of a video frame to be identified on a mapped surface (Lewis et al., 2011). The FMV Image Analyst extension within ArcGIS Pro facilitates the playback and analysis of any FMV-compliant video stream (Environmental Systems Research Institute (Esri), n.d.). An FMV-compliant file refers to a video file that contains specific metadata, making the FMV file spatially aware. The required metadata to spatially enable a video stream in accordance with the Motion Imagery Standards Board (MISB), include position, orientation, and altitude. Within a drone system, its location is recorded as metadata, including a timestamp, drone and camera position, angles, and field of view. When this metadata is encoded into the video stream collected by the drone, each video frame has an associated geographic position (Esri, n.d.).

The combination of GIS software and FMV provides the capability to observe and manipulate the video stream, allowing for the analysis and editing of feature data within the drone's field of view. This information can then be displayed and further analysed in the map view within ArcGIS Pro (Esri, n.d.). In this study, the combination of UAV FMV with georeferenced underwater footage offers a novel alternative to the mapping of shallow water reef flat habitat dynamics.

1.7 Aims and objectives

This research applied a novel UAV FMV technique, recently developed at the Auckland University of Technology (AUT) by Hinchliffe (2022) to survey and map a shallow reef flat near the village of Vavanga, Kolombangara Island, Solomon Islands. The study paired low-cost drones and a Sublue Whiteshark MixPro underwater scooter equipped with GoPro cameras, to collect spatially enabled underwater footage of reef flat biota and substrata. The combination of GoPro and UAV video provided a multiscale approach, with high-resolution ground truth data and contextual imagery of the survey area.

FMV allows imagery captured by a drone over water to be spatially georeferenced, as aircraft telemetry and camera variables can be post-processed as metadata into the video stream (Hinchliffe, 2022). In this study, underwater video imagery was synchronized with

aerial FMV collected from a drone flown overhead. Frames from the underwater video were geolocated allowing underwater features to be identified and directly compared with objects visible in aerial imagery at the same location.

Video from above and below the water can be displayed simultaneously for visual interpretation and the underwater video of reef flat biota and substrata can be used to train and ground truth classifications of photo orthomosaics generated from the matching drone data. The ability to repeatedly map the same reef habitats, lifeforms and even species through time using accurate spatial coordinates provides a powerful tool to monitor fine-scale changes without having to rely on artificial markers.

Through the development of cost-efficient coral reef survey strategies, we can provide better estimates of the conservation status of coral reefs and better understand how to mitigate anthropogenic threats, provide sustainable food security for coastal communities, and assess the effectiveness of ecosystem management.

This study aimed to trial the techniques described above to map spatial patterns in the zonation of benthic biota and substrata across a coral reef flat adjacent to a small village and river where logging has occurred in the catchment. The overall research question investigated is as follows:

Can fine-scale spatial patterns and zones in benthic biota and substrata on a coral reef flat be accurately quantified through a robust combination of UAV FMV techniques and underwater imagery, and what can this tell us about the health and functioning of these ecosystems?

This question will be investigated through the following objectives:

1. Combine Unoccupied Aerial Vehicle (UAV) Full Motion Video (FMV) with georeferenced underwater video to provide transects of substrate variation across the reef flat.
2. Determine the effectiveness of novel UAV FMV for shallow-water substrate mapping in a tropical reef flat environment.

3. Spatially quantify reef flat zones and gradients using a combination of geospatial and statistical sampling and analyses.
4. Investigate the potential of the open access Artificial Intelligence (AI) platform ReefCloud.AI, to classify reef flat substrata using georeferenced underwater imagery.
5. Determine the utility of geospatially referenced aerial and underwater video data to coral reef research, conservation, and management.

1.8 Structure of thesis

Chapter 1 has provided background knowledge, reviewed relevant literature, and addressed the aim and objectives of this study. Chapter 2 describes the methods applied in this study including the location, equipment used and data collection processes, followed by the data processing and analysis. In chapter 3 I will present the results of my analysis, before discussing the relevance and implications of my findings in Chapter 4.

2 Methods

2.1 Location

The Solomon Islands lie east of Papua New Guinea and north-west of Vanuatu, consisting of six larger islands, and over 900 smaller islands (Figure 2). Kolombangara Island is one of 35 islands that belong to the New Georgian chain of islands lying within the Western Province of the Solomon Islands. This region harbours a diverse range of habitat types spanning from lowland rainforests, with summits reaching up to 1000m, to low-lying atolls and coral reef systems, which provide a home to an extensive range of marine and terrestrial biodiversity (Tigulu et al., 2018).

Kolombangara Island is a mountainous island with a dense tropical rainforest, and an extensive fringing reef system that extends approximately 200m-300m offshore (Wenger et al., 2020). Data collection for this study took place between 5th – 14th of December 2022 and was carried out across a fringing reef flat over an area extending up to 2km either side of the river mouth at Vavanga Village (8°03'39.4"S 156°58'04.3"E), Kolombangara Island, Solomon Islands (Figure 3).

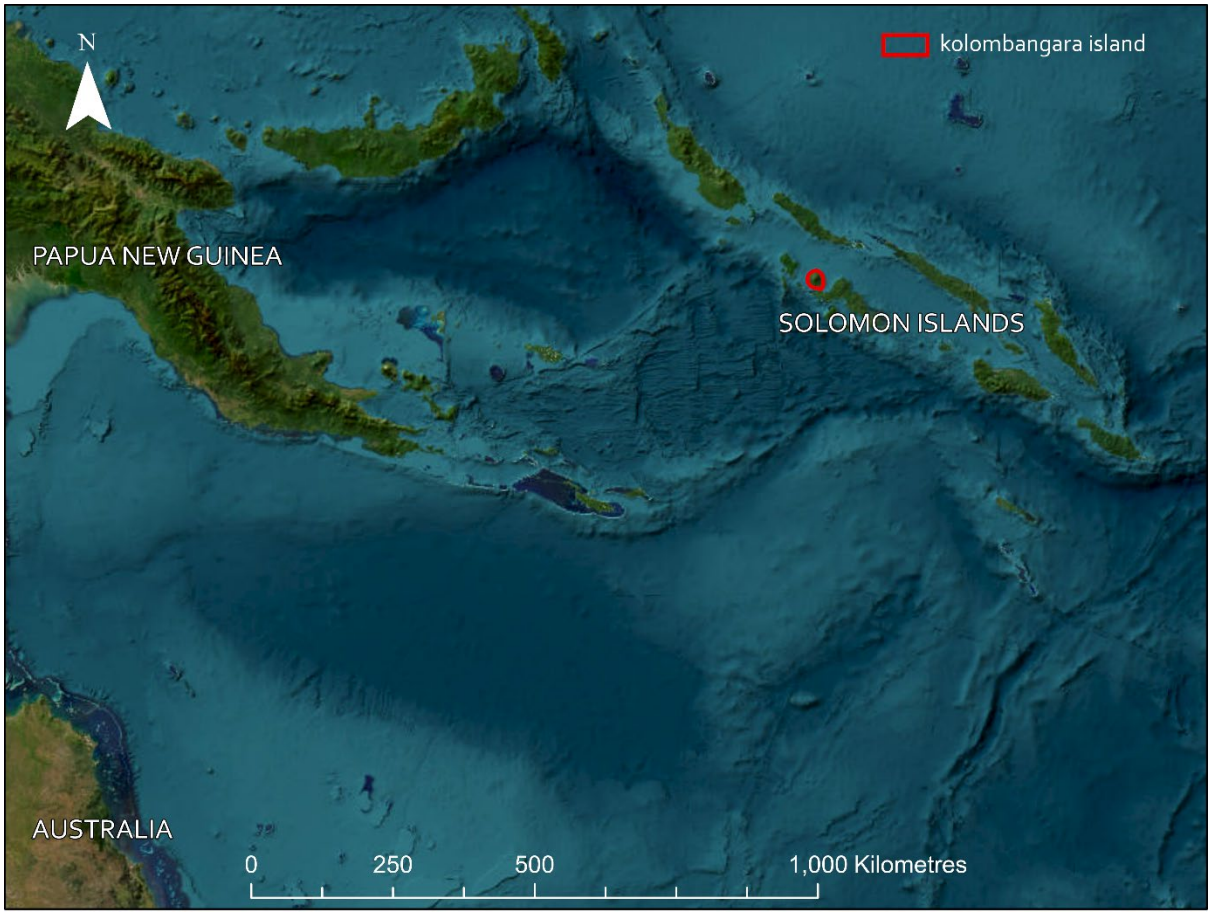

Figure 2. Location of Kolombangara Island, Solomon Islands. (Source: Esri, Maxar, Earthstar Geographics, and the GIS User Community).

The Solomon Islands are one of the six archipelago nations that lie within The Coral Triangle, an area renowned for its immensely diverse aquatic environment (Green & Mous, 2008). Although this region comprises only 2% of the world's oceans, it boasts a wealth of marine biodiversity spanning the Philippines, Indonesia, Malaysia, Timor Leste, Papua New Guinea, and the Solomon Islands (Aalbersberg et al., 2012). The coral triangle includes 76% of the world's scleractinian coral species, 37% of coral reef fish species, and 50% of the global tuna supply (Hoegh-Guldberg et al., 2009). During a Solomon Island Marine Assessment survey conducted by Green et al. (2006), 1019 species of coral reef fish and 485 coral species from 76 genera were identified across 66 sites. These corals were found across a diverse assemblage of reef types, including narrow fringing reefs, lagoons, patch reefs and atolls. The survey also identified other macroinvertebrate species inhabiting the coastal waters of

the Solomon Islands including 19 species of sea cucumber, six giant clam species, three species of pearl oyster, four main crayfish species, and multiple sea snail species. Additionally, the region hosts several marine reptiles, such as turtles, sea snakes, and a single species of crocodile, as well as a diverse range of marine mammals, including nine species of dolphins, eight species of whales, and a solitary species of dugong (Green et al., 2006).

The natural resources in the Solomon Islands play a vital role in sustaining the lives and aspirations of many local communities. This is especially crucial as over 80% of the Solomon Islands population resides in rural areas and primarily depend on their natural resources for their daily sustenance (Green et al., 2006). The reef flat in the Solomon Islands remains as a key foraging area for subsistence fishers, as it provides up to 60% of the population's consumption needs (Bell et al., 2009; Molea & Vuki, 2008). Revenue generated from the sale of fish and other marine products primarily in local markets also offers indirect advantages, allowing for the acquisition of additional food, commodities, and services (Molea & Vuki, 2008; Weeratunge et al., 2011).

Although the marine habitats of the Solomon Islands are still in relatively 'good' condition compared to other areas within the Coral Triangle (Aalbersberg et al., 2012), its abundant biodiversity still faces many threats. These include substantial pressures stemming from ongoing logging on primary islands, overexploitation of marine resources, sedimentation, pollution from inadequate waste management and the adverse consequences of climate change (Tigulu et al., 2018).

Rising sea surface temperature, sea levels and ocean acidification are likely to accelerate existing coral bleaching, mortality and disease and potentially create detrimental impacts on mangroves, seagrass meadows, and other coastal ecosystems (Albert et al., 2012). As reef flats are positioned in shallow waters, it is likely that this zone, along with the communities it supports, will be the most severely affected by climate change (Harborne, 2013). Thus, an understanding of reef flat habitat dynamics will be essential in the management and conservation of the goods and services it provides.

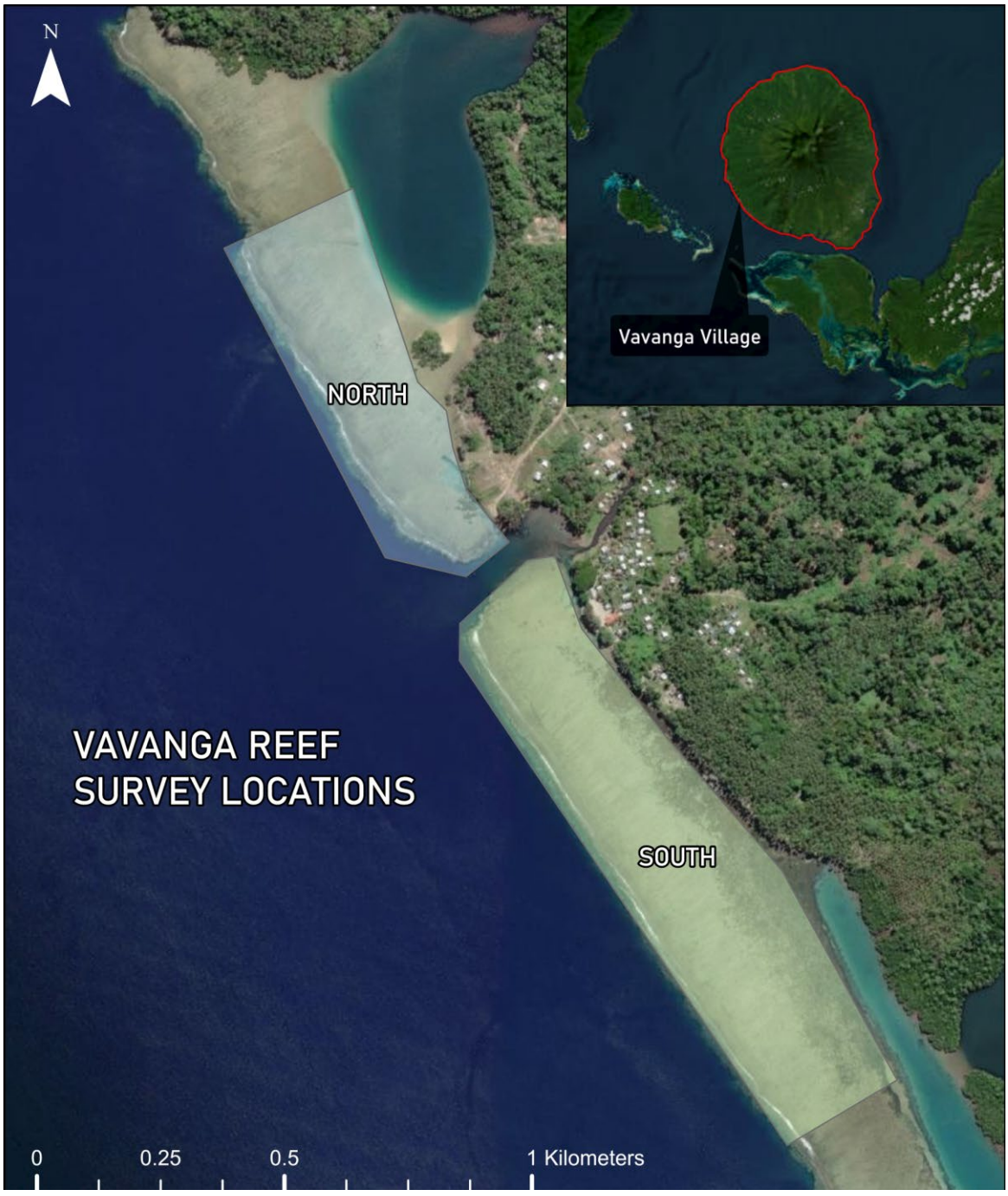

Figure 3. Overview of the north and south survey locations, Vavanga Village, Kolombangara Island, Western Province, Solomon Islands (Source: Esri, Maxar, Earthstar Geographics, and the GIS User Community).

2.2 Equipment

A DJI Mavic 2 Pro drone was used to collect all aerial FMV data and photo surveys across the two sampling sites, using the built-in three-band (RGB) camera and sensors (Figure 4). All drone footage was captured in 2.7k resolution (2704 x 1520 pixels), at a frame rate of 50 frames-per-second (fps). To increase visibility while flying, a strobe light and high-vis tape was attached to the drone.

A Sublue Whiteshark MixPro underwater scooter was used to propel a snorkeler through the water while collecting underwater video imagery (Figure 4). Underwater footage was captured simultaneously with a GoPro Hero 8 and GoPro Hero 9 camera, both with a 2.7k resolution, 50 fps frame rate, and stabilization set to low. A frame rate of 50fps was chosen to increase temporal fidelity when pausing the video, as this increased our chance of capturing a precise frame that matched the geographic position of the underwater scooter seen in the corresponding drone frame. The cameras were mounted to the front of the underwater scooter using a double GoPro mount. The cameras were mounted at 90° angles to each other to provide two points of view underwater (straight down and straight ahead).

All drone and underwater footage collected was downloaded from the SD card's and backed up onto two portable hard drives at the end of each day.

Figure 4. Image of data collection team and equipment. Pictured from left to right is Daniel Breen (safety team), Grace Martin (snorkeler), holding the Sublue Whiteshark MixPro Underwater Scooter with GoPro's attached, and supervisor Graham Hinchliffe (drone pilot).

2.3 Synchronised drone and underwater scooter video transects

The drone was piloted by supervisor Graham Hinchliffe, who holds a CASA RePL (Remote Pilot License). All flights were taken following Solomon Island regulations regarding UAV use. Specifically, this included visibility of the surrounding airspace, operating under 122m (400ft), below the cloud base and not within 4km of any airfield. Moreover, the safety ranges for the DJI Mavic 2 Pro were followed, including not flying in wind speeds over 10m/s and aborting flights in the event of any rain. During all surveys, Hinchliffe was piloting from one of the three drone operation sites along the shoreline (Figure 20). Depending on the terrain of each operation site, a flat wooden board was used as a stable drone launching surface. While most flights were flown from the shore, where required to work from a boat, the pilot used a 3D printed hand catch pole for safe launch and landing.

The following data collection steps are shown in Figure 5. To ensure that the UAV and GoPro video could be analysed together, a syncing action was captured by all cameras at the beginning of each video recording. At the start of each transect, the snorkeler would get into position in the water, turn on both GoPro cameras, and begin recording video. The safety team would then signal the pilot to launch the drone. Once the drone was in position

at a low flying height, the safety team would signal to the pilot that the snorkeler was ready to start the transect. The snorkeler would then perform a waving action that could be seen in both GoPro and drone video frames. This allowed for accurate synchronisation between the UAV and underwater video footage.

The snorkeler then began the transect, heading straight out towards the reef crest for approximately 300m. Once over the reef crest, the snorkeler would swim parallel to the shoreline, then turn around and come back towards the shore. Maintaining a consistent swimming speed was unnecessary as the sampling along transects was conducted based on distance intervals as opposed to time intervals. Each day, there was a small window of time that provided a tide high enough for the snorkeler to pass over the reef crest. Occasionally this window was missed due to weather or swell conditions, preventing the snorkeler from crossing over the reef crest, which resulted in slightly shorter transects.

During each transect, the pilot would follow the snorkeler, ensuring they remained in the drone's field of view. Depending on the light refraction and surface interference, the angle of the drone's point of view was chosen by the pilot to achieve the best view of the snorkeler. The battery life of the drone and the scooter was approximately 25 minutes, with flights typically resulting in 18-20 minutes of survey time. The drone returned to land once battery levels reached 30%, providing a safety buffer in case of any difficulty. Once the snorkeler had reached the shore, the video recordings were stopped and battery packs exchanged, ready for the next transect. A total of 14 combined UAV surveys were taken across the north and south survey areas (Table 1). Figure 6 displays six example GoPro frames extracted from the first transect taken on the 7th of December, highlighting the variation in substrate types seen across the reef flat.

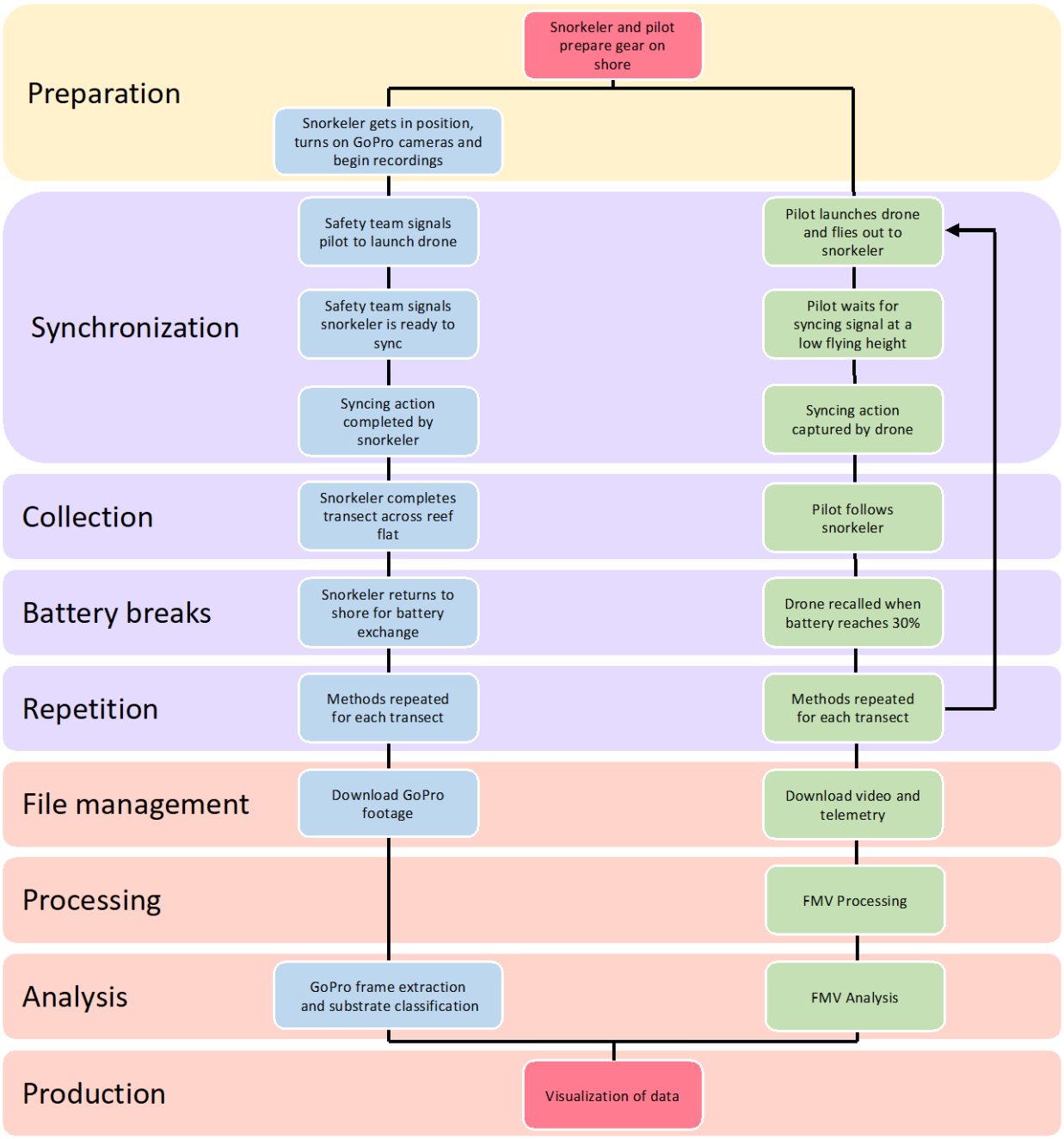

Figure 5. Data collection timeline showing the simultaneous snorkeling (blue boxes) and drone (green boxes) methods occurring in the field. The individual steps occur in one of three main phases: Preparation (yellow), data collection (purple), and data analysis (pink).

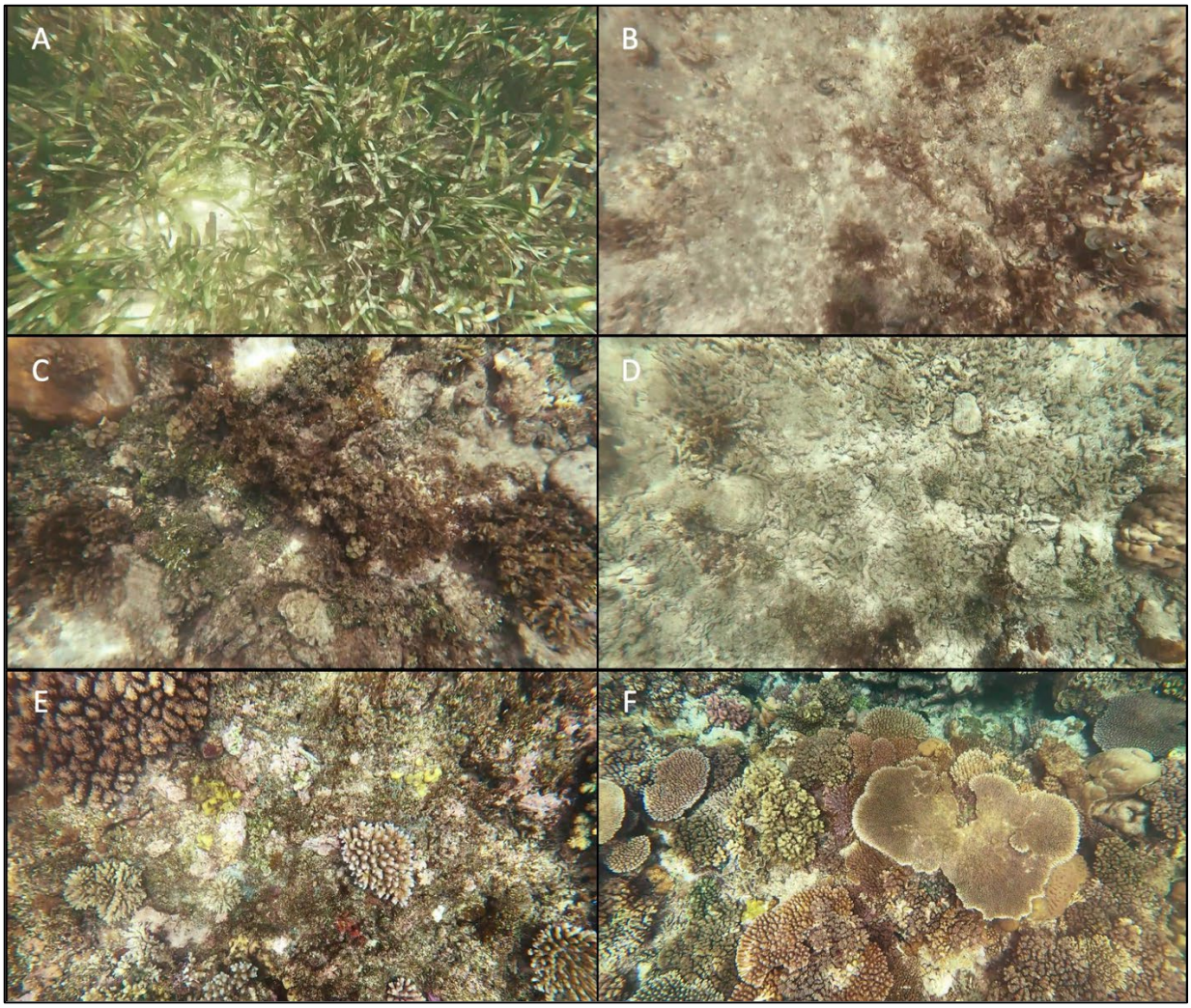

Figure 6. Example GoPro frames extracted from the first transect taken on the 7th of Dec, highlighting the variation in substrate types across the reef flat. (A) area close to the shoreline, dominated by the seagrass species *Thallassia hemprichii*; (B) beyond the seagrass beds, there is a mixture of sandy substrate and macroalgae such as *Padina*; (C) further out, there is a mixture of macroalgae species such as *Sargassum echinocarpum*, *Turbinaria ornata*, and *Halimeda*; (D) before reaching the reef crest, the area becomes dominated by coral rubble and consolidated coral rock substrate; (E) consolidated coral rock dominates, with some small *Acropora spp.* colonies and *Pocillopora verucosa* seen in the top left; and (F) live corals dominate at the reef crest.

2.1 Automated aerial photo flights

Photo flights were planned and conducted using UgCS control software, with a double grid method to maximize wave-free coverage over any particular area. Flights were configured for a normal ground spacing distance (GSD) of 2.6 and 2.8cm for the grids, giving Above Ground Level (AGL) flight heights of 102m and 110m respectively (Figure 7).

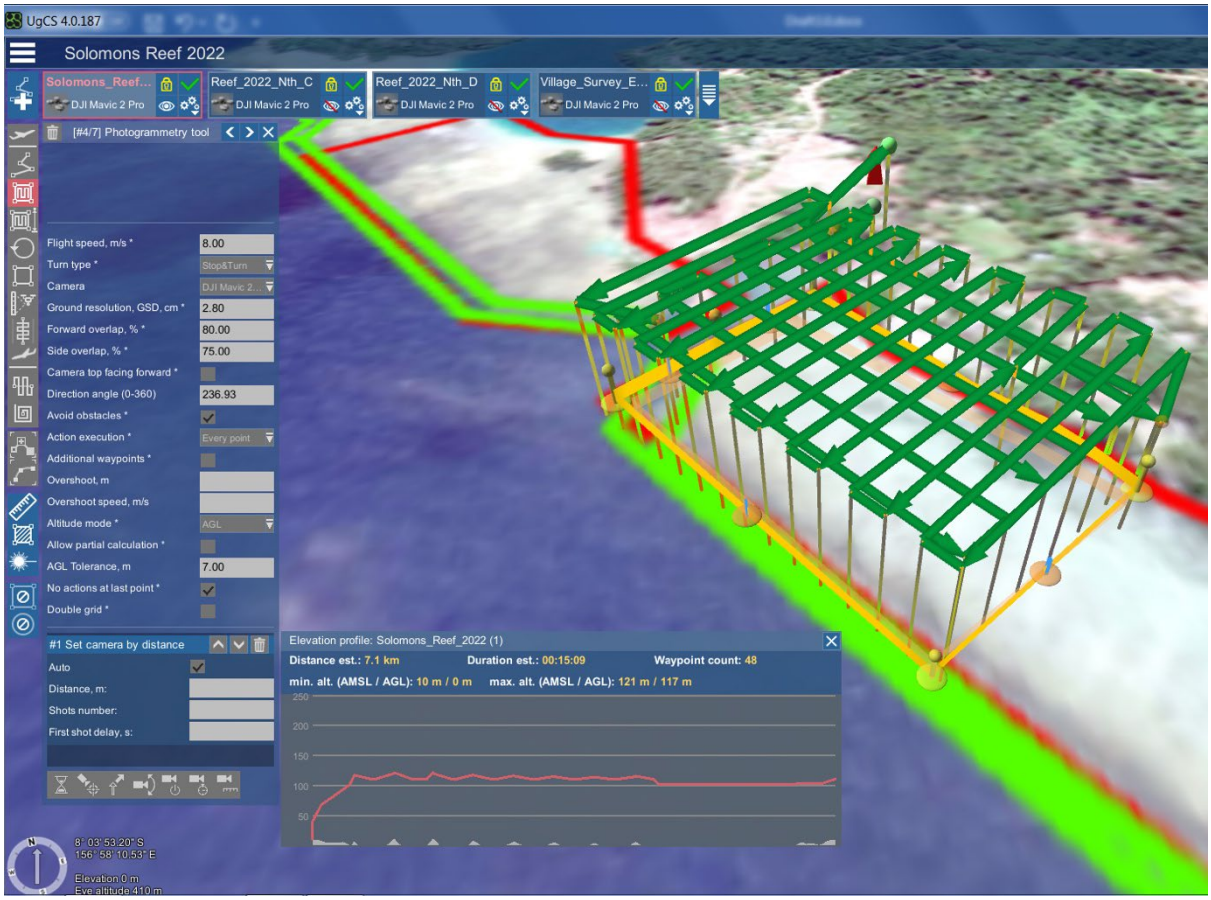

Figure 7. Example of a UgCS flight plan undertaken on the south reef flat in front of Vavanga village.

Table 3. Drone flight timeline

Monday 5th	*Flight 1:* Preliminary test flight scouting the reef survey locations
	Flight 2: UgCS route flight – photo survey of the South Reef flat zone A
	Flight 3: UgCS route flight continued
	Flight 4: FMV continuous drone video following snorkeler for three transects along south reef
	Flight 5: FMV continuous drone video following snorkeler for two transects along south reef
Tuesday 6th	*Flight 1:* UgCS route flight photo survey of South Reef zone B
	Flight 2: UgCS route flight continued
	Flight 3: DJI video transects along South Reef
	Flight 4: DJI video transects along North Reef, with dwell videos
	Flight 5: FMV continuous drone video following snorkeler for two transects along north reef
	Flight 6: FMV continuous drone video following snorkeler for two transects along north reef
	Flight 7: FMV continuous drone video following snorkeler for two transects along north reef
Wednesday 7th	*Flight 1:* UgCS route flight photo survey flights over North reef
	Flight 2: Surveillance flight.

	Flight 3: FMV continuous drone video following snorkeler for two transects along south reef (near lagoon)
	Flight 4: FMV continuous drone video following snorkeler for two transects along south reef
	Flight 5: FMV continuous drone video following snorkeler for two transects along south reef (closest to village)
Thursday 8th	*Flight 1:* FMV continuous drone video following snorkeler for two transects along north reef
	Flight 2: continued FMV drone video following snorkeler for two transects along north reef
Friday 9th	*Flight 1:* FMV continuous drone video following snorkeler for two transects along north reef
	Flight 2: continued FMV drone video following snorkeler for two transects along north reef
Wednesday 14th	*Flight 1:* FMV continuous drone video following snorkeler South lagoon area
	Flight 2: Continued FMV drone video following snorkeler South lagoon area

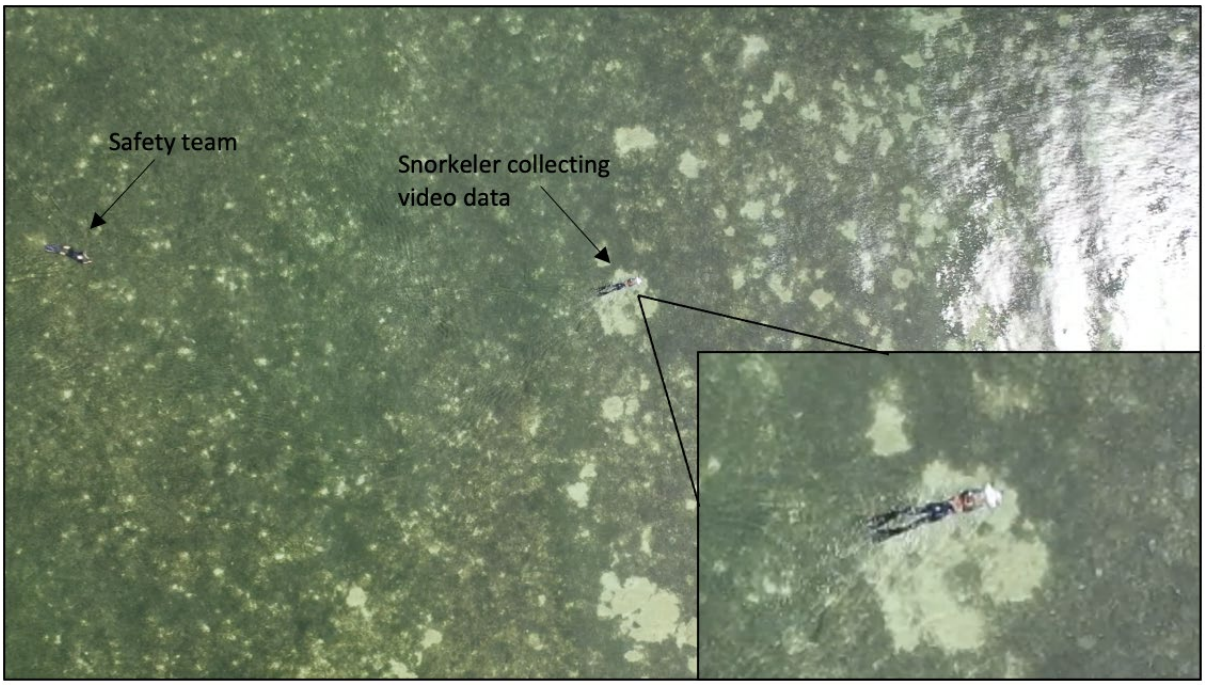

Figure 8. Screenshot of UAV footage with snorkeler videoing underwater habitat using the underwater scooter. Safety team is close behind.

Figure 9. Aerial photo of the south reef flat survey area. Darker areas inshore have dense seagrass.

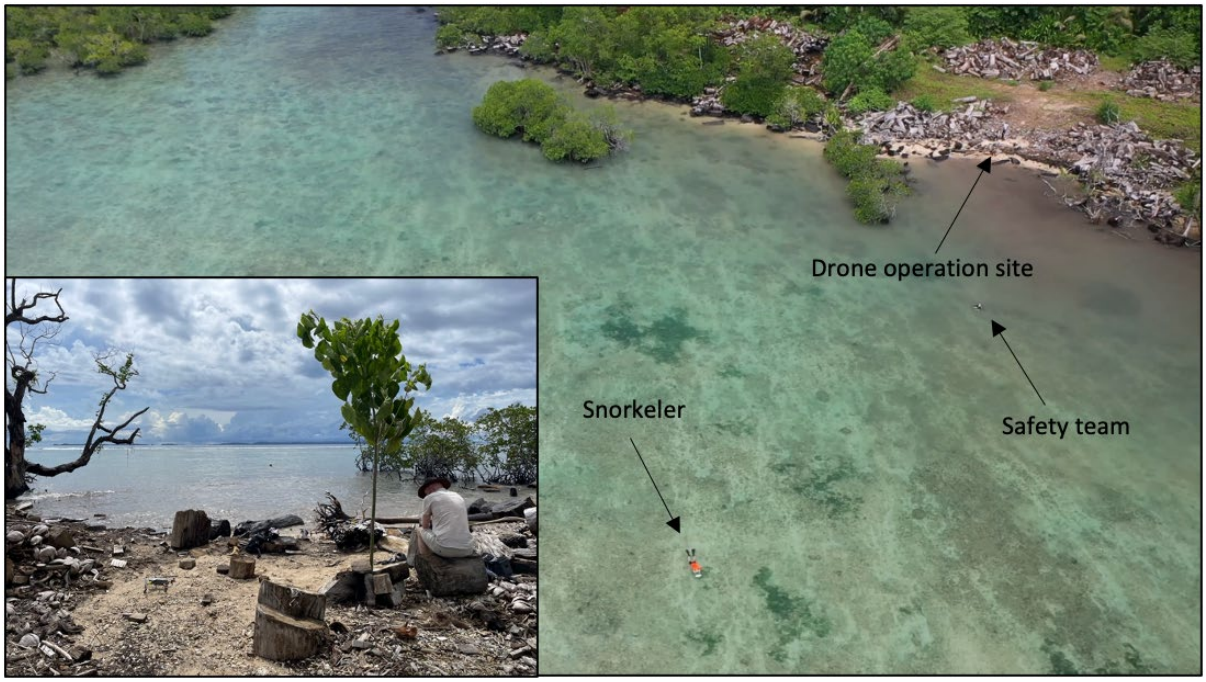

Figure 10. UAV image of the drone operation site on the north reef. The photo inserted in the bottom left corner shows the pilot's point of view from the drone operation site.

2.2 Software

- UgCS – used by Hinchliffe to create the flight routes for all photo surveys. The flights were flown using UgCS on a laptop that communicated via a wifi hotspot provided by the Samsung Galaxy Active3 Tab, to the tablet that was running the UgCS for DJI app. The DJI Mavic controller was connected to the tablet via a USB port.
- Desktop Esri ArcGIS Pro 2.5.0 - an adaptable software used for most of the data processing and analysis. The data analysis in ArcGIS Pro used the WGS 1984 UTM Zone 57S coordinate system and the World Imagery internal base map.
- FFMPEG - a free and open-access software used to convert GoPro files into a lower resolution, colour-correct all GoPro footage, and extract all GoPro frames for substrate classifications.
- Agisoft Metashape – software used by Hinchliffe to create the photo orthomosaics across the north and south survey areas.
- Microsoft Excel (version 16.73) - used alongside ArcGIS Pro for a portion of the data analysis.

- ReefCloud.AI - an open-access platform that uses artificial intelligence (AI) to classify images of coral reefs and estimate the abundance of coral reef substrate types (QUT, 2023). ReefCloud.AI was used to classify the substrata and biota within a subset of 260 extracted GoPro frames.

2.3 Data processing

2.3.1 Data pre-processing

Data pre-processing was conducted by thesis supervisor Hinchliffe. Due to the large size of each drone and GoPro video file, each video was automatically split and saved into 3.5 GB segments during recording and assigned sequentially coded file names. To improve the speed of processing and rendering in the early stages, all drone and GoPro video data was converted into a lower resolution of 1080p (1920 x 1080 pixels) and a frame rate of 30 fps. This was done using two free, open-access software programs: HandBrake for all UAV files; and FFmpeg for all GoPro files. FFmpeg was also used to colour-correct all GoPro footage to account for the rapid attenuation of red wavelengths underwater and improve substrate classification accuracy. Once all video files had been converted into a lower resolution and colour-corrected, the video segments were stitched back together using MP4Joiner.

2.3.2 Drone telemetry

The following data processing was carried out in accordance with Whittaker (2022) and Hinchliffe (2022). All individual flight records (telemetry) were converted into Motion Imagery Standards Board (MISB) compliant telemetry data for Full Motion Video (FMV) processing. This was carried out following the procedure described by Hinchliffe (2022). Drone telemetry data is collected every $1/10^{th}$ of a second and stored as an encrypted .txt file during the flight, however, this data format is not compatible with multiplexing. Therefore, the .txt files for each flight had to be decrypted into readable .csv files. Following this, the decrypted .csv files were then run through a Python script supplied by Hinchliffe (2021) and transformed into a MISB-compatible format appropriate for multiplexing. To create accurate telemetry outputs, two variables needed to be determined within the script's code for each .csv file:

1. *Heading correction:* The drone's compass calibration at the start of each flight has a margin of error and a magnetic offset of approximately 3-5 degrees. The magnetic

offset can be larger depending on the compass calibration and local conditions during UAV initialization. These discrepancies need to be considered to improve the spatial accuracy of the telemetry data. The .csv flight telemetry was imported into ArcGIS Pro as a standalone table. The direction of the flight path was then visualized by plotting the X and Y coordinates as point data and symbolised with directional triangles. A representative data point was then selected along a straight flight path and the relative craft heading was found in the attribute table. This craft heading could then be compared to the bearing measured using the measurement tool in ArcGIS, by drawing a straight line through the corresponding flight path data points. An error in the drone's compass calibration was evident if the bearing from the ArcGIS measurement tool differed from the flight data bearing. The 'heading correction' was entered into the script as the positive or negative difference between them.

2. *GPS offset:* The base altitude reading in the drone telemetry required adjustments to enhance spatial accuracy due to the elevated take-off height of the drone. Depending on the location of the drone take off, the take-off height was approximated by Hinchliffe for each flight and ranged between 0.4m - 1.5m. The resulting value was then entered into the 'GPS offset' variable within the Python script to account for the take-off elevation, thus providing a more accurate elevation reading from sea level. Once the appropriate heading correction and GPS offset variables were determined (Table 2), the Python script was executed for each flight individually.

Table 4. Flight Telemetry variables: Heading corrections and GPS offsets used as inputs per flight in the Python script provided by Hinchliffe (2021).

Site and Flight number	**Heading Correction**	**GPS Offset**
5th South: Flight 4	2°	1m
5th South: Flight 5	1°	1m
6th North: Flight 5	0°	0.5m
6th North: Flight 6	0°	0.5m
6th North: Flight 7	9°	0.5m

7th South: Flight 3	3°	0.6m
7th South: Flight 4	3°	0.6m
7th South: Flight 5	0°	0.6m
8th North: Flight 1	2°	0.4m
8th North: Flight 2	3°	0.4m
9th North: Flight 1	0°	0.4m
9th North: Flight 2	2°	0.4m
14th South: Flight 1	0°	1.5m
14th South: Flight 2	0°	1.5m

Occasionally, more than one video was taken throughout a drone flight, which meant the telemetry associated with multiple video files were within one telemetry file. Therefore, the flight telemetry file for that flight had to be cut and edited to eliminate the data from the previous video within the same flight. This would ensure that each drone video file corresponded to the correct segment of the telemetry file. The beginning of each video file was found by identifying gaps within the UNIX timestamps in the flight telemetry. Once the gap was found, the preceding video telemetry data was removed from the entire flight telemetry and saved as a new telemetry file specific to that video (Hinchliffe, 2022).

2.3.3 Multiplexing

The MISB-compliant telemetry data was then multiplexed with its associated drone video to produce an FMV-compliant video file (Figure 11). An ArcGIS Pro multiplexing toolbox model, provided by Hinchliffe (2022), was used to embed the output telemetry data into the associated drone video. The process involved several steps. Firstly, an elevation raster was generated using the create constant raster tool in ArcGIS. The raster had a value of 0, a cell size of 1m, and an extent matching the survey area, which served as a baseline sea level reference. This elevation raster was incorporated into the map as an elevation source and input into the multiplexing model. A re-mapping file supplied by Hinchliffe (2022) was used as the second model input to rename the telemetry field headings produced by the Python script. The renamed headings conform to the official MISB standards, which were required for the model to interpret the data accurately (MISB, 2020). The last two model inputs included the drone video and the associated MISB flight telemetry file. The pre-configured

multiplexing model was then executed separately for each output telemetry file and its corresponding drone video, resulting in the generation of FMV-compliant drone video outputs with embedded spatial data.

To assess the accuracy of the multiplexing, the FMV video file was added to a map in ArcGIS Pro. The add graphics tool was used to plot random data points onto the drone video frame. The video was then played to determine whether there was a lag between the drone frame movements and the plotted points. If a lag was evident, this meant that there was a slight delay between the time that the drone video began recording, and when the telemetry data began recording. To account for this delay, the first UNIX timestamp in the associated telemetry file was edited to be approximately 0.7 seconds earlier. This was done by editing the .csv file in Notepad++. Once the first UNIX timestamp within the telemetry data had been edited, the multiplex model was run again using the adjusted telemetry file to further improve the spatial accuracy of the FMV video file.

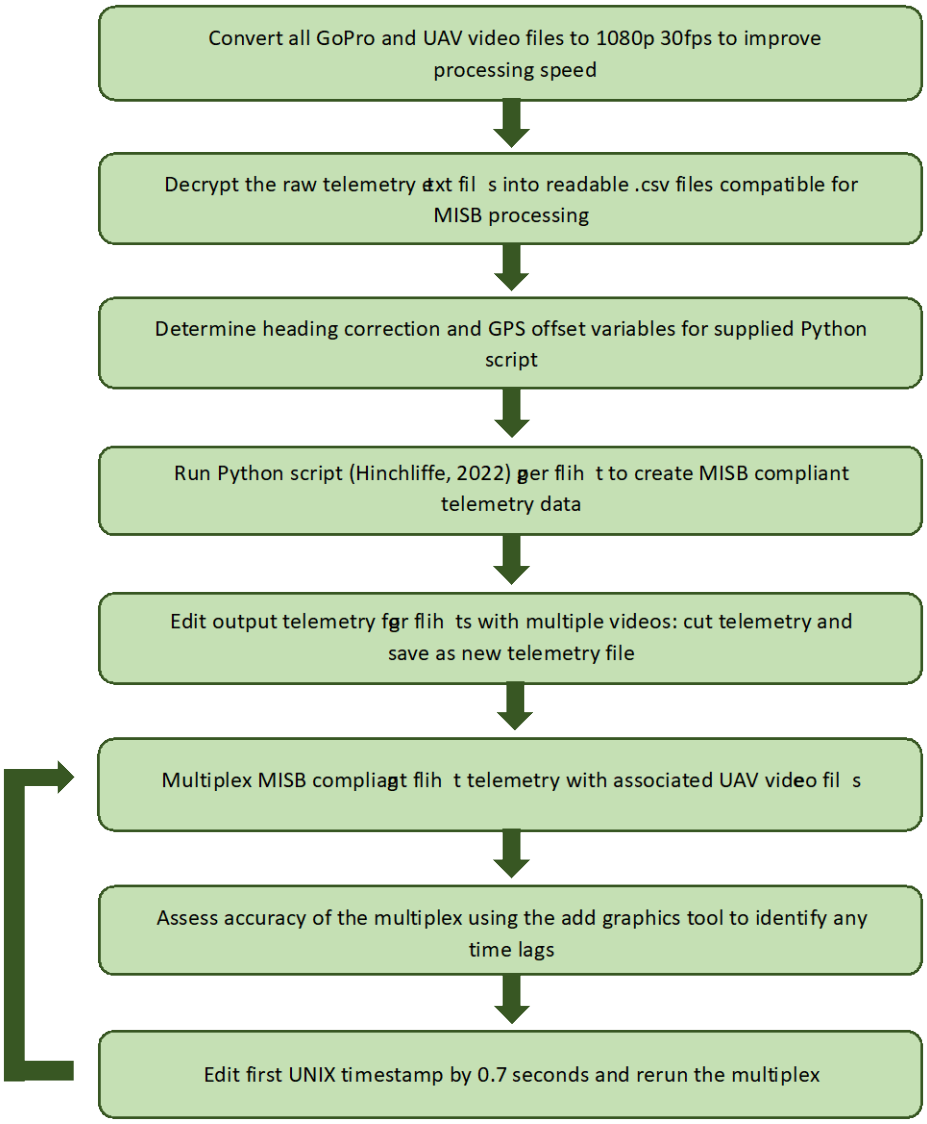

Figure 11. Flowchart displaying the steps to multiplex the data as per Hinchliffe (2022)

2.3.4 Georeferenced photo orthomosaics

High-resolution, georeferenced photo orthomosaics (.tif images) were created for the north and south reef survey locations. This was done using a total of 867 overlapping photos taken during UgCS-programmed flights on each side of the village and river. The photo orthomosaics were generated by Hinchliffe using the Agisoft Metashape software. Active wave areas within the input images were masked to produce clean wave-free mosaic raster files for the north and south reef flat. Two UgCS flights were taken across the south reef flat, therefore, two separate mosaics were created. The images collected during UgCS flights had a resolution of 2.5 cm providing a much higher resolution than background satellite imagery (Figure 12).

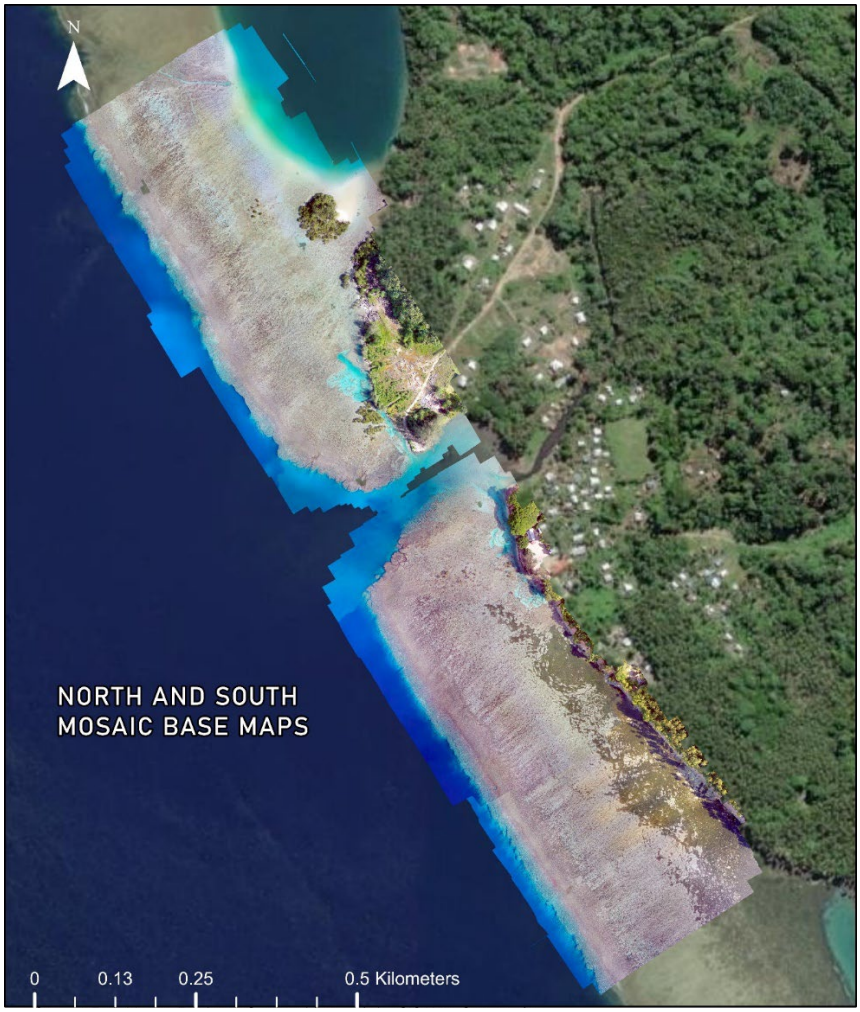

Figure 12. High-resolution, georeferenced photo orthomosaics of the reef flat on each side of the river at Vavanga village, generated from 867 UAV photos (background satellite imagery from Esri, Maxar, Earthstar Geographics, and the GIS User Community).

2.4 Geospatial and statistical analyses

2.4.1 Georeferencing snorkeler video transects from UAV FMV

The position of the snorkeler, scooter, and underwater video cameras along transects were digitised using the ArcGIS Pro FMV Image Analyst extension. The add graphics tool in the FMV player was used to plot points along the snorkeler path, while the FMV played out. Each point was placed on the scooter approximately 2m apart (Figure 13). As each point was plotted in the FMV player, the points simultaneously appeared on the map in the correct location. Once the entire transect had been plotted, the points were saved to the map as a

feature layer using the save graphics tool. Each point in the feature layer was assigned a unique MissionID in the attribute table. The MissionID signified the exact time in the drone video that the point was plotted on the map. These timestamps were essential for the extraction of associated GoPro frames along each transect. Following this, a geoprocessing model was run to add fields to the feature layer attribute table to be used for the substrate classifications. These included an image link and 10 substrate type and substrate proportion fields. This process was carried out for each FMV across the south reef flat.

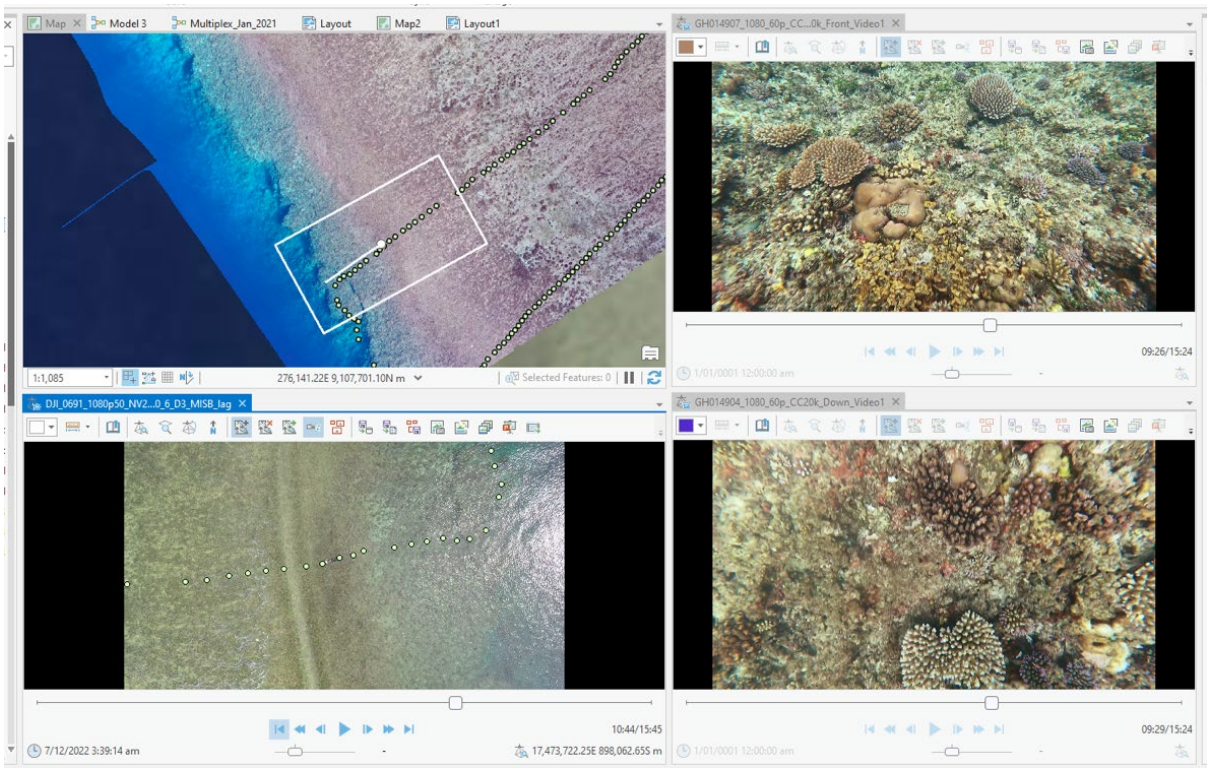

Figure 13. ArcGIS Pro display of synchronised FMV drone and spatially referenced underwater video. This allows features visible from the drone to be identified from underwater video recorded at the same location. Top left, the drone flight path across the photo orthomosaic, with the spatial perspective highlighted in the white rectangle. Plotted transect points are highlighted in yellow. Bottom left, drone video frame perspective with overlaid synchronised data points. Top right, synchronised georeferenced underwater image from forward facing GoPro camera. Bottom right, synchronised georeferenced underwater image from downward facing GoPro video camera.

2.4.2 Extraction of still images from underwater GoPro video frames

Still images of underwater substrata and biota were extracted from the GoPro video frames that aligned with the georeferenced points along the transect. Synchronisation points in the UAV and GoPro videos were identified. The UAV and underwater GoPro videos were played together to identify the points where the snorkeler signals to start and end the transects. In most instances, the syncing action carried out by the snorkeler was a hand swipe in front of the GoPro cameras. On occasions where the hand swipe was missed in the UAV video, the point at which the GoPro's were submerged into the water was used as the sync point. An Excel spreadsheet created by Hinchliffe was used to develop an FFMPEG script that would extract the associated GoPro frames from the video file (Figure 14). The script also applied a 10-point overlay to each GoPro frame to be used when classifying the substrate within the image. The 10-point overlay was designed to provide a systematic sample across the image while avoiding the edges which were more affected by visual distortion due to the GoPro lenses and underwater housing (Figure 15). This systematic approach allowed us to use a single template generated image that could be efficiently applied to each extracted GoPro frame. The Excel spreadsheet had a series of requirements to be fulfilled:

1. The first MissionID from the FMV flight telemetry
2. The MissionID's associated with each point in the transect feature layer
3. The offset (in seconds) between the GoPro and UAV sync points
4. The folder location of the 10-point overlay
5. The folder location of the GoPro Video
6. The output folder location for the extracted GoPro frames

			Remember to have the \				
GH014904_1080_60p_CC20k_Down_Video1		Infolder\	F:\FMV_Trial_1\Solomons_Trial\GoPro\				
3	seconds	Outfolder\	F:\FMV_Trial_1\Solomons_Trial\GoPro\Output-captures_7th_1\				
2	seconds before each frame	Prefix	Down				
0	seconds after each frame						Offsets (convert to secs)
Leave these alone					First MissionID in Telem	16703837101280	-75
Seconds	Video start	Video stop	Step	MissionID	Elapsed Time in the UAV Video (sec)		Elapsed Time Down GoPro
72.5	70.5	72.5	1	16703838576180	147.5	2.458166667	72.5
75.4	73.4	75.4	2	16703838605260	150.4	2.506633333	75.4
78.0	76.0	78.0	3	16703838631250	153.0	2.54995	78.0
81.2	79.2	81.2	4	16703838663350	156.2	2.60345	81.2
83.6	81.6	83.6	5	16703838687230	158.6	2.64325	83.6
86.2	84.2	86.2	6	16703838713150	161.2	2.68645	86.2
95.4	93.4	95.4	7	16703838805300	170.4	2.840033333	95.4
102.4	100.4	102.4	8	16703838875650	177.4	2.957283333	102.4
105.1	103.1	105.1	9	16703838902710	180.1	3.002383333	105.1
107.3	105.3	107.3	10	16703838924440	182.3	3.0386	107.3
109.7	107.7	109.7	11	16703838948350	184.7	3.07845	109.7
111.8	109.8	111.8	12	16703838968980	186.8	3.112833333	111.8
115.0	113.0	115.0	13	16703839001060	190.0	3.1663	115.0
117.4	115.4	117.4	14	16703839024950	192.4	3.206116667	117.4
125.4	123.4	125.4	15	16703839104900	200.4	3.339366667	125.4
128.2	126.2	128.2	16	16703839132810	203.2	3.385883333	128.2
130.2	128.2	130.2	17	16703839153480	205.2	3.420333333	130.2
132.6	130.6	132.6	18	16703839177410	207.6	3.460216667	132.6
135.2	133.2	135.2	19	16703839203370	210.2	3.503483333	135.2

Figure 14. Screenshot of the FFMPEG script maker in Excel.

Code created by Hinchliffe used the MissionID's and the offset to identify the exact time in the GoPro video that each point was plotted along the transect. Once all requirements were fulfilled, the script was copied into a .txt file in Notepad. The .txt file was then converted into a .bat file and run. For each time point, the script extracted the original GoPro frame, the GoPro frame with the 10-point overlay, and a three-second video leading up to each frame (with the 10-point overlay) into the appointed folder location. The MissionID was included in the name of each saved output so that the images could be linked to their geolocated point within ArcGIS. This process was repeated for each transect along the south reef flat.

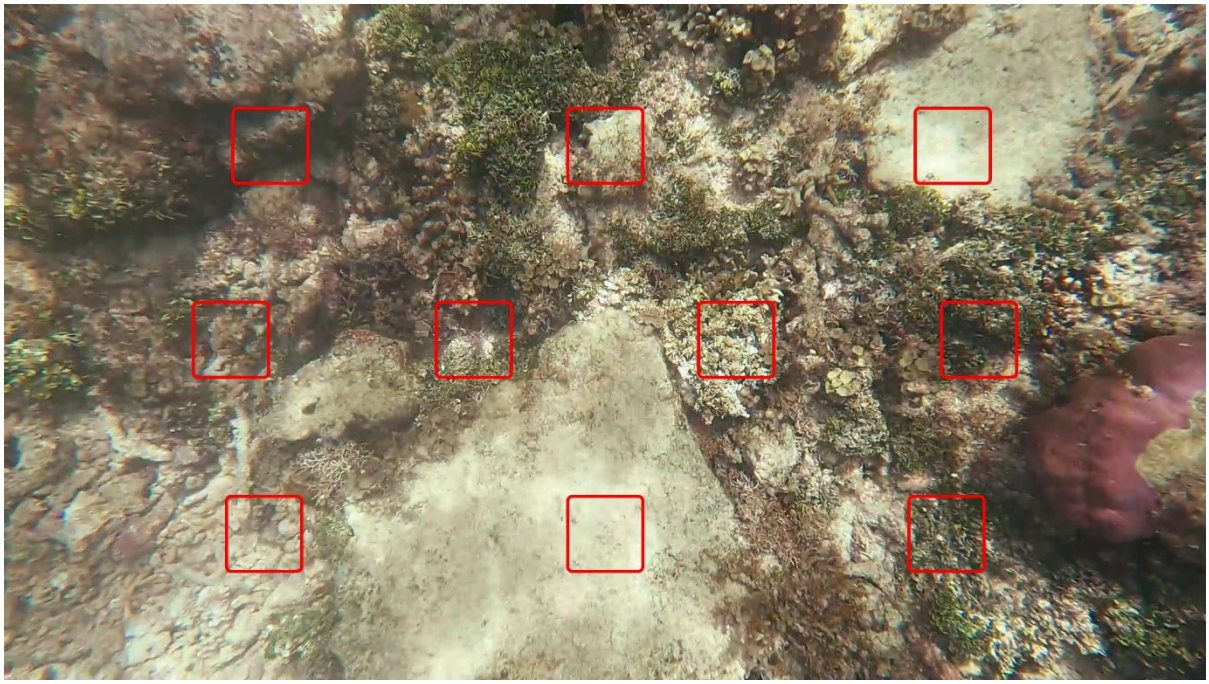

Figure 15. Example of extracted GoPro frame with 10-point overlay

2.4.3 Classification of reef flat substrata and biota

A hierarchical classification table of sessile reef macrofauna, algae, seagrass and substrata was created in Microsoft Excel by Breen based on previous Microsoft Access applications and similar to codes and groups used by the Australian Institute of Marine Science Great Barrier Reef Long Term Monitoring Program (Emslie et al., 2020; English et al., 1998). The reduced version included 192 taxonomic groups and classes of substratum specifically selected for species and habitats most frequently observed at the study sites. To allow results to be summarised across a range of taxonomic scales, codes were grouped by additional data fields including genus, family, order, phyla, morphology, common name, substrata, live or recently dead, and reliability of identification. Each taxonomic group was assigned a unique ID number. This classification table was used to create a drop-down classification domain in ArcGIS Pro. The domain required each class to have a unique code and description. The domain was first created in an Excel sheet, where the code field was populated with the unique ID number and the description field was populated with the species code and name. The table to domain tool was then used to import the Excel table into ArcGIS Pro as a domain.

GoPro frames were linked to their corresponding point locations using the Image_Link field that was populated with the folder location of the GoPro frame. Using the Image_Link field as an input, the configure pop-ups tool was used to create an image pop up for each data point. This meant the related GoPro frame for each data point would appear when clicking on any point along a transect (Figure 16).

The biota or type of substrata visible under 10 systematically placed sample points overlaid on each underwater video frame was then determined. The author undertook training in substrate classification from Breen, with additional sources from Veron (1986), and Wallace (1999). Any ambiguous classifications were checked by Breen to ensure high-quality classification. Visual classification and recording of biota and substrata were carried out using the drop-down classification domain in ArcGIS Pro. Biota and substrata under ten points (for precision, the centre of each overlaid square) on still video frames were assigned a unique code at the species level (or genus if this was not possible). The sum of each substrate proportion field would equate to 10 (100% cover) per GoPro frame, except where the substrate below a point could not be identified because of motion blur, water depth, shade, or other image artefacts. These points were recorded as not visible and percentage cover estimates for any frames affected were adjusted accordingly.

This process was repeated for all data points on transects across and along the south reef flat area. The merge tool was used to merge the individual transect layers into a single dataset. The original hierarchical classification table attributes supplied by Breen was then linked to the species and substrata codes recorded from video frames at georeferenced points along all transects for the southern reef flat area. This allowed data to be displayed across multiple classification levels, by mapping the distributions of singular species, genera, family, or substrata type. The steps undertaken to achieve this were completed within AcrGIS Pro and Microsoft Excel and are summarised in Figure 17 and appendices.

The percentage cover of benthic biota and substrata at different taxonomic scales was mapped for each georeferenced still underwater video frame. For comparison, overall summary statistics (means and standard errors) were calculated for whole transects, the whole reef flat and reef crest, and across the entire southern reef survey area.

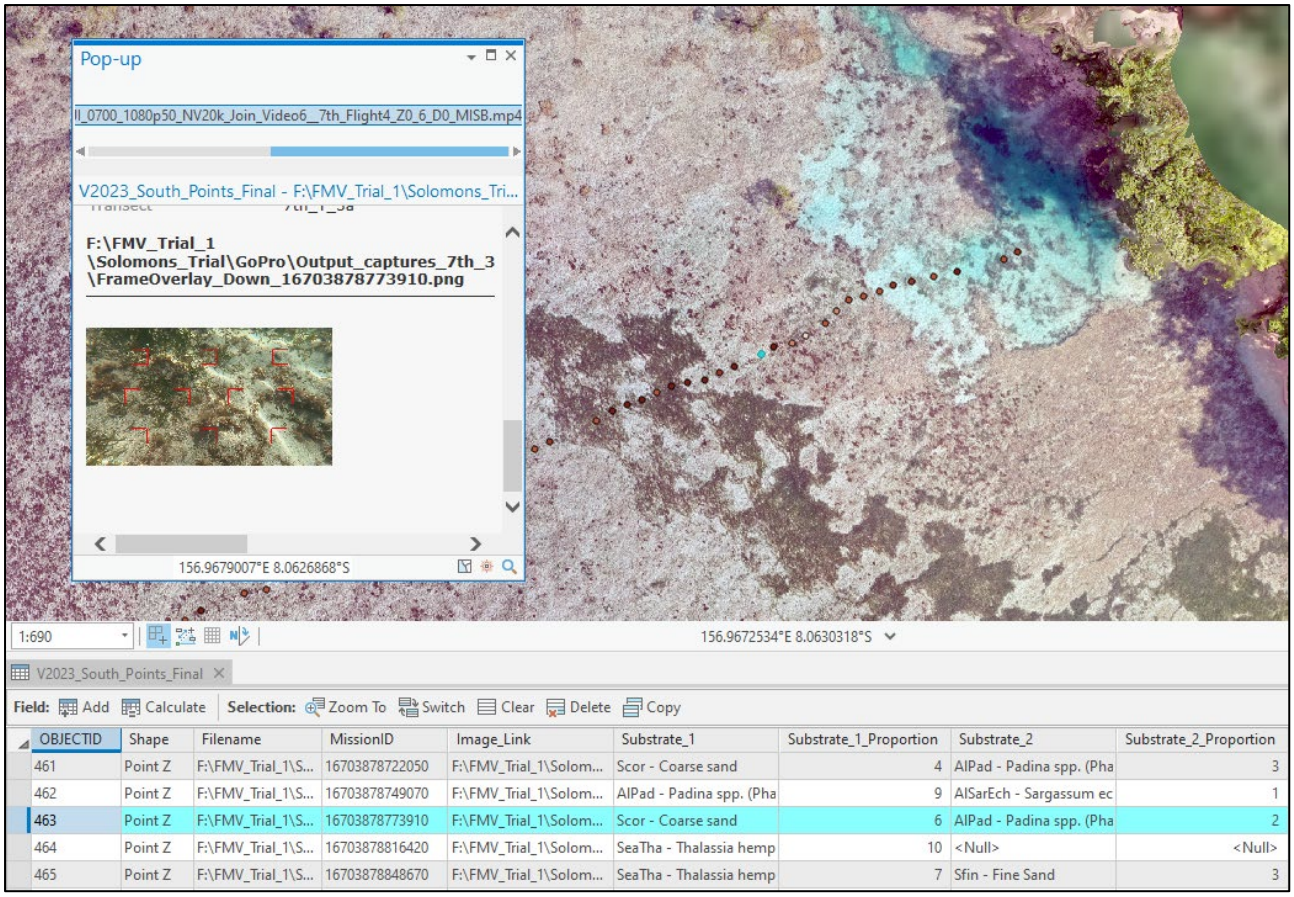

OBJECTID	Shape	Filename	MissionID	Image_Link	Substrate_1	Substrate_1_Proportion	Substrate_2	Substrate_2_Proportion
461	Point Z	F:\FMV_Trial_1\S...	16703878722050	F:\FMV_Trial_1\Solom...	Scor - Coarse sand	4	AlPad - Padina spp. (Pha	3
462	Point Z	F:\FMV_Trial_1\S...	16703878749070	F:\FMV_Trial_1\Solom...	AlPad - Padina spp. (Pha	9	AlSarEch - Sargassum ec	1
463	Point Z	F:\FMV_Trial_1\S...	16703878773910	F:\FMV_Trial_1\Solom...	Scor - Coarse sand	6	AlPad - Padina spp. (Pha	2
464	Point Z	F:\FMV_Trial_1\S...	16703878816420	F:\FMV_Trial_1\Solom...	SeaTha - Thalassia hemp	10	<Null>	<Null>
465	Point Z	F:\FMV_Trial_1\S...	16703878848670	F:\FMV_Trial_1\Solom...	SeaTha - Thalassia hemp	7	Sfin - Fine Sand	3

Figure 16. Example of an image pop-up for a random data point (highlighted in blue).

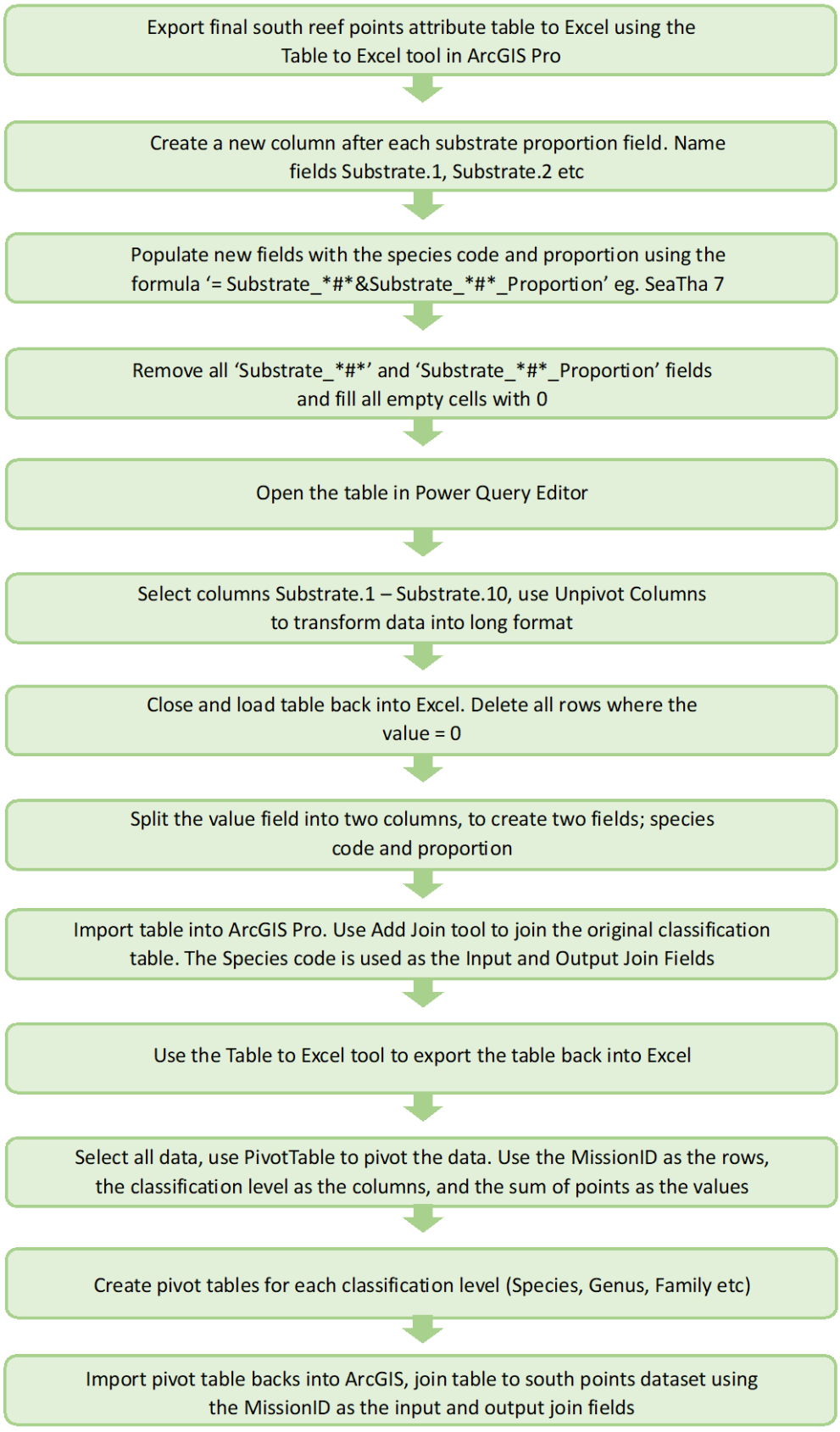

Figure 17. Flowchart describing the steps to join the taxonomic and substrata classification table to the georeferenced underwater video and percentage cover data in ArcGIS Pro.

2.4.4 Classification and regression tree zonation across the reef flat

Classification and regression trees (CART) identify and statistically test differences in one or more (MCART) dependent variables in response to categorical and/or continuous predictor variables (Kerrigan et al., 2010). They are useful in ecology as they use intuitive trees to partition the most variation in response variables that can be explained by different levels and combinations of the independent explanatory predictor variables and test the statistical significance of these splits (De'ath & Fabricius, 2000; Kerrigan et al., 2010). Permutation tests are used to test for statistical significance by cross-validating results with distributions generated by repeated random sub-sampling of the same data set or, as is the case here, by withholding part (40%) of the data set from the initial model building to cross-validate models produced from the remaining data set. These models are useful as they are distribution-free, handle missing values, detect complex interactions among variables, handle large data sets and can be used with multivariate species composition data (De'ath & Fabricius, 2000). If spatial explanatory variables (such as distance to reef crest, distance to river, x and y spatial coordinates) are used, results can be used to statistically predict and spatially interpolate species and substrata between sample points.

Exhaustive Chi-squared Automatic Interaction Detection (CHAID) decision trees in the statistical software SPSS (Statistical Package for the Social Sciences, version 29.01) were used to identify statistically different patterns in the percentage cover of benthic biota and substrata in relation to distance from the reef crest. The random forest classification and regression algorithm in ArcGIS Pro was also used for a similar purpose and provided similar results, so only the CHAID results are presented below.

2.4.5 Regressions of percentage cover on the reef flat and crest with distance from the river.

Data points along the snorkeler transects that ran across the reef flat were clipped to the extent of the shortest transect as low tides prevented the outer flat and crest from being accessed for some of the transects. These transects extended to the start of the shallow outer reef flat, inshore of the reef crest. The mean percentage cover of the most abundant biota and substrata for each reef flat and reef crest transect were graphed as a function of distance to river and regression models fitted using the statistical software Kyplot (version 6, 1997-2020, Kyens Lab Inc.).

2.4.6 Automated underwater image classification with ReefCloud.AI

In addition to a trained observer classifying underwater images, the ReefCloud.AI deep learning software (AIMS, 2022) was used to classify basic biota and substrata on still video frames of reef flat on a sample transect from the total dataset. The first transect taken on the 7th of December was chosen for this analysis, which included 260 images. To set up the project in ReefCloud, there were several required specifications, including a project name, project code, description, location, sampling protocol, data collection method, and field of view estimation (Table 3). To set up the AI model, a label set and the number and distribution of points were chosen to determine how the information would be extracted from the images. To compare the AI classifications against the manual classifications completed in the previous analysis section, the classification domain was used as the label set. The classification domain was imported into the project as a .csv file that included a code (species code), description (species name), and functional group (substrate type). The 12-point grid overlay was chosen and replaced with our 10-point overlay during the bulk upload process.

Site creation required a site name, position, reef name, reef zone, reef type, exposure level, depth, country, and country region (Table 4). To position the sample points in the same position as the 10-point overlay, ReefCloud provides a 'Bulk Import' option when uploading the survey images. The bulk import required two Excel files. The first file contains the survey information, which includes the survey location, start date and time, survey collection method, and survey image directory (the name of the folder containing the images to upload into ReefCloud.AI) (Table 5). The second file contained the point information, which included the point image path, point x coordinate, point y coordinate, and point annotation. Microsoft Paint was used to determine the x and y coordinates of the 10-point overlay. The point image path applied each point to a specified image within its folder location. The optional point annotation field was populated using the substrate classifications determined from earlier analysis.

Table 5. Project specifications.

Project name	Solomon_Islands_Vavanga_5.0
Project code	Ps6516g3l9hza
Description	Substrate classification on the Vavanga south reef flat
Location	Solomon Islands
Sampling protocol	Geo-referenced transects
Data collection method	Snorkel
Field of view	50-100cm

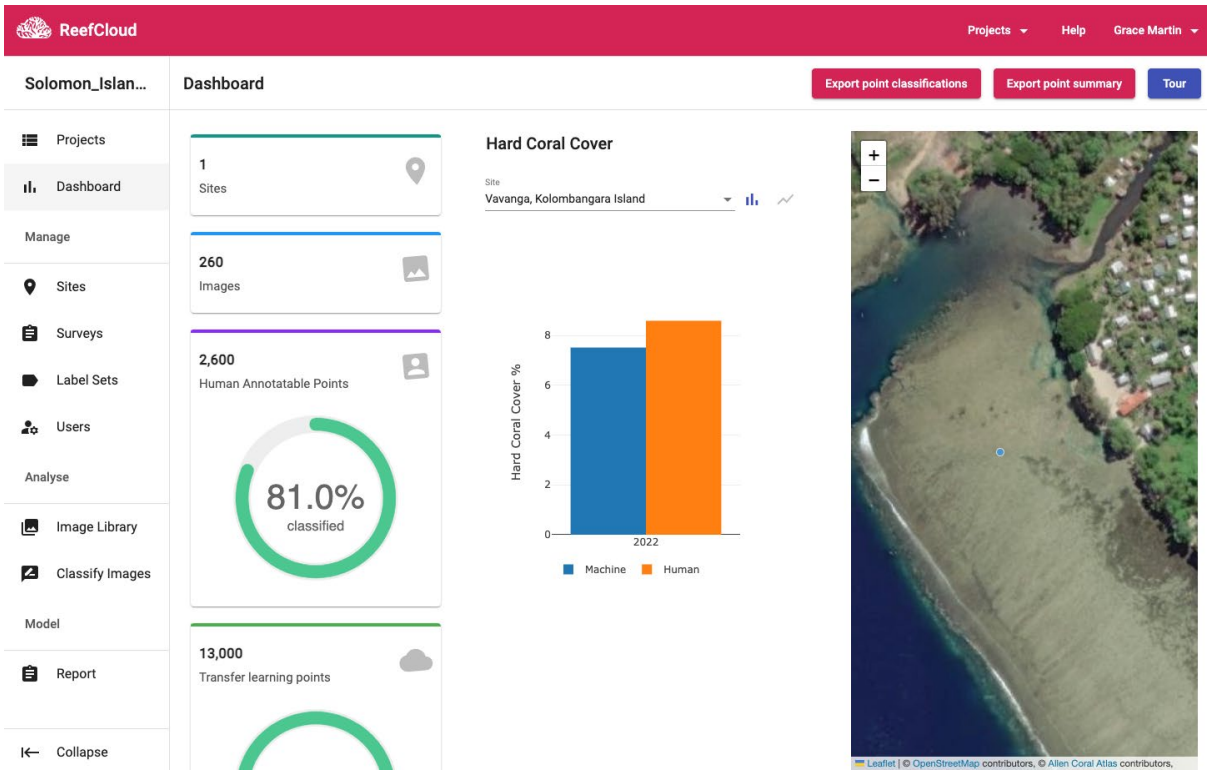

Figure 18. Screenshot of the ReefCloud.AI dashboard.

Table 6. ReefCloud.AI site specifications.

Site Name	Vavanga, Kolombangara Island
Position	-8.062576, -156.967356
Reef Name	Vavanga south reef
Reef Zone	Back reef
Reef Type	Fringing
Exposure Level	Semi-exposed
Depth	1.5m
Country	Solomon Islands
Country Region	Western Province

Table 7. Excel sheet survey specifications.

Survey Site	Vavanga, Kolombangara Island
Start Date, Time	07/12/2022 1:30pm
Survey Collection Method	Snorkel
Survey Image Directory	7th_transect_1_ReefCloud
Transect Number	1
Depth	1.5

To reduce manual classification time within ReefCloud.AI, 50% of the images were uploaded with their point annotations. Once the images had been uploaded into ReefCloud, another 30% of the images were manually classified using the classification domain label set. Each point had an associated human classification and machine classification. As the points were annotated, the AI would continue to improve its algorithm, and began to predict the substrate types in the remaining images automatically. The last remaining 20% of images were left without human classifications, so that they could be used to conduct an accuracy assessment.

To assess the accuracy of the ReefCloud.AI classifications the compute confusion matrix tool in ArcGIS Pro was used to compare the machine classifications to the human classifications found in the original dataset. The accuracy assessment was conducted for the last 20% of images that had not been manually classified within ReefCloud. Another accuracy assessment was then performed across the whole ReefCloud dataset. The confusion matrices produced an overall accuracy, and user's and producer's accuracies for each substrate class. The confusion matrices assessed the accuracy of the machine classifications at a species and main substrate type classification level. The specific steps undertaken to produce the confusion matrices are provided in the appendices.

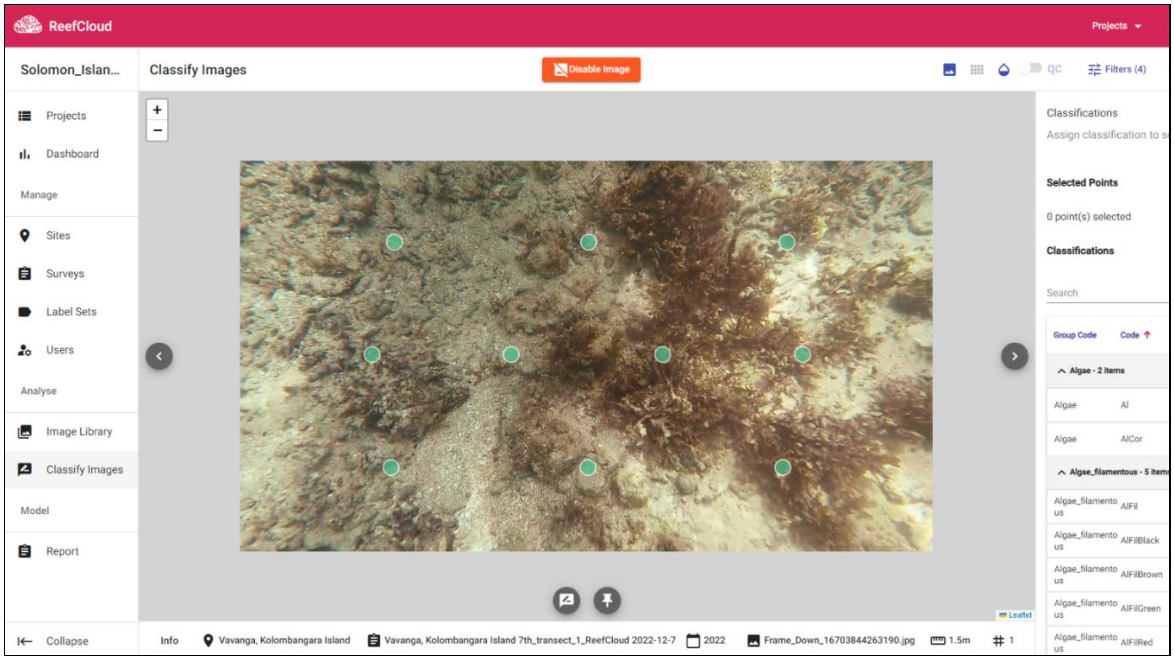

Figure 19. Screenshot of the ReefCloud image classification interface. The image to be classified is seen in the middle, with the label set in the bottom right corner.

2.4.7 Object-based image analysis of the aerial drone photo orthomosaic

An object-based image analysis (OBIA) was run on a sample of the georeferenced drone photo orthomosaic from the southern reef flat. It included a representative sample of habitat types from seagrass meadows to the coral-dominant reef crest. A subsection of the south reef flat photo orthomosaic that included two transect lines was clipped out using the ArcGIS Pro clip raster tool. The segment mean shift tool was then used to divide the clipped mosaic into segments based on a segmentation algorithm that groups pixels together based on spectral and spatial characteristics. The tool had three parameters: segment size (minimum number of pixels per segment), spectral detail (colour characteristics) and spatial detail. An iterative process was carried out to produce an output that best identified visible reef features, by visually assessing the results, adjusting the three parameters, and re-running the segmentation. The final output was created using a minimum segment size of 300 (2.5 cm pixel size), spectral detail of 17, and spatial detail of 18.

The training samples manager in ArcGIS Pro was used to create a classification schema and collect training samples. These samples were used to train the classifier to assign polygons within the segmented raster to a specific class. Class categories were created in the classification schema including dense seagrass, sparse seagrass, macroalgae, sand/algal mix, coral rock/algal mix, and coral rock/hard coral mix. These classes were chosen based on what was visible to the naked eye within the photo orthomosaic. To collect random training samples, 300 random points were plotted across the segmented raster. The segment under each point was then used as a training sample. The class for each segment was determined using visual assessments of the photo orthomosaic, field knowledge, and validated through the overlaid georeferenced underwater images.

To ensure the training samples could be validated through accurately positioned ground control points, the positional accuracy of the digitized transect points was determined using a subset of 38 points along the transects that intersected the clipped raster. In the FMV player, the frame snapshot tool was used to extract drone video frames along the transect

path. The frames were then inserted into the map as raster files, and georeferenced using the photo orthomosaic as a reference. New points were then plotted directly above the underwater scooter visible in the extracted frames. The distance and bearing were then determined between the original transect points and the newly plotted points using the measurement tool. The average distance and bearing were then determined across the 38 points. The newly plotted points with high positional accuracy were used to help train and validate the classification.

The supervised Support Vector Machine (SVM) classifier was chosen to classify the segmented raster as it is well suited for segmented raster inputs and is less susceptible to noise and an unbalanced number of training samples within each class (Esri, n.d.). To evaluate the accuracy of the classification, the compute confusion matrix tool was used to compare the reference data to the image classification data. The confusion matrix was used to calculate the associated accuracy statistics, which included the overall accuracy, and user's and producer's accuracies for each class. To create the confusion matrix, all training sample polygons were first removed from the segmented image. Following this, 500 stratified random points were distributed across the image using the create accuracy assessment points tool. Each point was assigned class values for the 'classified' field, while the 'ground truth' field remained empty. The ground truth field for each point was manually populated using a visual assessment of the reference data (the high-resolution photo orthomosaic and field survey data), and expert field knowledge. The compute confusion matrix tool was then used to compute an error matrix, using the accuracy assessment points as the input.

3 Results

3.1 Location of drone flight paths and snorkel transects

A total of 14 drone flights were taken across the north and south reef flats between the 5th – 14th of December 2022. FMV processing was only undertaken on the south reef footage (7 drone flights) due to time constraints. However, georeferenced drone photo orthomosaics with a resolution of 2.5 cm for the north and south reef flat survey locations were generated from hundreds of photos taken on automated UgCS flights. The resulting high-resolution images provide a far more detailed view of the reef and adjacent coast than the satellite imagery available in Esri's base maps visible at the southernmost section of the reef flat as seen in Figure 20.

Figure 20 illustrates the location of the three drone operation sites, as well as the flight paths taken while following the snorkeler for all transects undertaken across the north and south reef flat. Figure 21 maps the coordinates of the snorkeler and underwater video along transects across the southern reef flat, as determined from the FMV processing.

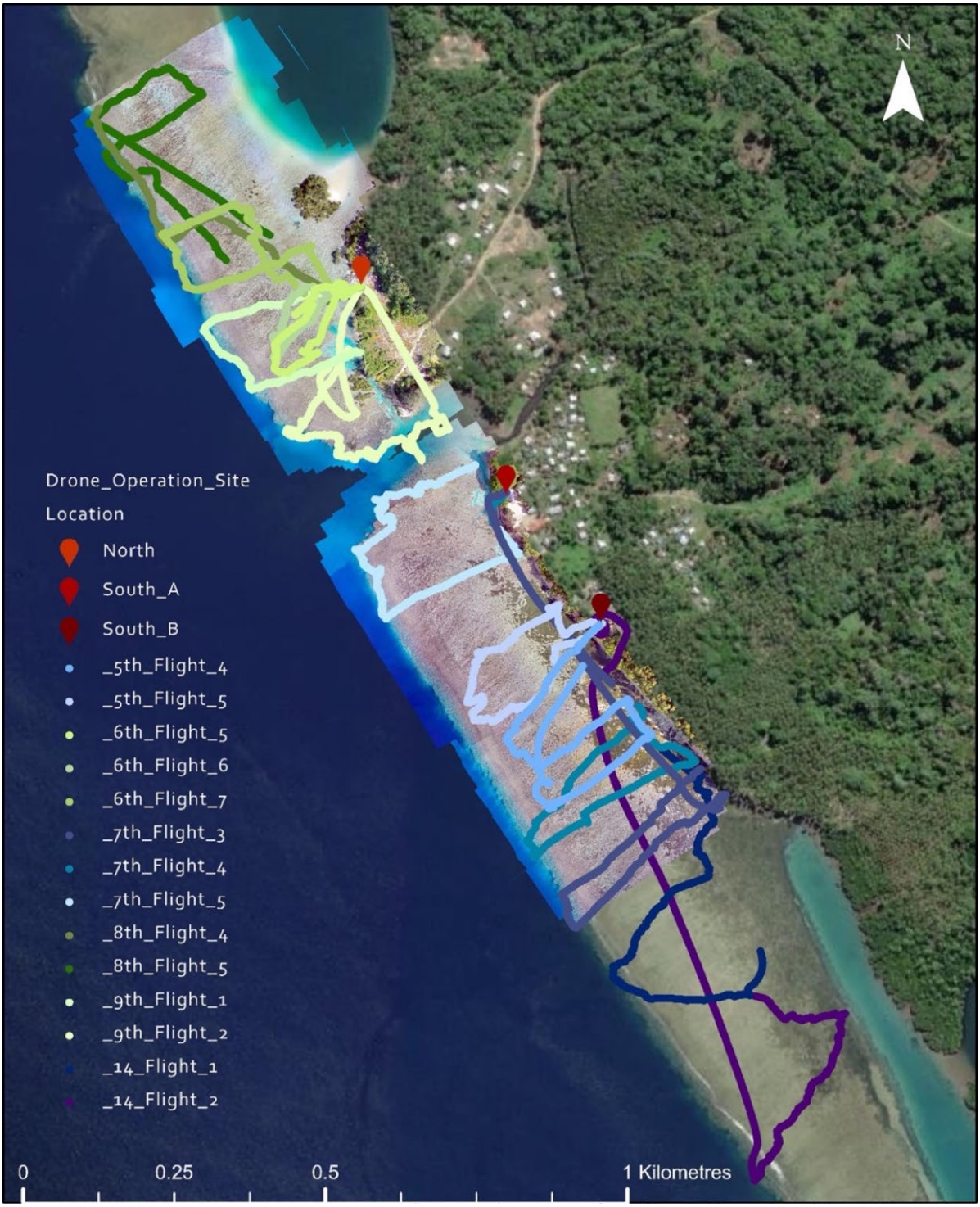

Figure 20. Drone flight paths between the 5th to 14th of December, following the snorkeler and scooter across the north and south reef flats (Additional data sources: Esri, Maxar, Earthstar Geographics, and the GIS User Community).

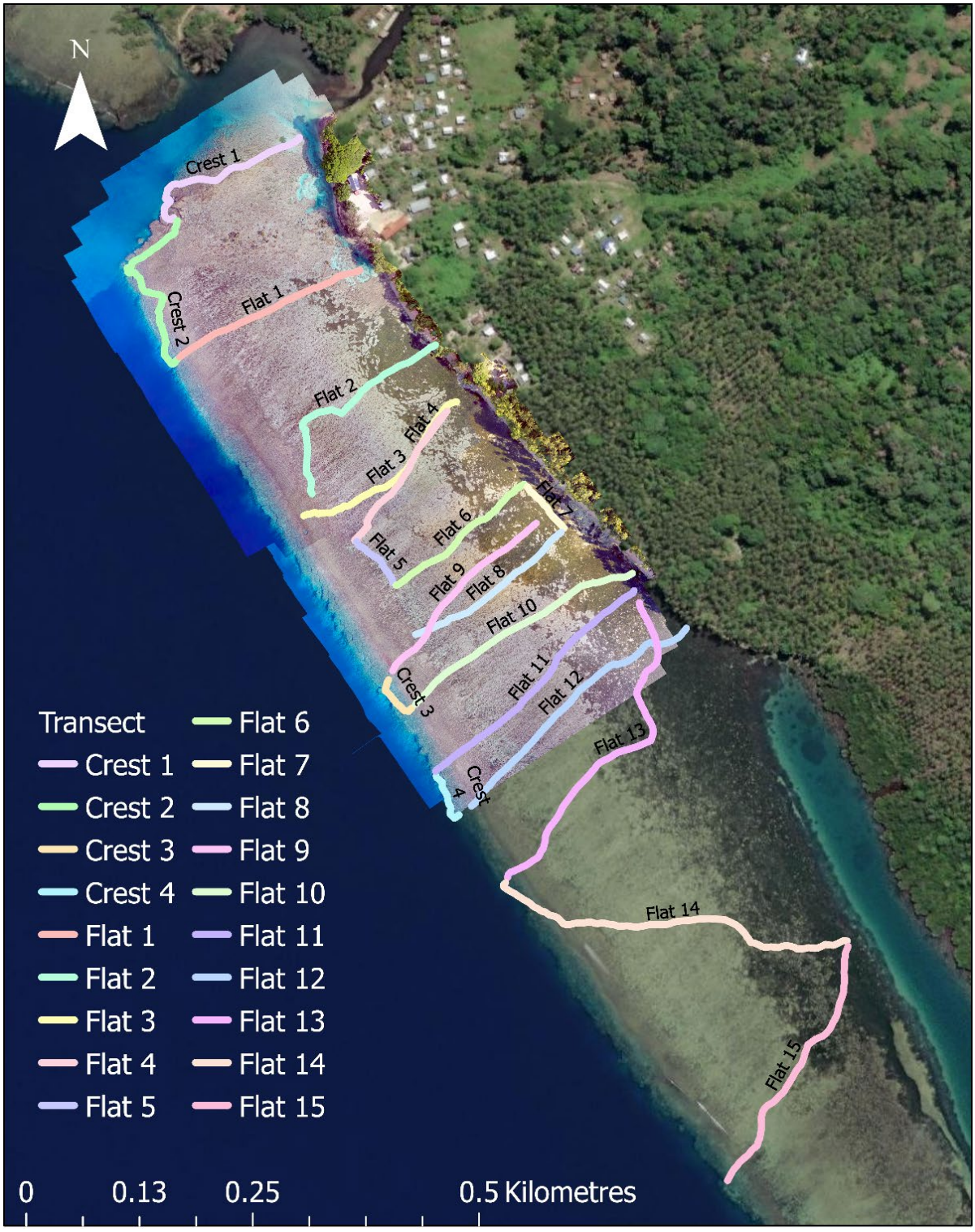

Figure 21. Snorkeler transect paths from 5th – 14th of December across the south reef flat. (Additional data sources: Esri, Maxar, Earthstar Geographics, and the GIS User Community).

3.2 Fine scale spatial distribution maps of reef flat biota and substrata

Figure 22 to Figure 24 map the spatial distributions of point estimates of percentage cover from individual georeferenced underwater video frames on transects for three examples of benthic biota on the southern reef flat. These include the seagrass species *Thalassia hemprichii* (Figure 22), the macroalgae species *Sargassum echinocarpum* (Figure 23) and hard coral (Figure 24). Similar maps for other biota and substrata including coral rock, coral rubble, *Acropora* and the macroalgae *Padina* can be seen in Appendix.

Figure 25 shows the composition of the most abundant categories of biota and substrata identified in each extracted GoPro frame from the reef crest to the shore across the southern reef flat. Each data point is represented by a stacked bar graph, with the proportion of colour representing the percentage cover of the most abundant categories of biota or substrata. Figure 26 displays a more detailed visual of the stacked bar graph for transect 'Flat 11' from the 7th of December, 2023.

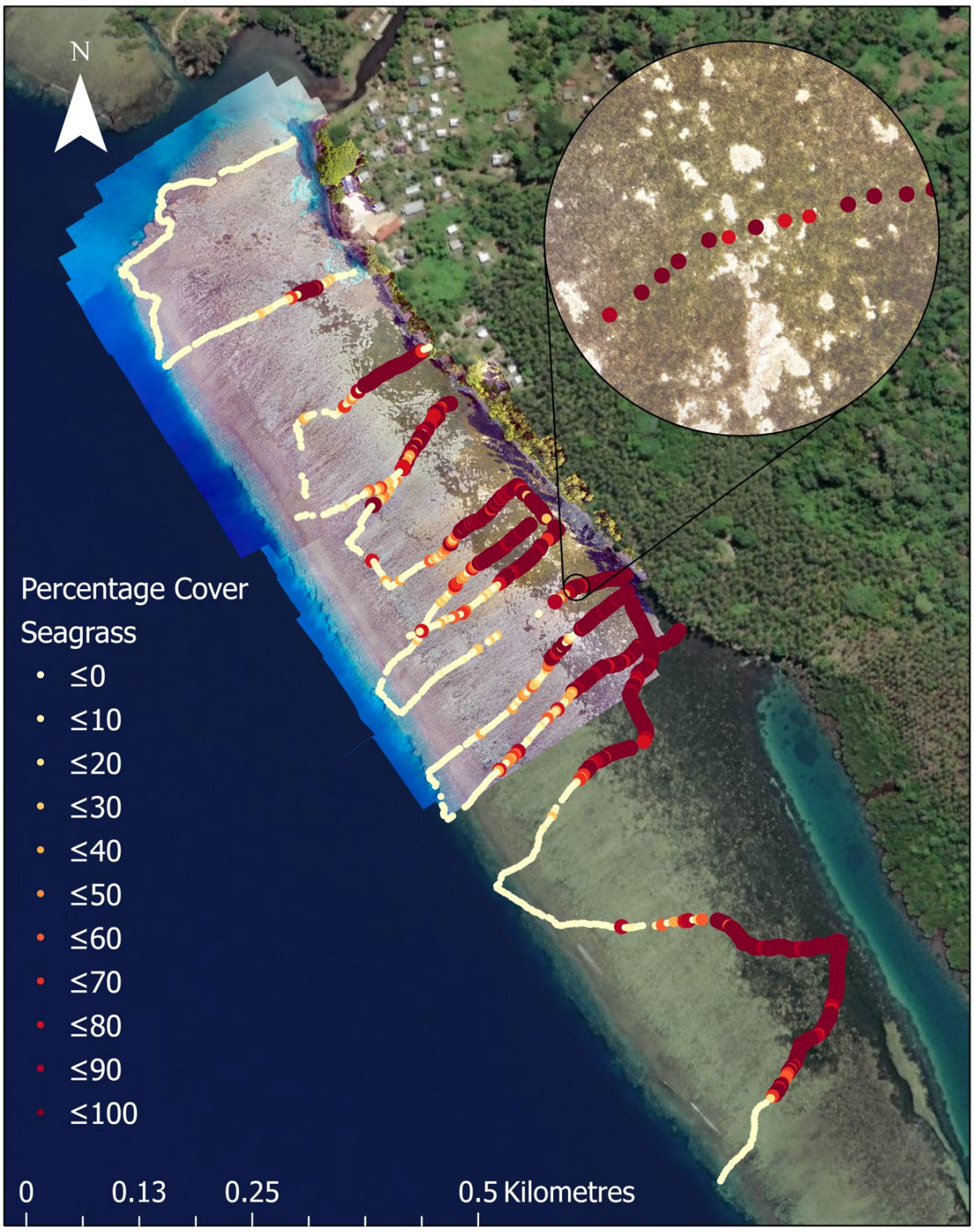

Figure 22. Distribution of the seagrass species *Thalassia hemprichii* across the southern reef. Percentage cover symbolized by colour; dark red (≤100%) to light yellow (≤0%) (Additional data sources: Esri, Maxar, Earthstar Geographics, and the GIS User Community).

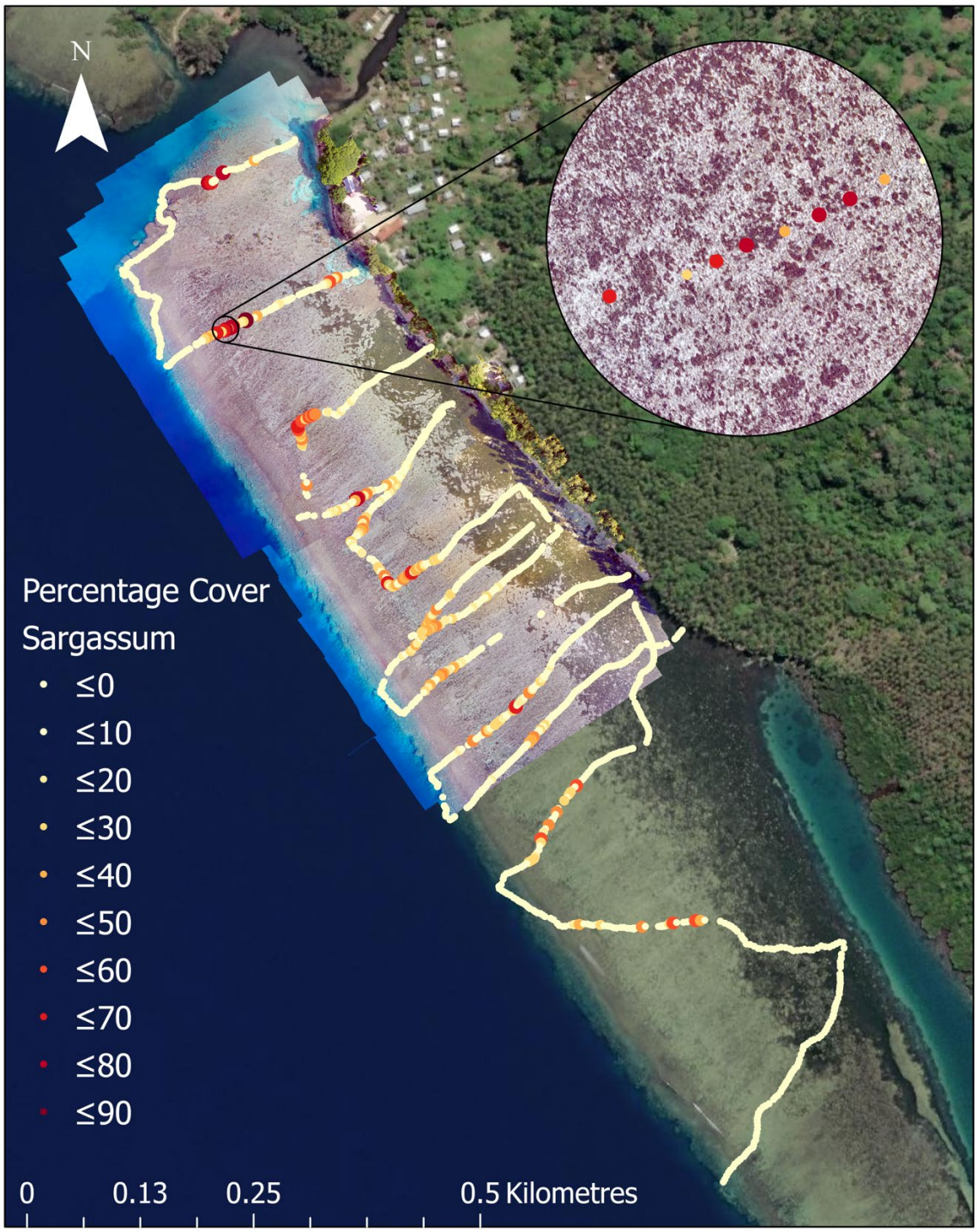

Figure 23. Distribution of the brown macroalgae species *Sargassum echinocarpum* across the south reef. Percentage cover symbolized by colour; dark red (≤90%) to light yellow (≤0%). (Additional data sources: Esri, Maxar, Earthstar Geographics, and the GIS User Community).

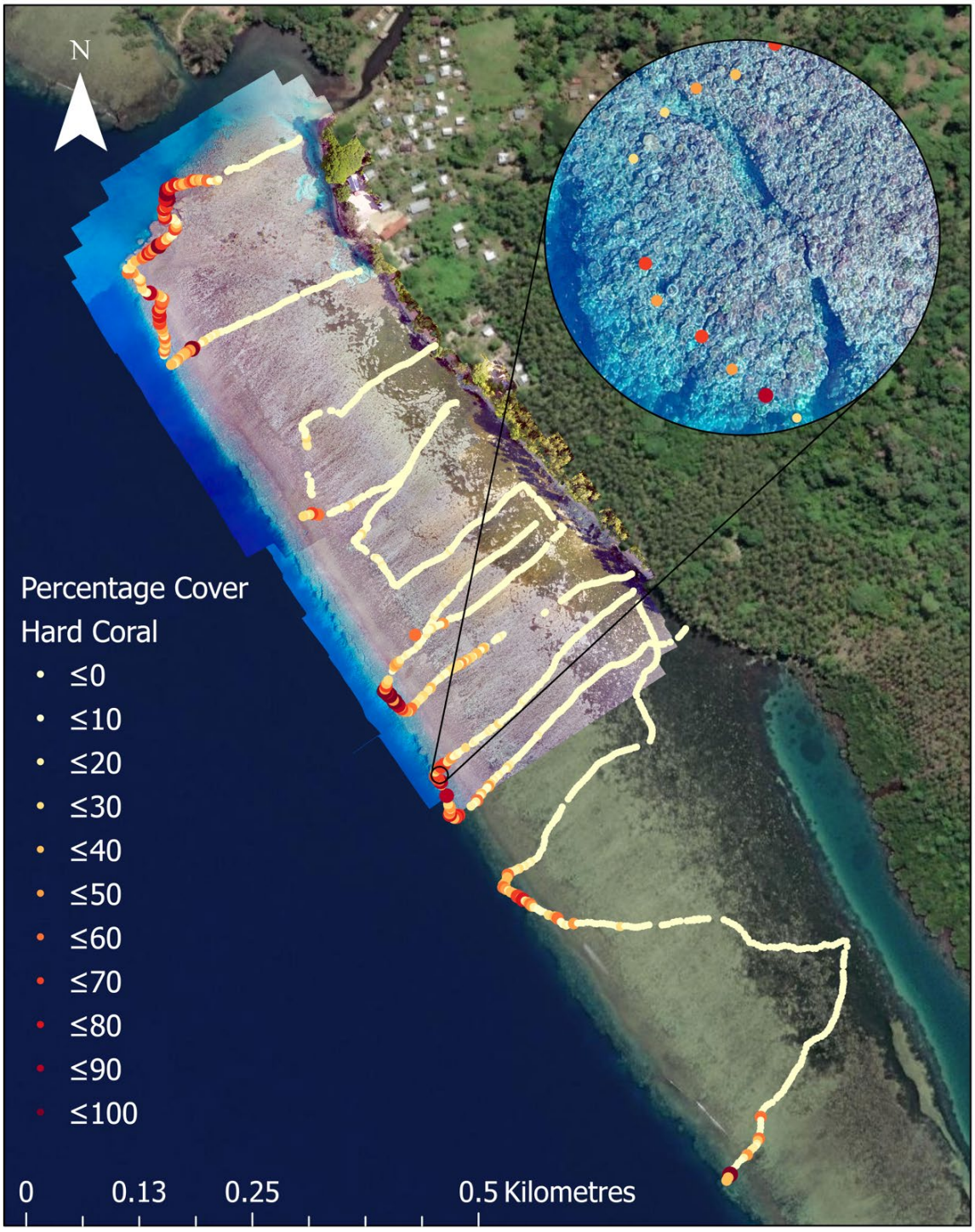

Figure 24. Distribution of hard coral across the south reef. Percentage cover symbolized by colour; dark red (≤100%) to light yellow (≤0%). (Additional data sources: Esri, Maxar, Earthstar Geographics, and the GIS User Community).

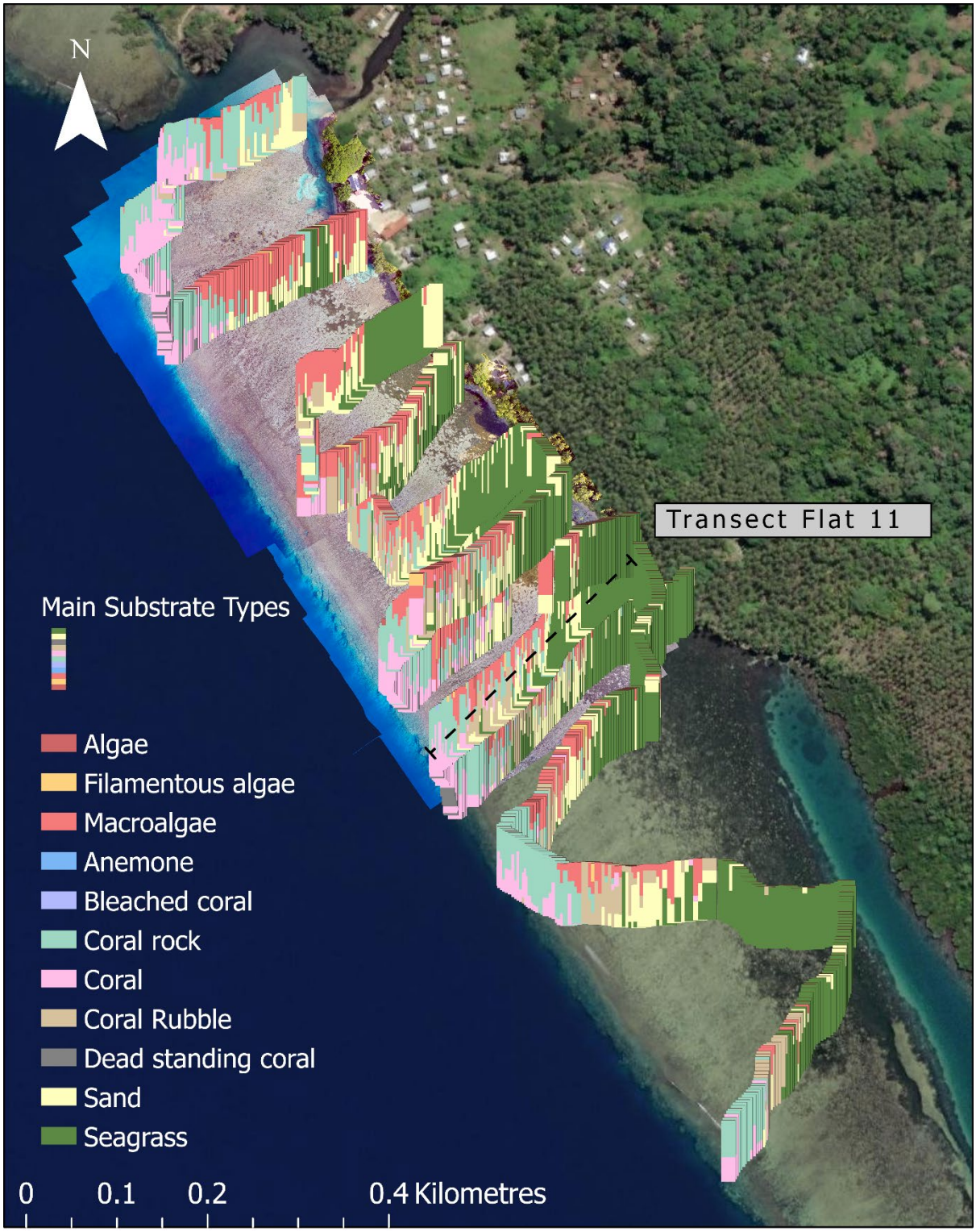

Figure 25. Map displaying the composition of main substrate types at each GoPro frame location, represented as stacked bar graphs approximately 2m apart. The proportion of each colour corresponds to the percentage cover of each substrate type.

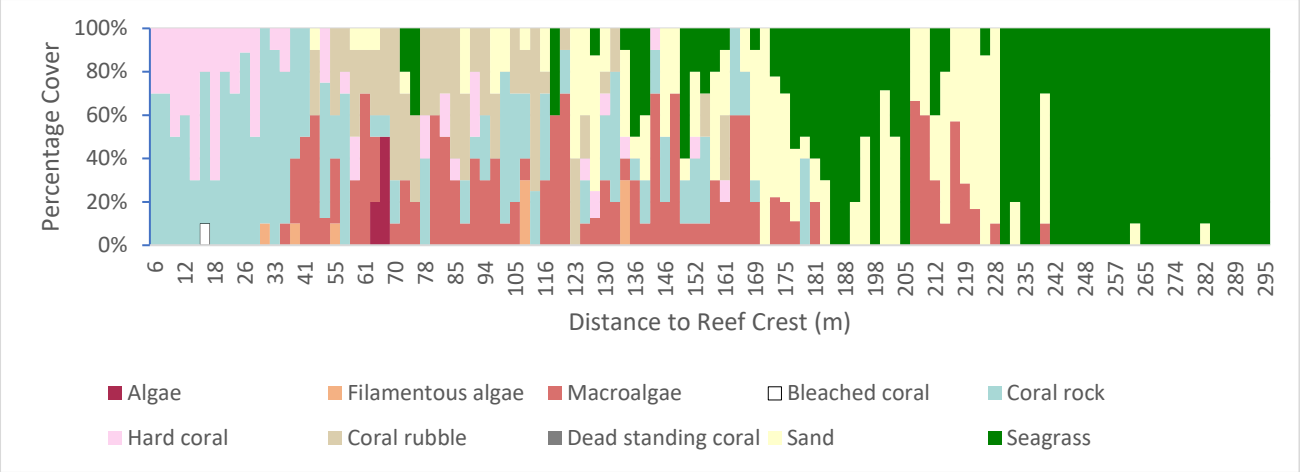

Figure 26. Relative proportions of most abundant biota and substrata estimated from georeferenced still video frames for transect Flat 11. Each bar represents the percentage cover of biota and substrata for a single GoPro image along the transect.

3.3 Summary statistics for percentage cover on the reef flat and reef crest

Statistics summarizing overall percentage cover for large areas of reef are frequently used in monitoring reef biota and substrata. Figure 27 and Table 7 summarise the overall mean percentage cover (+/- standard error) of the most abundant categories of benthic biota and substrata estimated from underwater videos across and along the reef flat and reef crest south of the river at Vavanga. Figure 28 and Table 8 display the overall mean percentage cover (+/- standard error) of the most abundant coral genera identified across the southern reef survey area.

Along the reef crest, hard coral (45.4% ± 8.0 SE) and coral rock (43.6% ± 3.8 SE) covered the most area with some macroalgae (3.7% ± 2.8 SE), sand (3.2% ± 3.1 SE), and coral rubble (1.3% ± 1.3 SE) (Figure 27).

The most abundant hard coral genera across the reef crest were *Acropora* (20.3% ± 8.0 SE), followed by *Pocillopora* (8.5% ± 2.4 SE), *Montipora* (5.6% ± 2.5 SE), *Porites* (6.0% ± 1.2 SE), and the family *Faviidae* (2.5% ± 1.3 SE) (Figure 28).

Seagrass (38.6% ± 4.3 SE) had the highest mean percentage cover across the reef flat, followed by macroalgae (17.1% ± 3.0 SE), sand (16.3% ± 1.8 SE), coral rock (12.0% ± 1.6 SE), coral rubble (10.1% ± 2.2) and hard coral (4.6% ± 0.7 SE) (Figure 27).

Macroalgae across the reef flat was predominantly composed of three brown macroalgae genera: *Padina* (6.9% ± 1.8 SE); *Sargassum* (6.7% ± 1.2 SE); and *Turbinaria* (2.0% ± 0.6); and one green macroalgae genus, *Halimeda* (1.6% ± 0.4 SE) (Figure 27).

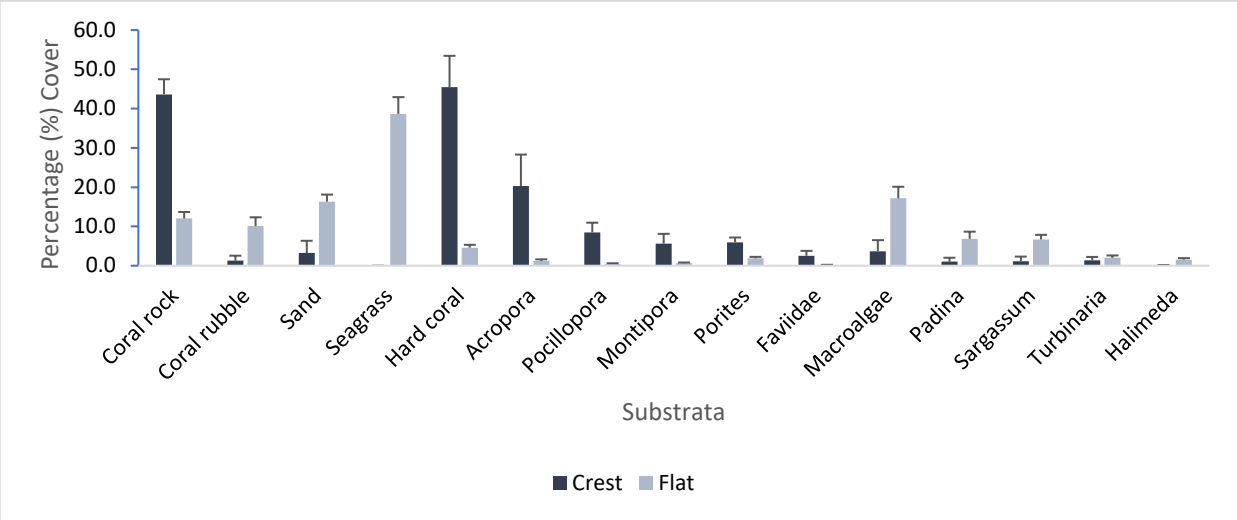

Figure 27. Mean percentage cover of common substrata and biota across the reef flat and reef crest.

Table 8. Mean percentage cover substrata and biota across the reef flat and reef crest

Substrata	**Reef crest**	**Reef flat**
Coral rock	43.6% ± 3.8 SE	12.0% ± 1.6 SE
Coral rubble	1.3% ± 1.3 SE	10.1% ± 2.2 SE
Sand	3.2% ± 3.1 SE	16.3% ± 1.8 SE
Seagrass	0.0% ± 0.0 SE	38.6% ±4.3 SE
Hard coral	45.4% ± 8.0 SE	4.6% ± 0.7 SE
Acropora	20.3% ± 8.0 SE	1.2% ± 0.4 SE

Pocillopora	8.5% ± 2.4 SE	0.4% ± 0.2 SE
Montipora	5.6% ± 2.5 SE	0.6% ± 0.2 SE
Porites	6.0% ± 1.2 SE	1.9% ± 0.4 SE
Faviidae	2.5% ± 1.3 SE	0.2% ± 0.0 SE
Macroalgae	3.7% ± 2.8 SE	17.1% ± 3.0 SE
Padina	1.0% ± 1.0 SE	6.9% ± 1.8 SE
Sargassum	1.2% ± 1.2 SE	6.7% ± 1.2 SE
Turbinaria	1.4% ± 0.8 SE	2.0% ± 0.6 SE
Halimeda	0.1% ± 0.1 SE	1.6% ± 0.4 SE

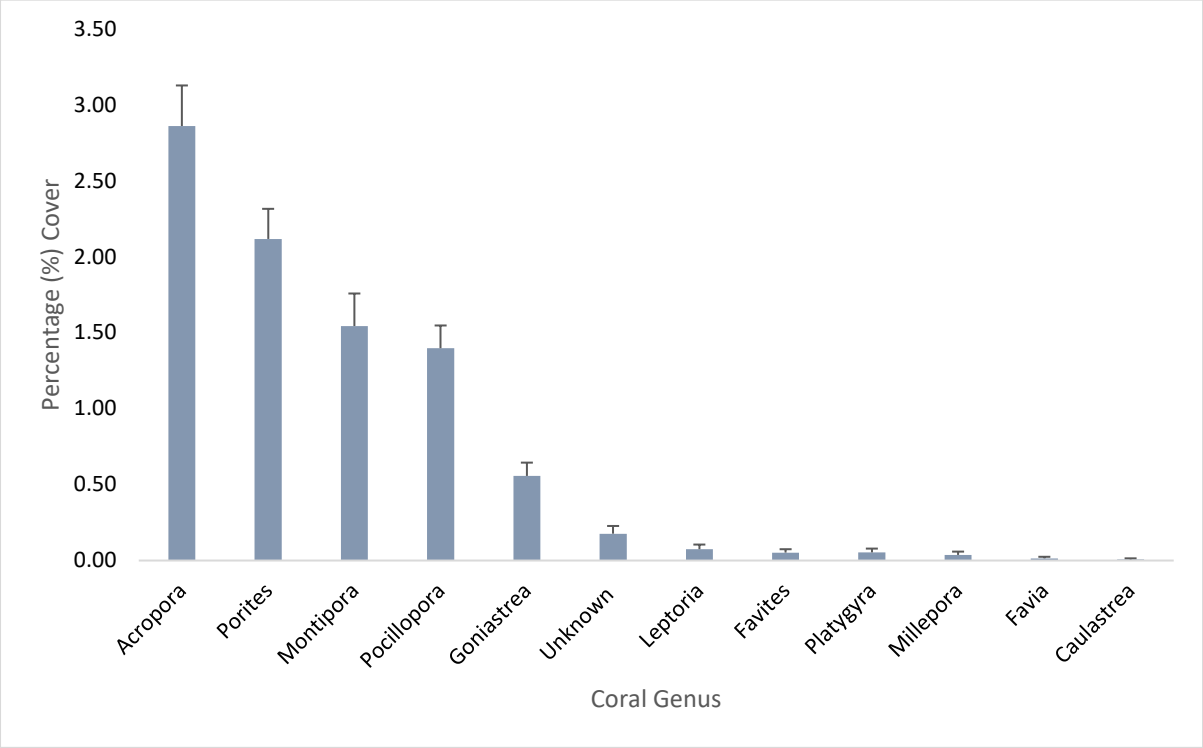

Figure 28. Total mean percentage cover of coral genera identified across the southern reef study area (including reef flat and reef crest), ranging from highest to lowest in percentage cover.

Table 9. Mean percentage cover of coral genera

Coral Genera	**Mean percentage cover**
Acropora	2.86% ± 0.27 SE
Porites	2.12% ± 0.20 SE
Montipora	1.40% ± 0.15 SE
Pocillopora	1.4% ± 0.15 SE
Goniastrea	0.56% ± 0.09 SE

Leptoria	0.07% ± 0.03 SE
Favites	0.05% ± 0.02 SE
Platygyra	0.05% ± 0.03 SE
Millepora	0.04% ± 0.02 SE
Favia	0.01% ± 0.01 SE
Caulastrea	0.01% ± 0.01 SE

3.4 Classification and regression tree zonation across reef flat

Exhaustive Chi-squared Automatic Interaction Detection (CHAID) decision trees were computed to test for differences in the percentage cover of the most abundant benthic biota and substrata with increasing distance (m) from the reef crest. The mean percentage cover of each substrate type was predicted for each significant distance range.

Figure 29, Figure 31 and Figure 33 show three examples of CHAID classification and regression trees predicting the percentage cover of seagrass, *Sargassum* and hard coral. An explanation of the tree components as well as additional trees for coral rubble, *Acropora* and *Padina* are provided in the Appendix.

Figure 30, Figure 32 and Figure 34 map the predicted zones across the reef flat with statistically different percentage cover for seagrass, *Sargassum* and hard coral based on the tree model partitions and the distance offshore of 1 m^2 polygon grid cells generated using the create tessellation function in ArcGIS Pro.

The mean percentage cover of seagrass was estimated as 0.3% ($P< 0.001$) within 76m of the reef crest; 8.2% ($P< 0.001$) between 76m and 129m; 24.0% ($P< 0.001$) between 129m and 163m; 61.0% ($P< 0.001$) between 163m and 192m; 73.2% ($P< 0.001$) between 192m and 219m; and 90.4% ($P< 0.001$) more than 219m from the reef crest (Figure 29 and Figure 30).

The mean percentage cover of the genus *Sargassum* was estimated at 0.9% ($P< 0.001$) within 47m of the reef crest; 8.5% ($P< 0.001$) between 47m and 80m; 21.3% ($P< 0.001$) between 80m and 102m; 13.5% ($P< 0.001$) between 102m and 137m; 6.9% ($P< 0.001$) between 137m and 168m; and 0.4% ($P< 0.001$) more than 168m from the reef crest (Figure 31 and Figure 32).

The mean percentage cover of hard coral was estimated as 44.6% ($P< 0.001$) within 19m of the reef crest; 30.8% ($P< 0.001$) between 19m and 44m; 5.3% ($P< 0.001$) between 44m and 131m; 0.9% between 131m and 158m; and 0.1% ($P< 0.001$) more than 158m from the reef crest (Figure 33 and Figure 34).

The results of the remaining CHAID classification and regression trees are found in the Appendix. However, the main patterns observed are as follows.

The highest predicted mean percentage cover of coral rock was estimated as 50.4% (P> 0.001), within 19m of the reef crest and decreased consistently towards the shoreline. The highest predicted mean percentage cover of coral rubble was estimated as 29.1% (P> 0.001) between 47m and 99m from the reef crest and decreased from this point towards the reef crest and shoreline. The highest predicted mean percentage cover of sand was estimated as 36.1% (P> 0.001) between 105m and 164m from the reef crest and decreased towards the reef crest and shoreline.

The highest predicted mean percentage cover of macroalgae was estimated as 25.8% (P> 0.001) between 48m and 168m from the reef crest and decreased from this point towards the reef crest and shoreline. The highest predicted mean percentage cover of the macroalgae genus *Padina* (17.8% (P> 0.001)) was found closer to shore, between 132m and 160m from the reef crest, whereas the highest predicted mean percentage cover of *Turbinaria ornata* (7.1% (P> 0.001)) was found closer to the reef crest between 50m and 82m.

The highest mean percentage cover of the coral genus *Acropora* was estimated as 21.1% (P> 0.001) within 18m of the reef crest, whereas the genus *Montipora* was estimated as 6.6% (P> 0.001) within 51m of the reef crest.

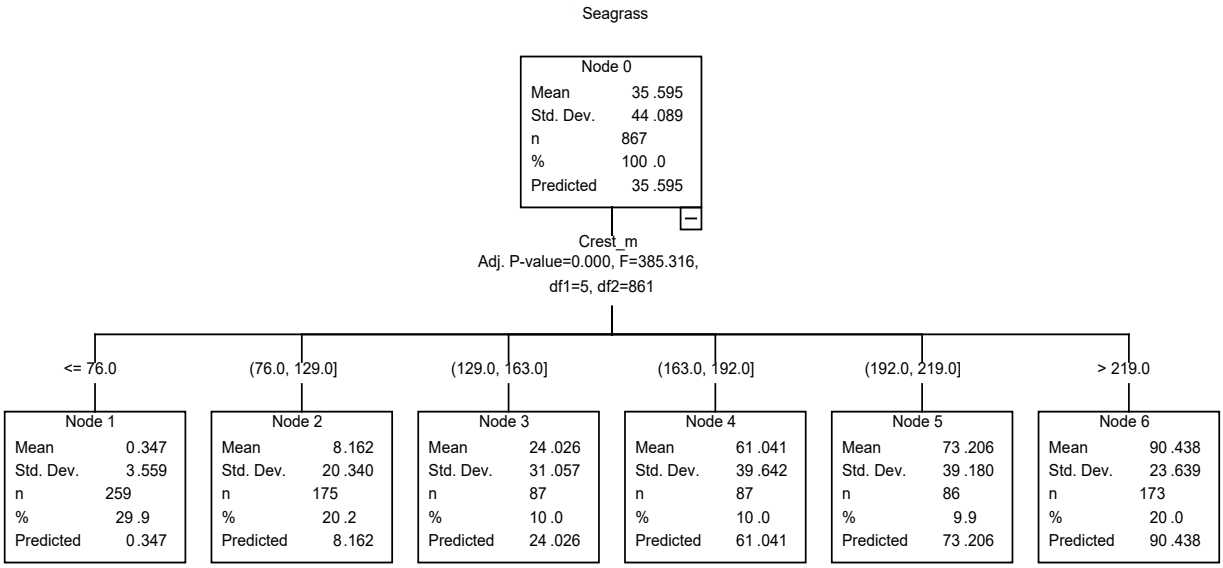

Figure 29. Predicted classification and regression zones of seagrass in response to distance from the reef crest. Percentage cover of seagrass was predicted at < 76m from crest (0.3% (P< 0.001)); 76m - 129m (8.2% (P< 0.001)); 129m - 163m (24.0% (P< 0.001)); 163m - 192m (61.0% (P< 0.001)); 192m - 219m (73.2% (P< 0.001)); and >219m (90.4% (P< 0.001)).

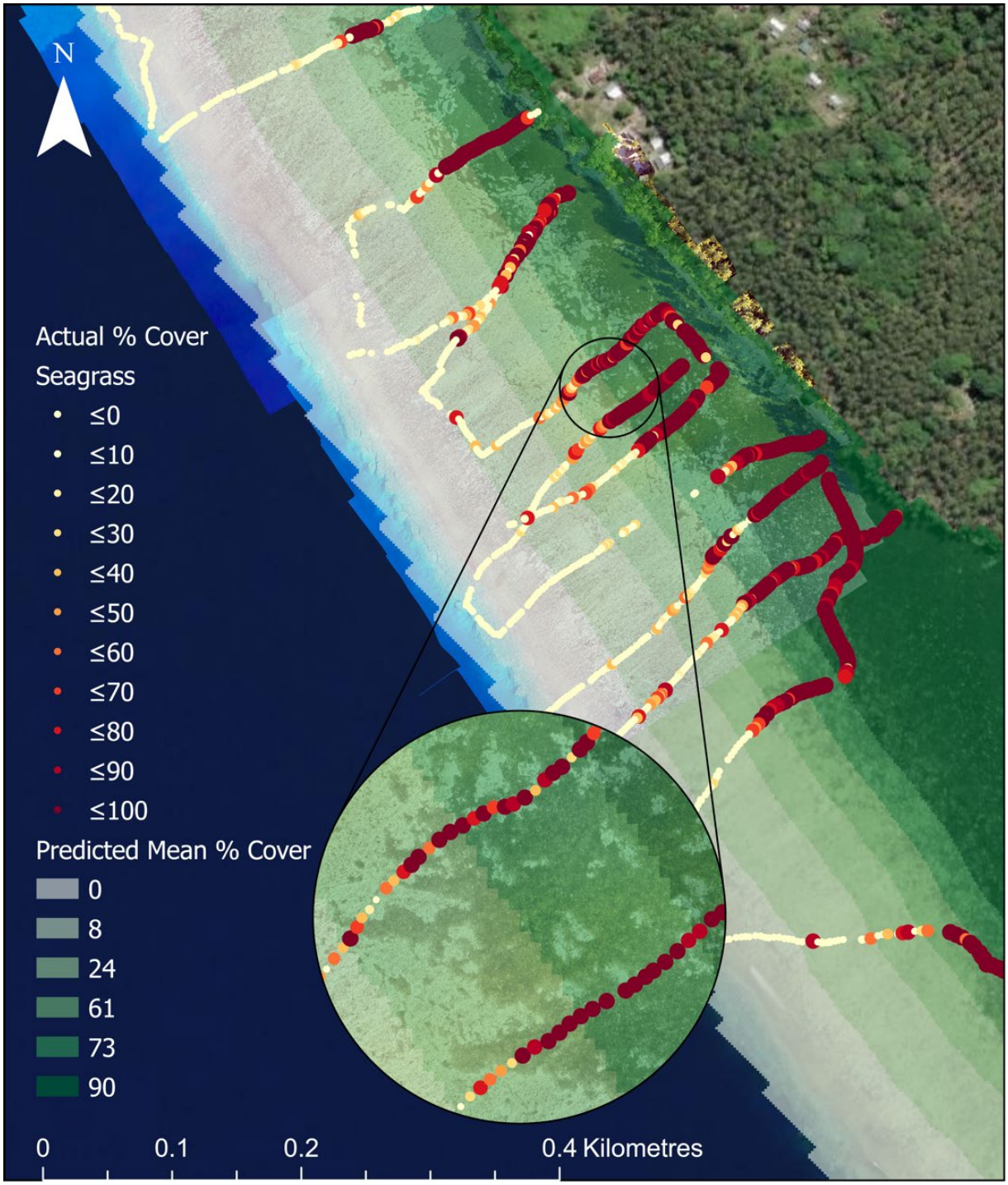

Figure 30. Predicted zones of mean percentage cover (and video survey point estimates) of seagrass from classification and regression tree analysis.

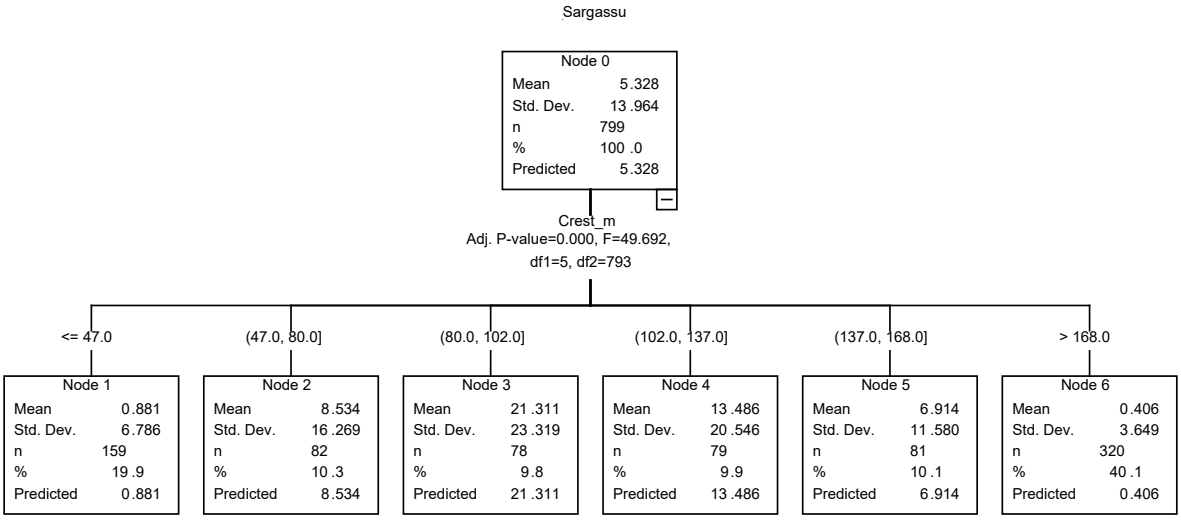

Figure 31. Predicted classification and regression zones of *Sargassum* in response to distance from the reef crest. Mean percentage cover of *Sargassum* was predicted at <47m (0.9% (P< 0.001)), 47m – 80m (8.5% (P< 0.001)), 80m – 102m (21.3% (P< 0.001)), 02m – 137m (13.5% (P< 0.001)), 137m – 168m (11.6% (P< 0.001)), and > 168m (0.4% (P< 0.001)).

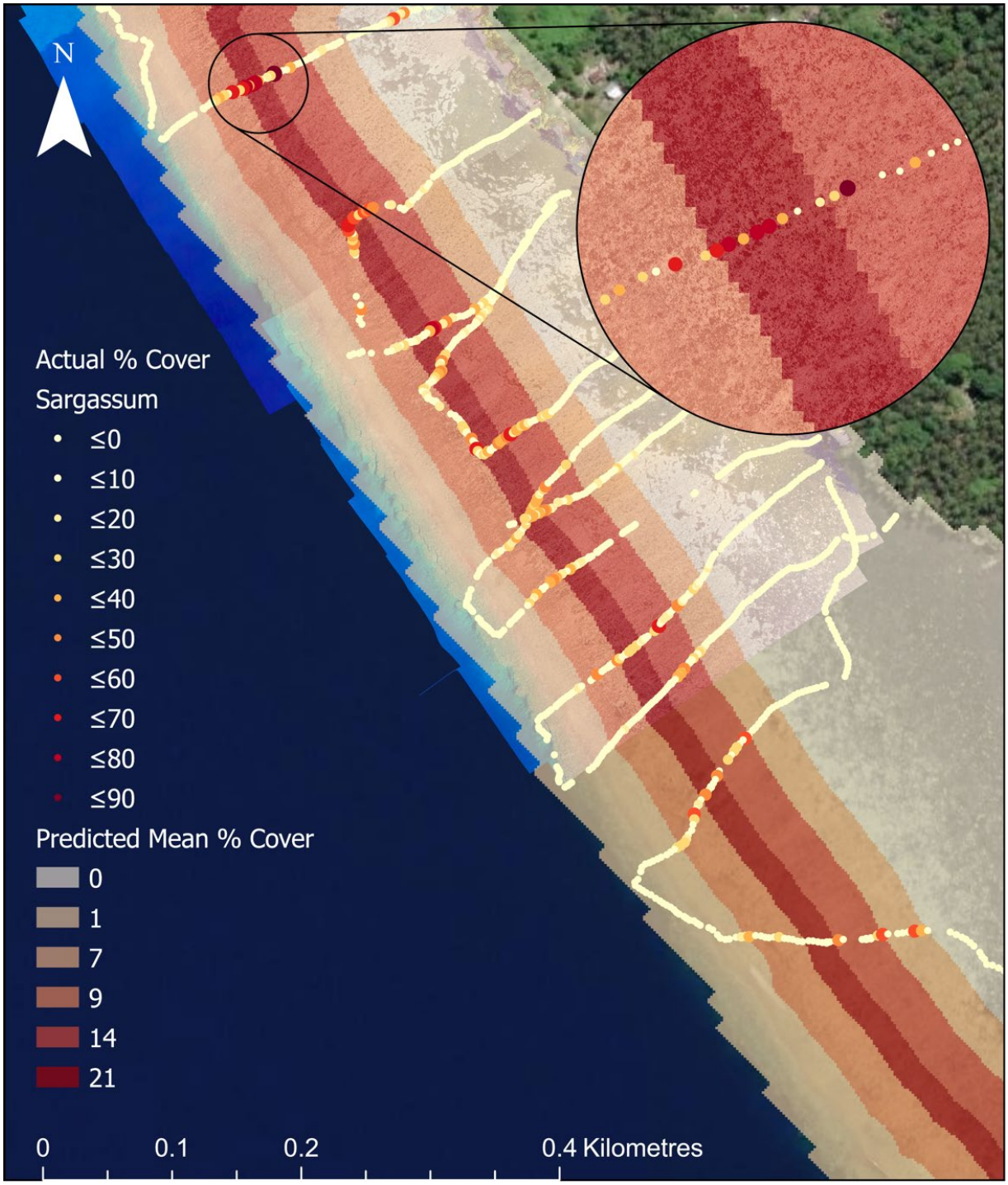

Figure 32. Predicted zones of mean percentage cover (and video survey point estimates) of *Sargassum* from classification and regression tree analysis.

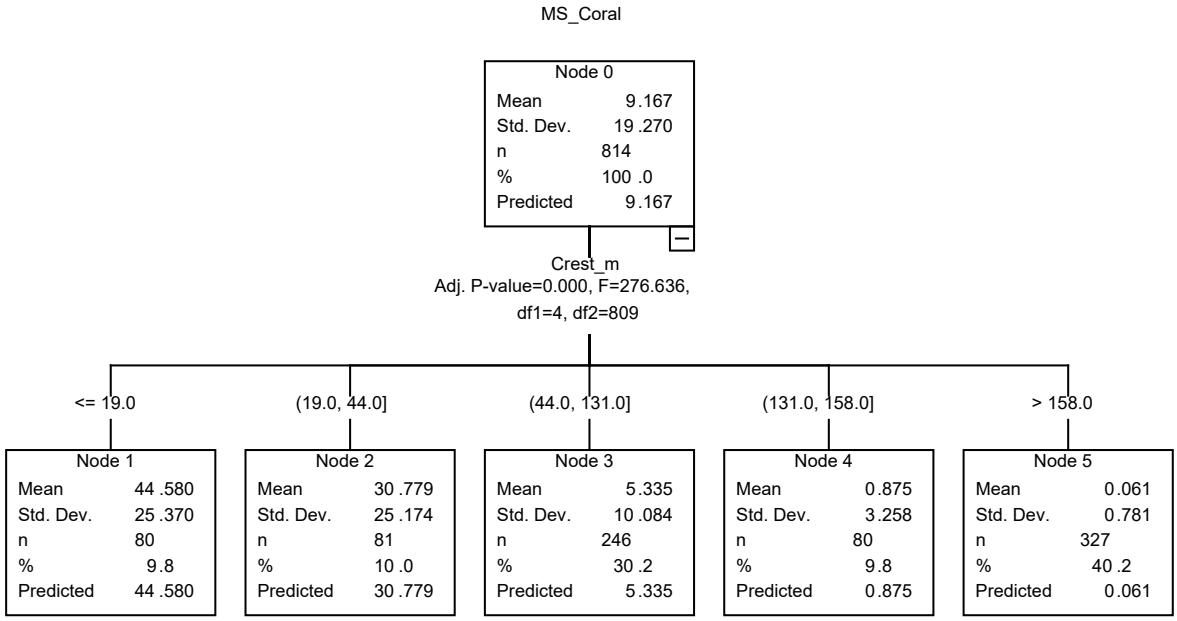

Figure 33. Predicted classification and regression zones of hard coral in response to distance from the reef crest. Mean percentage cover of hard coral was predicted at <19m (44.6% (P< 0.001)), 19m – 44m (30.8% (P< 0.001)), 44m – 131m (5.3% (P< 0.001)), 131m – 158m (0.9% (P< 0.001)), and >158m (0.1% (P< 0.001)).

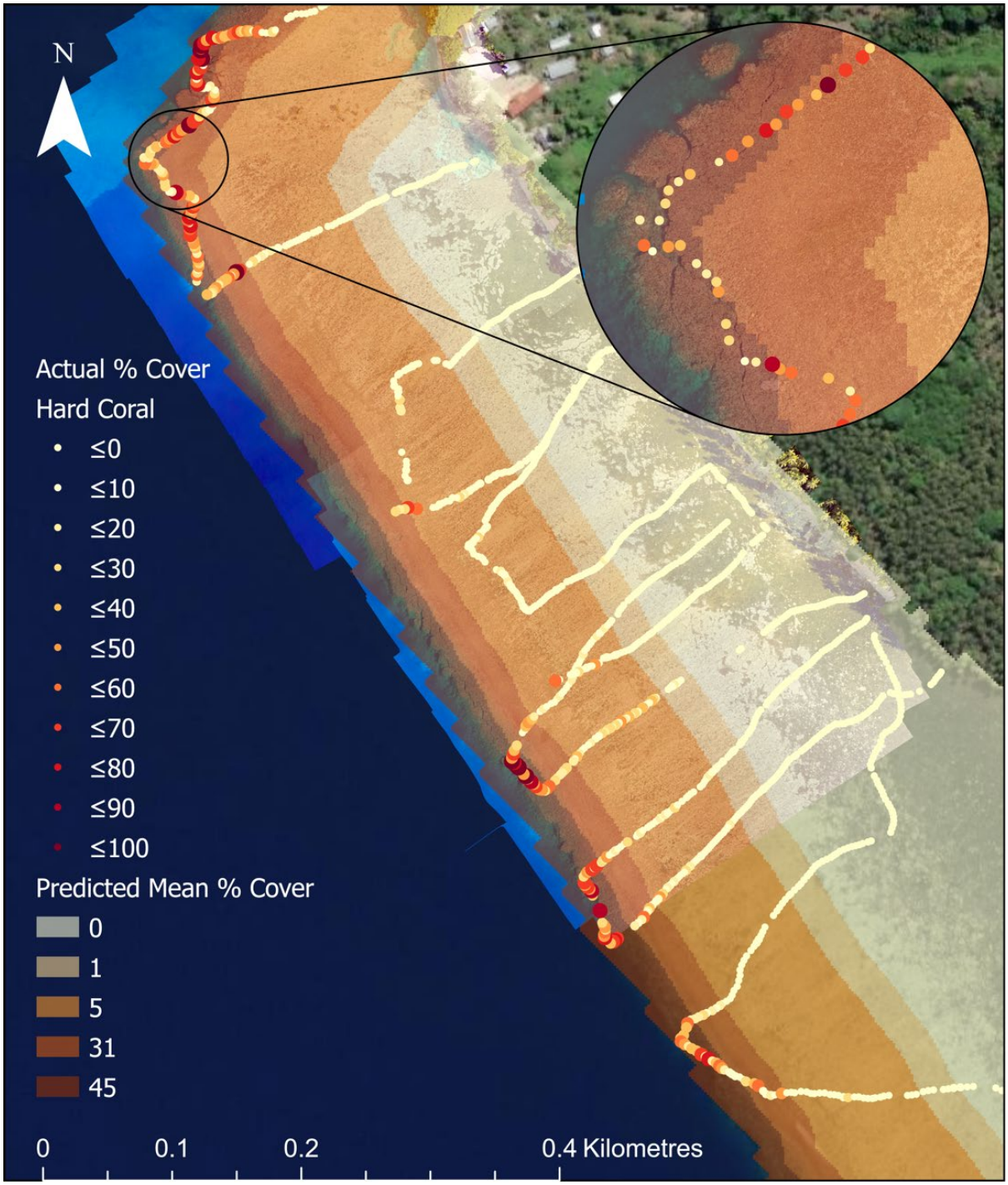

Figure 34. Predicted zones of mean percentage cover (and video survey point estimates) of hard coral from classification and regression tree analysis.

3.5 Regression of reef flat and crest percentage cover with distance from the river

Figure 35 to Figure 40 show changes in mean percentage cover among reef flat transects (n=11) with increasing distance from the river at Vavanga for those biota and substrata where there was a significant regression or of particular interest. Figure 41 and Figure 42 show the same for mean percentage cover on reef crest transects.

The percentage cover of macroalgae on the reef flat transects (greater than 70m from the crest) decreased from 66% near the river to 6% 1.2km south of the river. A statistically significant linear regression of the relationship explained 80% of the variation in the percentage cover of macroalgae among transects (Figure 35). Most of this was due to the mean percentage cover of the genus, *Sargassum* decreasing from 32% near the river to 0% 1.2km south of the river. A statistically significant linear regression of the relationship explained 80% of the variation in the percentage cover of *Sargassum* among transects (Figure 36).

The percentage cover of the genus, *Padina*, also contributed to the decrease in macroalgae. Percentage cover of *Padina* decreased from 31% near the river to 1% 800m south of the river but then increased to 9 and 6% 1km and 1.2 km from the river. A statistically significant 2nd order polynomial curvilinear regression of the relationship explained 80% of the variation in the percentage cover of *Padina* among transects (Figure 37).

The percentage cover of seagrass on the reef flat transects increased from 3% near the river to 39% 1.2km south of the river. A statistically significant linear regression of the relationship explained 43% of the variation in the percentage cover of macroalgae among transects (Figure 38).

The percentage cover of live coral on the reef flat transects generally ranged between 1 and 8% except for a transect 650m south of the river (19% cover, mostly of the coral genus *Porites)*. There was no statistically significant relationship between distance from the river and the percentage cover of hard coral (Figure 39).

The mean percentage cover of coral rubble on the reef flat transects increased from 1% near the river to 44% 1.2km south of the river. A statistically significant linear regression of the relationship explained 57% of the variation in the percentage cover of coral rubble among transects (Figure 40).

There were only five short reef crest transects for which there was a non-significant trend in coral rock decreasing from approximately 50% cover near the river to 0% cover 800m south (Figure 41). There was no linear relationship for live coral on reef crest transects with distance from the river and percentage cover ranged from 0% to 45% (Figure 42).

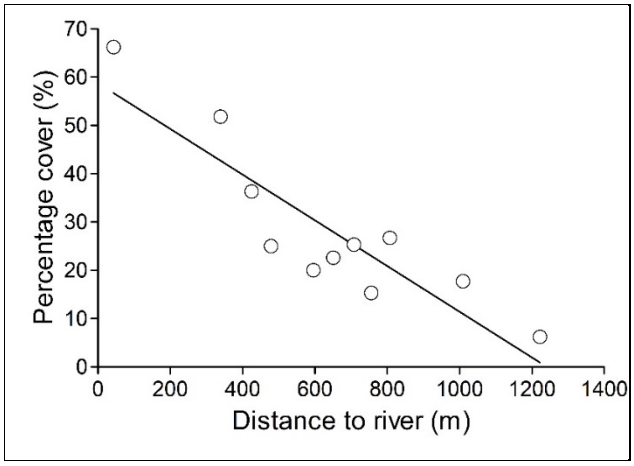

Figure 35. Linear regression of percentage cover of reef flat macroalgae with distance from river (m). (r^2 = 0.8, P<0.001, n=11).

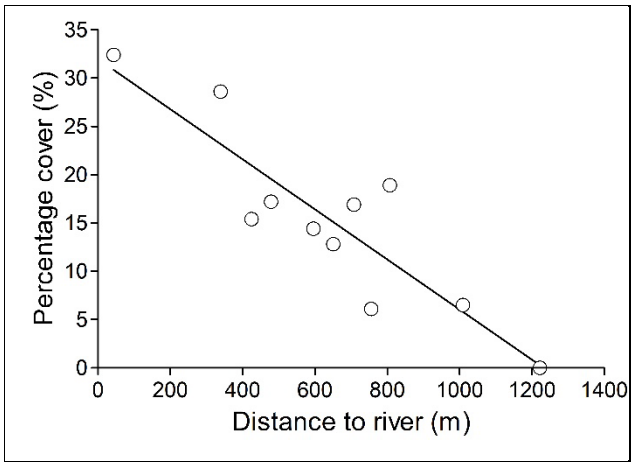

Figure 36. Linear regression of percentage cover of reef flat genus *Sargassum* with distance from river (m). (r^2 = 0.8, P<0.001, n=11).

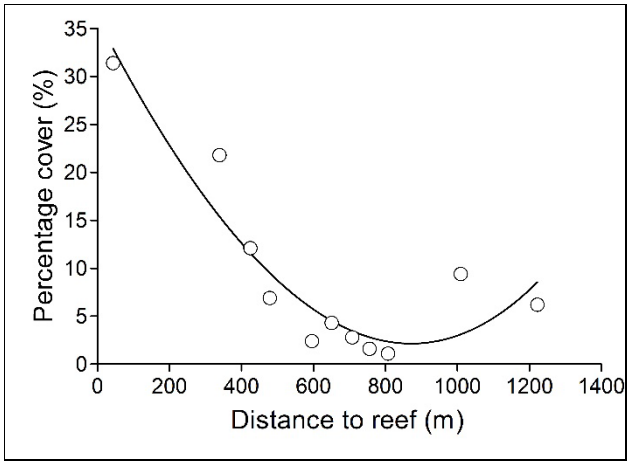

Figure 37. Curvilinear regression of percentage cover of reef flat genus *Padina* with distance from river (m). (r^2 = 0.8, P<0.001, n=11).

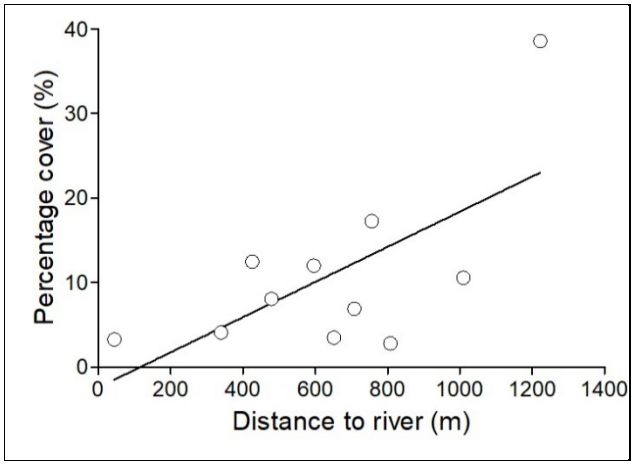

Figure 38. Linear regression of percentage cover of reef flat seagrass with distance from river (m). (r^2 = 0.43, P<0.03, n=11).

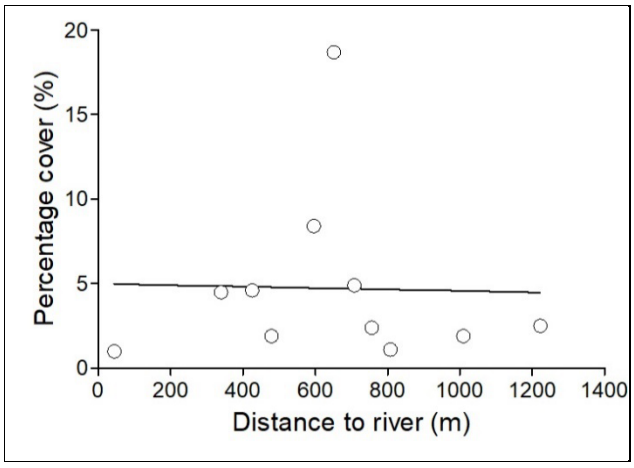

Figure 39. Linear regression of percentage cover of reef flat coral with distance from river (m). (r^2 = 0.001, P>0.9, n=5, not significant).

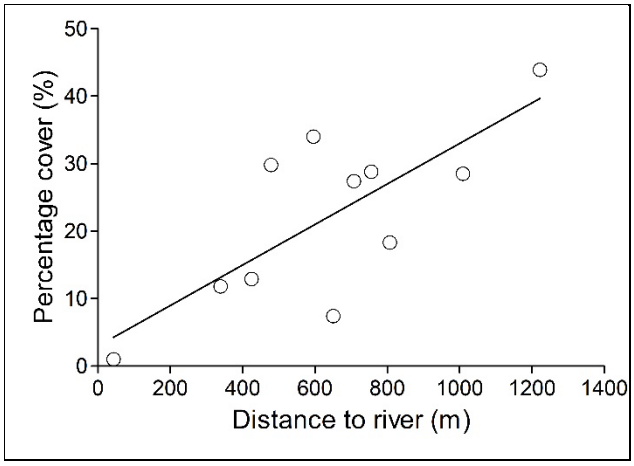

Figure 40. Linear regression of percentage cover of reef flat coral rubble with distance from river (m). (r^2 = 0.57, P<0.01 n=11).

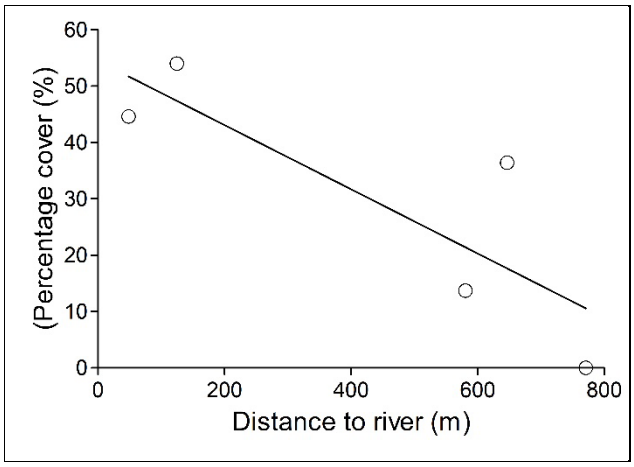

Figure 41. Linear regression of percentage cover of reef crest coral rock with distance from river (m). (r^2 = 0.7, P=0.08, n=5, not significant).

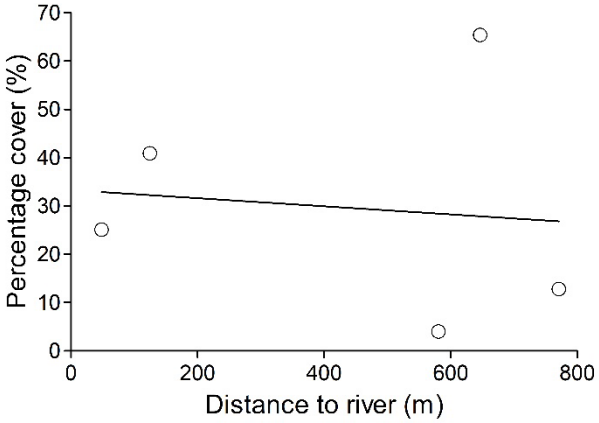

Figure 42. Linear regression of percentage cover of reef crest coral with distance from river (m). (r^2 = 0.01, P=0.9, n=5, not significant).

3.6 Automated underwater image classification with ReefCloud AI

A total of 260 images were analysed using ReefCloud AI. 80% of all images were annotated manually. The model produced an accuracy score of 0.68 (68% accuracy) and an F1 score of 0.66 (66% accuracy). The accuracy score reflects the amount of agreement between all human and machine classifications (ReefCloud, 2024). The F1 score considers two metrics, precision (the correct positive predictions relative to total positive predictions) and recall (the correct positive predictions relative to actual positives). Figure 43, Figure 44 and Figure 45 illustrate three examples of ReefCloud model validation outputs that compare the total percentage cover of different substrate categories between the human and machine classifications. These include seagrass (Figure 43), hard substrate (Figure 44), and macroalgae (Figure 45).

The last 20% of images uploaded to ReefCloud were not human annotated. These were used to produce an accuracy assessment of the model. Table 9 displays the accuracy of the model at the main substrate level and produced an overall accuracy score of 0.70 (70% accuracy). The highest individual class accuracy was seen in seagrass (94% P accuracy), followed by sand (79% P accuracy), hard coral (69% P accuracy), coral rubble (55% P accuracy), coral rock (45% P accuracy), filamentous algae (20% P accuracy), and algae (0% P accuracy). Table 10 displays the accuracy of the model at a species level and produced an overall accuracy score of 0.63 (63%). The highest individual class accuracy was again seen in seagrass (94%), followed by fine sand (70%), coarse sand (57%), and coral rubble (55%).

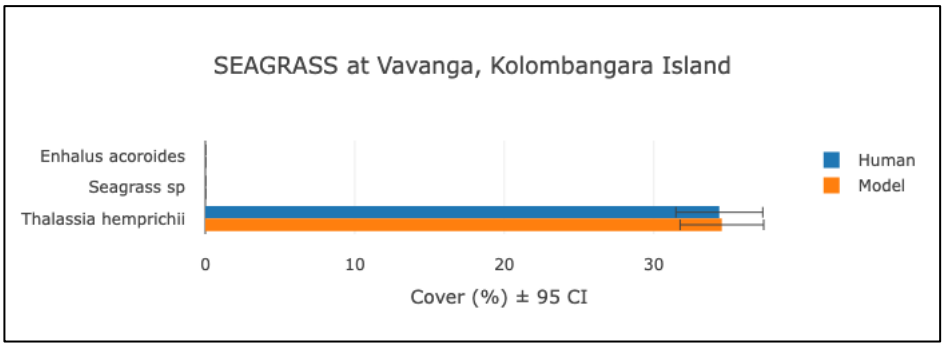

Figure 43. ReefCloud model validation output comparing the percentage cover of seagrass between the human and model annotations. Percentage cover of *Thalassia hemprichii* was 34.4 ± 2.9 (human) and 34.5 ± 2.8 (model).

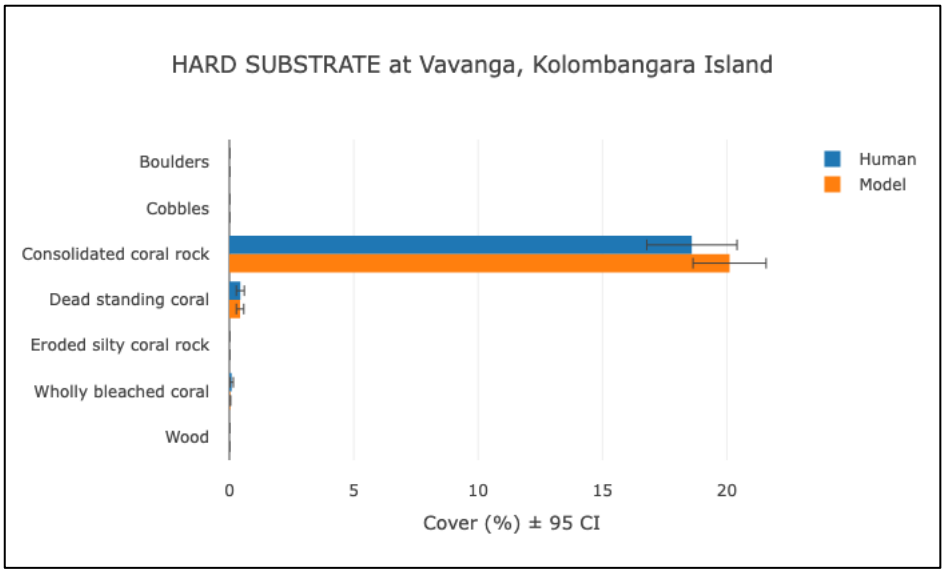

Figure 44. ReefCloud model validation output comparing the percentage cover of hard substrate between the human and model annotations. Percentage cover of consolidated coral rock was 18.59 ± 1.82 (human) and 20.11 ± 1.47 (model). Dead standing coral produced a percentage cover of 0.44 ± 0.16 (human) and 0.43 ± 0.15 (model).

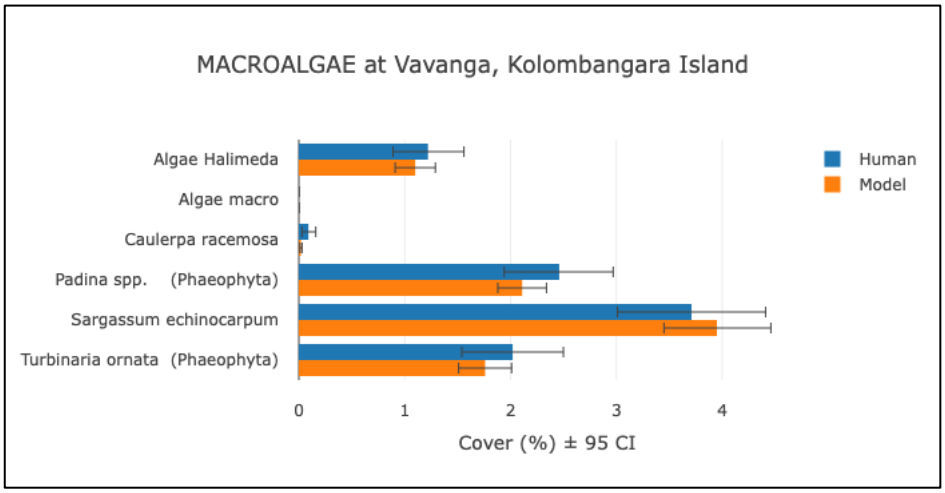

Figure 45. ReefCloud model validation output comparing the percentage cover of macroalgae between the human and model annotations. Percentage cover of Algae *Halimeda* was 1.22 ± 0.33 (human) and 1.1 ± 0.19 (model). Percentage cover of *Caulerpa racemos*a was 0.09 ± 0.06 (human) and 0.02 ± 0.01 (model). Percentage cover of *Padina* spp. was 2.46 ± 0.51 (human) and 2.11 ± 0.23. Percentage cover of *Sargassum*

echinocarpum was 3.71 $\pm$ 0.70 (human) and 3.95 $\pm$ 0.51 (model). Percentage cover of *Turbinaria ornata* was 2.02 $\pm$ 0.48 (human) and 1.76 $\pm$ 0.25 (model).

Table 10. Confusion matrix displaying the accuracy of the ReefCloud.AI main substrate classifications from the last 20% of images uploaded to ReefCloud.

KEY	ClassValue	Coral Rock	Coral Rubble	Sand	Seagrass	Algae	Filamentous Algae	Macroalgae	Hard Coral	Total	U_Accuracy	Kappa
Human	Coral Rock	22	9	2	1	0	3	12	6	55	0.40	0.00
Machine	Coral Rubble	10	16	1	0	0	0	6	0	33	0.48	0.00
Correct class	Sand	10	1	48	5	0	3	15	1	83	0.58	0.00
0 < ≥ 5	Seagrass	1	0	5	133	0	0	2	0	141	0.94	0.00
5 < ≥ 10	Algae	0	0	0	0	0	0	0	0	0	0.00	0.00
10 <	Filamentous Algae	1	1	0	0	0	2	1	0	5	0.40	0.00
	Macroalgae	3	2	5	3	1	2	26	1	43	0.60	0.00
	Hard Coral	2	0	0	0	1	0	1	18	22	0.82	0.00
	Total	49	29	61	142	2	10	63	26	382	0.00	0.00
	P_Accuracy	0.45	0.55	0.79	0.94	0.00	0.20	0.41	0.69	0.00	0.69	0.00
	Kappa	0.00	0.00	0.00	0.00	0.00	0.00	0.00	0.00	0.00	0.00	0.61

Table 11. Confusion matrix displaying the accuracy of the ReefCloud.AI species classifications from the last 20% of images uploaded to ReefCloud.

ClassValue	Coral Rock	Coral Rubble	Fine Sand	Coarse Sand	Seagrass	Algae	Fill Algae	Halimeda	Sargassum	Turbinaria	Padina	Acroclat	Acrocor	Acrohya	Acromill	Pociver	Pormass	Porann	Total	U_Accuracy	Kappa
Coral Rock	22	9	2	0	1	0	3	1	2	1	8	0	0	1	0	1	4	0	55	0.40	0.00
Coral Rubble	10	16	0	1	0	0	0	0	2	1	3	0	0	0	0	0	0	0	33	0.48	0.00
Fine Sand	9	1	38	2	5	0	0	0	1	0	13	0	0	0	0	0	0	0	69	0.55	0.00
Coarse Sand	1	0	4	4	0	0	3	0	0	0	1	0	1	0	0	0	0	0	14	0.29	0.00
Seagrass	1	0	5	0	133	0	0	1	0	0	1	0	0	0	0	0	0	0	141	0.94	0.00
Algae	0	0	0	0	0	0	0	0	0	0	0	0	0	0	0	0	0	0	0	0.00	0.00
Fill Algae	1	1	0	0	0	0	2	0	1	0	0	0	0	0	0	0	0	0	5	0.40	0.00
Halimeda	2	1	0	0	0	0	0	0	0	0	0	0	0	0	0	0	0	0	3	0.00	0.00
Sargassum	1	0	0	0	2	1	0	0	10	1	2	0	0	0	0	0	0	1	18	0.56	0.00
Turbinaria	0	1	1	0	0	0	1	1	2	2	0	0	0	0	0	0	0	0	8	0.25	0.00
Padina	0	0	4	0	1	0	1	0	3	0	5	0	0	0	0	0	0	0	14	0.36	0.00
Acroclat	0	0	0	0	0	0	0	0	0	0	0	0	0	0	0	0	0	0	0	0.00	0.00
Acrocor	1	0	0	0	0	0	0	0	0	0	0	0	3	1	1	1	0	0	7	0.43	0.00
Acrohya	0	0	0	0	0	0	0	0	0	0	0	2	0	2	0	0	0	0	4	0.50	0.00
Acromill	0	0	0	0	0	0	0	0	0	0	0	0	0	0	0	0	0	0	0	0.00	0.00
Pociver	0	0	0	0	0	0	0	0	0	0	0	0	2	0	1	2	0	0	5	0.40	0.00
Pormas	1	0	0	0	0	1	0	0	1	0	0	0	2	0	0	0	1	0	6	0.17	0.00
Porann	0	0	0	0	0	0	0	0	0	0	0	0	0	0	0	0	0	0	0	0.00	0.00
Total	49	29	54	7	142	2	10	3	22	5	33	2	8	4	2	4	5	1	382	0.00	0.00
P_Accuracy	0.45	0.55	0.70	0.57	0.94	0.00	0.20	0.00	0.45	0.40	0.15	0.00	0.38	0.50	0.00	0.50	0.20	0.00	0.00	0.63	0.00
Kappa	0.00	0.00	0.00	0.00	0.00	0.00	0.00	0.00	0.00	0.00	0.00	0.00	0.00	0.00	0.00	0.00	0.00	0.00	0.00	0.00	0.54

3.7 Object-based image analysis of the aerial drone photo orthomosaic

Figure 46 displays the results of the object-based image classification undertaken across a subset of the south reef flat photo orthomosaic, using six defined classifications. Table 8 displays the confusion matrix highlighting the overall and individual class accuracies of the object-based image classification. The confusion matrix produced an overall accuracy of 70.9%. The highest individual class accuracy was seen in coral/coral rock mix (94% P accuracy), followed by sand/algal mix (82% P accuracy), dense seagrass (64% P accuracy), coral rock/algal mix (56% P accuracy), macroalgae (48% P accuracy), and sparse seagrass (38% P accuracy). Sand/algal mix was frequently misclassified as coral rock/algal mix, while coral rock/algal mix was most often misclassified as sand/algal mix. Dense seagrass was also frequently misclassified as coral rock/algal mix. Macroalgae was most often misclassified as dense seagrass. Figure 47 displays a comparison of the mean spectral values for each RGB band between the six classifications. The mean spectral values were derived from 10 random samples taken across the photo orthomosaic for each class. The similar spectral values of the sand/algal mix and coral rock/algal mix classes may help to explain the frequent classification confusion between these classes.

Table 9 displays the adjusted distance and bearing measurements between the original transect points and the newly plotted points used to validate the training and validation of the classification. The average adjusted distance and bearing between the original and adjusted points were 0.89m and 138.03°, respectively.

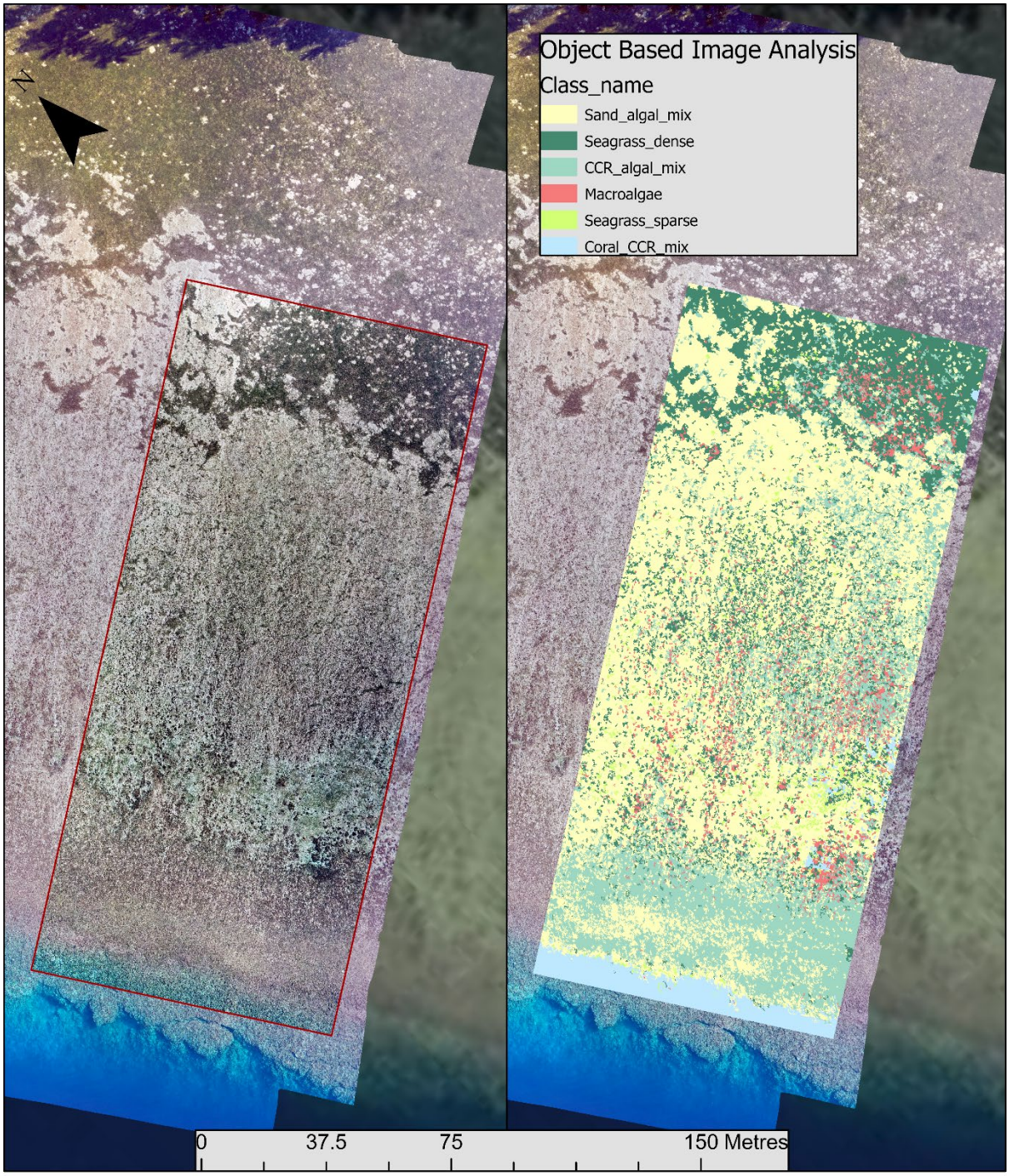

Figure 46. Map displaying the results of the object-based image classification undertaken on a subsection of the south reef flat photo orthomosaic, using six defined classifications; sand and algae (yellow), dense seagrass (dark green), coral rock and algae (aquamarine), macroalgae (pink), sparse seagrass (lime green), and coral rock and live coral (blue).

Table 12. Confusion matrix: Benthic community map of the south reef flat derived from the object-based image classification of the UAV photo orthomosaic.

KEY	ClassValue	Sand_algal_mix	Seagrass_dense	CCR_algal_mix	Macroalgae	Seagrass_sparse	Coral_CCR_mix	Total	U_Accuracy	Kappa
Ground Truth	Sand_algal_mix	205	9	31	3	6	1	255	0.80	0
Classified	Seagrass_dense	9	59	8	10	1	0	87	0.68	0
Correct class	CCR_algal_mix	33	15	54	2	3	0	107	0.50	0
0 < ≥ 5	Macroalgae	0	7	1	14	0	0	22	0.64	0
5 < ≥ 10	Seagrass_sparse	2	1	1	0	6	0	10	0.60	0
10 <	Coral_CCR_mix	1	1	1	0	0	17	20	0.85	0
	Total	250	92	96	29	16	18	501	0	0
	P_Accuracy	0.82	0.64	0.56	0.48	0.38	0.94	0	0.71	0
	Kappa	0	0	0	0	0	0	0	0	0.56

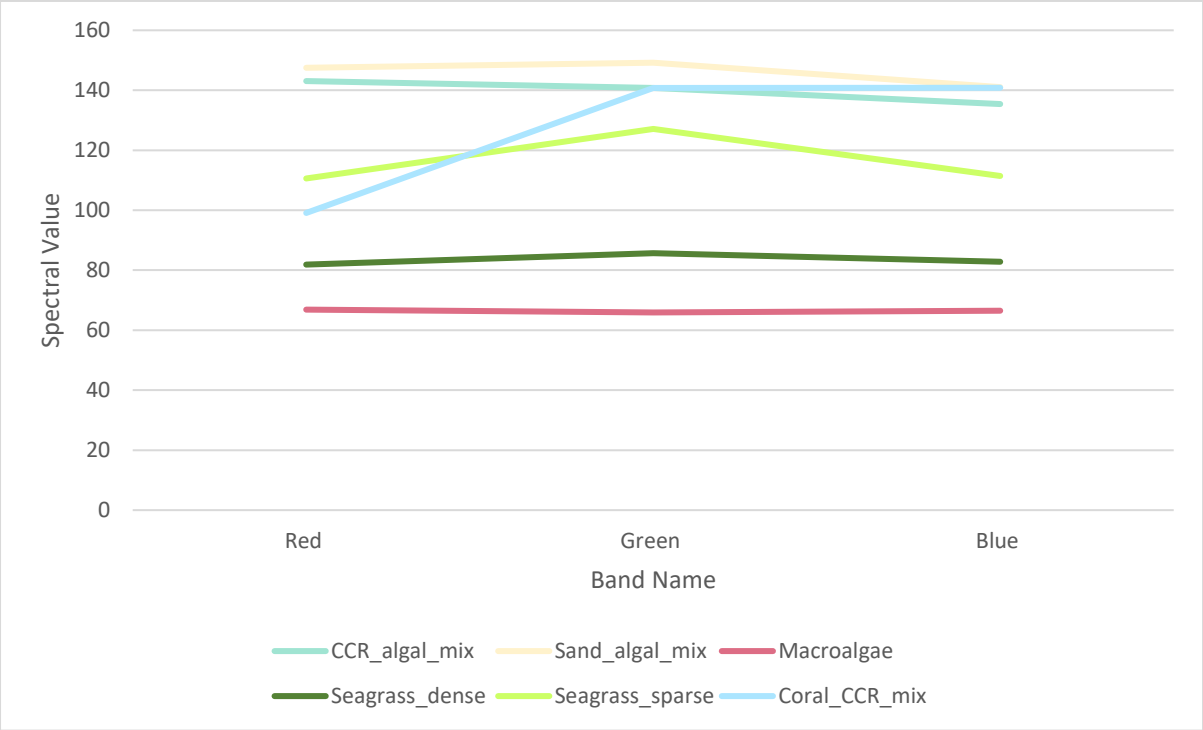

Figure 47. Stacked line graph displaying comparison of mean spectral values for the three RGB bands, across the 6 substrate classes used in the object-based image classification. Mean values for each class were derived from 10 random samples across the photo orthomosaic. Mean spectral values of the red band: 143 (CCR_algal_mix), 148 (Sand_algal_mix), 67 (Macroalgae), 82 (Seagrass_dense), 111 (Seagrass_sparse), and 99 (Coral_CCR_mix). Mean spectral values of the green band: 141 (CCR_algal_mix), 149 (Sand_algal_mix), 66 (Macroalgae), 86 (Seagrass_dense), 127 (Seagrass_sparse), and 141

(Coral_CCR_mix). Mean spectral values of the blue band: 134 (CCR_algal_mix), 141 (Sand_algal_mix), 67 (Macroalgae), 83 (Seagrass_dense), 112 (Seagrass_sparse), and 141 (Coral_CCR_mix).

Table 13. Adjusted distance and bearing measurements.

Mission ID	Adjusted dist (m)	Bearing (degrees)
16703839024950	1.43	139
16703839203370	1.46	182
16703839346590	1.42	227
16703839470710	1.13	130
16703839598130	1.58	136
16703839725610	1.61	129
16703839848950	1.66	165
16703839991860	1.58	105
16703840100930	1.35	101
16703840218010	1.17	139
16703840326820	0.71	220
16703840435600	1.06	97
16703840549760	1.16	116
16703840664790	0.81	109
16703840775130	0.56	99
16703840887870	0.58	71
16703841005160	0.21	193
16703841118180	0.27	123
16703841232240	0.45	89
16703841360830	0.3	94
16703841467560	0.63	91
16703841578370	0.46	127
16703841703790	0.38	145
16703843677020	1.01	97
16703843878900	0.96	67
16703844036300	0.59	92
16703844168920	1.16	71
16703844344010	0.78	137
16703844504690	0.74	143
16703844636280	0.74	114
16703844797040	0.63	73
16703844942160	0.38	90
16703845117130	0.84	216
16703845279690	0.22	166
16703845455990	1.64	291
16703845580550	0.37	239

16703845719450	0.78	204
16703845867720	0.97	218
Mean	0.89	138.03

4 Discussion

Coral reef flats include a variety of habitat types that support a diverse assortment of marine organisms. These highly dynamic environments also provide a range of ecological goods and services to local and surrounding human coastal populations (Adams et al., 2006; Davis et al., 2017; Sheppard et al., 2005). Given their location in shallow waters, it is probable that reef flats and the associated communities they support will face the most significant impacts from climate change and other anthropogenic stressors (Harborne, 2013). Thus, the development of accurate and precise assessments of reef flat habitat dynamics is essential for the mapping, monitoring, and conservation of these unique environments (Cresswell et al., 2021). The overall aim of this research was to investigate the ability of novel UAV FMV techniques to effectively quantify the dynamics of habitat zonation across the reef flat on Kolombangara Island, Solomon Islands. To achieve this aim, I addressed the following objectives:

1. Combine Unoccupied Aerial Vehicle (UAV) Full Motion Video (FMV) with georeferenced underwater video to map the spatial distributions of reef flat substrata and biota across the reef flat.
2. Determine the effectiveness of UAV FMV for shallow-water substrate mapping in a tropical reef-flat environment.
3. Spatially quantify reef flat zones and gradients using a combination of geospatial and statistical sampling and analyses.
4. Investigate the potential of the open access Artificial Intelligence (AI) platform ReefCloud.AI to classify reef flat substrata using georeferenced underwater imagery.
5. Determine the utility of geospatially referenced aerial and underwater video data to coral reef research, conservation, and management.

The integration of spatially referenced UAV photography and FMV with underwater video provided a quantitative and visually intuitive analysis of how reef flat zonation responds to environmental gradients adjacent to Vavanga. This approach combined the advantages of remotely sensed drone data from 100-110m and underwater video from approximately 1 metre away, to allow both video streams to be viewed simultaneously in geographic space within the ArcGIS Pro FMV Image Analyst extension.

The resulting data from the UAV FMV analysis was then manipulated to produce substrate distribution maps across multiple classification levels. Several different approaches to data analysis were employed in this study, each providing complementary information on the distributions of reef flat substrata and biota. These methods included simple summary statistics averaged over whole transects, habitats and areas, as well as simple linear regressions, and classification and regression trees for factors such as distance to the reef crest and river. A subset of 260 georeferenced images was also used to test the classifying capability of ReefCloud.AI, and accuracy assessments were performed. Additionally, a sample from the high-resolution drone photo orthomosaic was analysed using object-based image segmentation and classification, with validation from georeferenced underwater imagery.

This chapter is divided into four sections to assess the aim and objectives presented in this research. The first section will discuss spatial patterns in the distribution of benthic biota and substrata. The second section will examine the success and significance of the study and the uncertainty and limitations of the methods. Recommendations for future research and potential applications will be discussed in the third section, followed by concluding statements.

4.1 Spatial distribution of substrata and biota on the reef flat and reef crest

4.1.1 Summary statistics

Averaging percentage cover across whole habitats provided a summary of obvious differences between reef flat and reef crest substrata and biota. Hard coral and coral rock each contributed over 40% of the area of reef crest habitats, but on the reef flat hard coral and coral rock covered only 5% and 12% of the area, respectively (Figure 27). The most

abundant corals on the reef crest included species of *Acropora*, *Pocillopora*, *Montipora,* and corals from the family Favidae (Figure 28). The high cover of these species is fairly typical of semi-exposed reef fronts in clear water (Morrissey, 1980; Pichon & Morrissey, 1982). The southern side of Kolombangara Island is sheltered by an archipelago of islands and reefs to the south-east and west where the predominant ocean swells originate, but there are passes through the reef that allow swell to reach the island and the reef crest. Strong tidal currents also circulate large amounts of water between the islands.

On a reef crest more exposed to large ocean swells, hard coral species such as *Isopora palifera*, *I. cuneata, I. brueggemanni*, *Acropora humilis*, and *Pocillopora eydouxi* would be common (Veron, 1986; Done, 1982, Pers. Comm. D. Breen), but these were relatively rare at Vavanga. Corals on the reef crest did not include many of the species often associated with highly turbid inshore fringing reefs. Species composition more closely resembled mid-shelf fringing reefs that are usually protected from large swells but have relatively high water clarity (Done, 1982). Visibility off the reef crest was normally more than 10m, the exception being when high rainfall resulted in large plumes of freshwater and sediments entering the ocean from river mouths and coastal lagoons.

Instead, some of the more common reef crest coral species included: *Pocillopora verrucosa* and *P. damicornis*; *Acropora hyacinthu*s plate corals; branching and corymbose *Acropora; Montipora digitata* and encrusting *Montipora*; *Porites* boulder corals and faviid corals including *Platygyra daedalea and Goniastrea*, similar to clear water mid-shelf and back reef communities described by Done (1982) and Morrissey (1980). This is likely due to the protection of large ocean swells provided by the surrounding islands, as well as strong currents that carry away turbid water and sediments from the rivers and coast. Many other environmental factors may influence the composition of coral communities within the Solomon Islands such as disturbance, predation, competition, and disease, among others. Appendix includes a list of all species identified during the surveys.

The high cover of coral rock on the reef crest is due in part to its exposure to breaking waves but also to limitations in identifying less conspicuous, but abundant biota such as encrusting coralline and filamentous turf algae and sponges, and the effects of grazing by herbivorous fishes.

In comparison, the highest average percentage cover of substrata and biota on the reef flat occurred for seagrass and sand (Figure 27), particularly closer to shore. Coral rubble and rock occurred across the remaining reef flat with overlapping zones of the brown macroalgae *Sargassum echinocarpum*, *Padina*, and *Turbinaria ornata,* and small amounts of *Montipora digitata* all peaking at varying distances across the mid to outer shelf reef flat. The dominant algal species identified across the Vavanga reef flat were also identified in varying abundance in the comprehensive algal survey conducted in the Solomon Islands by Womersley and Bailey (1970). *Porites* boulder corals, corymbose *Acropora,* the green macroalgae *Halimeda*, and encrusting corals were more abundant approaching the reef crest and increasing wave exposure. Similar zonation patterns across a fringing reef have been described in detail for fringing island reefs on the Great Barrier Reef (Bull, 1982; Morrissey, 1980; Pichon & Morrissey, 1981).

These descriptions are based on field observations and percentage cover averaged across reef habitats and transects. However, spatially referencing percentage cover estimates for each video frame permits a more detailed view of the distribution of substrata and biota and allows the extent of zones and gradients in abundance to be modelled and mapped.

4.1.2 Classification and regression analysis across the reef crest and reef flat areas

Permutation tests for CHAID classification and regression trees showed that several different reef flat substrata and biota varied with distance from the reef crest and identified the approximate limits of zones explaining the most variation in mean percentage cover. Although spatial patterns in abundance are usually more gradual than categorical, the classification and regression trees identified unimodal peaks in abundance with adjacent zones of decreasing abundance for hard coral, seagrass, sand, coral rock, coral rubble and macroalgae, including *Sargassum*, *Padina* and *Turbinaria*.

Mapping the spatial limits of these zones in ArcGIS Pro together with the high-resolution drone photo orthomosaic, and the original underwater estimates allowed these patterns across the reef flat to be readily interpreted and verified at a relatively fine spatial scale. Although not presented in detail here for the sake of brevity, the random forests tool in ArcGIS Pro provided a similar classification of point estimates of percentage cover in response to distance to the reef crest.

High densities of the seagrass species *Thalassia hemprichii* were visible in the shallow, sheltered, sandy nearshore areas of the southern reef flat (Figure 30). From the CHAID predictions, the highest abundance of seagrass peaked more than 219m away from the reef crest (nearest the shoreline) and decreased consistently towards the crest (Figure 29). This pattern is consistent with a typical reef flat as the presence of seagrass is typically driven by key drivers such as shelter from wave action, wind, and tidal energy (Grech & Coles, 2010; Morrissey, 1980).

In comparison, the highest density of hard coral (44.6%) was predicted within 19m of the reef crest and consistently decreased towards the shoreline, where the mean percentage cover was estimated at 1% beyond 131m (Figure 33). This pattern was highly expected as hard coral cover typically increases seaward across the reef flat, and peaks near the outer edge of this zone, where most coral species (approximately 75%) are found to occur (Morrissey, 1980). However, Morrissey (1980) found small groups of species such as *Montipora, Porites* and some corals from the family Favidae occur nearer the land on the reef flat, which was also evident through field observations in this study.

The highest density of macroalgae was evident between 48 and 168m from the crest. *Turbinaria ornata* dominated closest to the reef crest between 50 and 82m, followed by *Sargassum* between 80 and 102m (Figure 31), and *Padina* between 132 and 160m (Figure 56). *Turbinaria* and *Sargassum* are two reasonably large standing macrophytes that can be found in abundance closer to the reef crest, as higher wave action often decreases herbivory activity, therefore promoting their growth (Hay et al., 1983; Littler & Littler, 1988). Whereas *Padina* is often found towards the inner reef flat, where wave action is reduced (Morrissey, 1980). However, these analyses generalize across any alongshore or other gradients that may also be present. While zonation of macroalgae across reef flats has been documented elsewhere (Morrissey, 1980; Pichon & Morrissey, 1982), an increase in the abundance and extent of these species through time could indicate changes in the reef ecosystem from anthropogenic activities on land, sea and in the atmosphere.

Linear regressions showed clear patterns in the mean percentage cover of reef flat transects concerning alongshore gradients. The macroalgae *Sargassum* (Figure 36) and *Padina* (Figure 37) exhibited a decrease in mean percentage cover with proximity to the river, whereas

seagrass (Figure 38) and coral rubble (Figure 40) demonstrated an increase in mean percentage cover with distance from the river. Outlying points of slightly higher cover of *Padina* and seagrass at the greatest distances from the river indicate that these relationships may not extend beyond the sampling area and other possible influences, such as the presence of inshore lagoons and creeks may begin to have an effect. Linear regressions of the mean values for reef flat substrata in response to distance to the river were used instead of CHAID, as the transects occurred at a few discrete intervals along the shoreline, providing too few data points for CHAID, and biasing such a classification towards the distances of the chosen transect locations.

Although there were no statistical relationships for reef crest substrata and biota with distance to the river, the number and length of these transects were relatively small. Spatial patterns along the reef crest are being assessed from another larger continuous data set along the reef crest on either side of the river (McNie, 2020).

There were, however, strong spatial correlations for several reef flat substrata and biota with distance to the river at Vavanga. This does not necessarily imply a causal relationship and the decreases in macroalgae and increases in seagrass with distance to the river may be due to other influences including other sources of freshwater, natural transport and deposition of sand and other sediments, human activities in the village, the log processing site near the catchment, a combination of the above or other influences. To reliably determine the processes responsible, adverse, or otherwise, requires additional evidence. This could be provided by replicate studies at other river mouths and villages, monitoring of water quality, estimation of trends through repeated measurements in time and, where possible, experiments to exclude alternative hypotheses (Albert et al., 2008; Cabaco et al., 2013; Fabricius et al., 2005; Schaffelke et al., 2005).

4.2 Significance, success and limitations of the research

This research involved the use of a novel UAV FMV technique recently developed at AUT by one of the project's supervisors, Hinchliffe, to map and quantify fine-scale spatial patterns and zones in benthic biota and substrata across the southern reef flat near Vavanga village,

Solomon Islands. The following section provides an evaluation of the significance and successes of the study as well as its limitations.

4.2.1 Unoccupied Aerial Vehicle (UAV) Full Motion Video (FMV)

This study successfully used synchronous underwater video footage and UAV FMV to map the percentage cover of substrata and biota across the southern Vavanga reef flat, using ArcGIS Pro software. This innovative approach, developed by Hinchliffe as part of his working PhD, is one of the limited studies currently employing drone imagery at the consumer level for coastal marine research (Duffy, 2018). Postgraduate projects supervised by Hinchliffe (MacNie, 2020; Patterson, 2021; Whittaker, 2021), developed and applied these methods to temperate and coral reef environments, and in other applications such as tracking waves, wave energy, and surfers, using FMV drone imagery (Quilter, 2023). This study refined the field techniques and data analyses from these studies and efficiently mapped approximately 0.4km^2 of the reef flat south of Vavanga village with additional, yet-to-be-analysed data, acquired for a similar area to the north of the river mouth.

While MacNie (2020) acquired FMV-tracked underwater video estimates of the percentage cover of substrata and biota along the narrow reef crest in front of Vavanga, this study aimed to map the much broader area of the reef flat to quantify changes in substrata and biota composition between the shore and the reef crest and at increasing distances from the river and village.

By incorporating synchronized underwater video with geocoded UAV FMV, we were able to produce an accurate (within 2m) subtidal map of georeferenced transects displaying the distribution of substrata and biota identified at a range of classification and taxonomic levels. The use of UAV imagery also allowed us to create high-resolution (2.5cm pixels) aerial photo orthomosaics of the survey area, providing a much higher level of detail compared to what is currently publicly available for the Vavanga reef area. The anticipated outcomes of this project were achieved successfully, yielding precise images, maps, and statistical models of the subtidal area.

4.2.1.1 Time-efficiency

The use of a Sublue Whiteshark MixPro underwater scooter greatly reduced the time taken to film underwater transects along the southern reef flat. The device allowed the snorkeler to conserve significant amounts of energy, as minimal effort was exerted while being towed across the surface. The buoyancy of the device also assisted the snorkeler in remaining at a relatively consistent distance from the seafloor (<1m). The time taken to video a transect beginning at the shore, out to the reef crest, and back, took an average of 20 minutes. This covered an approximate distance of 600m. At this speed, a typical 50m transect would therefore take approximately 1.7 minutes. Comparatively, Leujak and Orman (2007) took 10 minutes to film along a 50m transect on SCUBA. Using the photo line-intercept and photo-quadrat method, Nakajima et al. (2010) found the time taken to photograph 20 points along five 10m transects took approximately 50 minutes of dive time. With the use of a tow camera, Cresswell et al., (2021), were able to complete a 50m transect in 2.5 minutes, proving to be a slightly slower method of collecting underwater footage. Thus, highlighting video transects with the additional use of an underwater scooter provides a highly time-efficient method for collecting subsurface video data.

However, the pre-processing and analysis of each underwater video frame took a considerable amount of time. This approach although particularly efficient in the field, still required a substantial amount of human time and skill to visually identify and record substrata and biota in the extracted underwater frames. For the reef flat south of Vavanga, the UAV FMV technique extracted 1,396 georeferenced underwater images along 14 transects, and on each image, the substrata or biota under each of the ten points was recorded manually in ArcGIS Pro. This required a significant amount of time and skill in taxonomy to interpret images taken from a moving camera. The analysis of the video frames and data entry into ArcGIS Pro ranged from 2-3 minutes per photo (except where the identification of cryptic species was difficult, or images were blurred). This was very similar to the time taken by Nakajima et al. (2010) to analyse each image using the photo line-intercept method, however, much faster than that of the photo quadrat method (10-15 minutes per quadrat). A total of 1,396 photos were analysed, bringing the total time for identification of substrata and biota to approximately 46-70 hours. However, if the time taken to only analyse 100 images (3-5 hours), and the time required to video 100m

(approximately. 3 minutes) is considered, the total time taken to collect and analyse the data was much faster than that of the photo quadrat method undertaken by Nakajima et al. (2010) (17-26 hours). The use of machine-learning algorithms to classify georeferenced underwater images has the potential to further reduce manual analysis time, and this method is explored and discussed in more detail below.

4.2.1.2 Spatial accuracy

The UAV photo orthomosaics were created based on the UAV internal GPS signal at the time of each UgCS flight, which has an accuracy level of approximately 1m. Although all UAV data was collected with the same equipment across the sampling period, GPS conditions changed quickly, therefore each UAV flight had a slightly different GPS signal at the time of data collection. This has resulted in slight offsets (within 1m) between the photo orthomosaic layers and all FMV flights. Ground control points with an accurate GPS reading were not collected in the field as we were unable to put down static markers across the water. To further improve the absolute accuracy of the photo orthomosaic, it would have been beneficial to swim, wade or kayak out into the water with a GPS attached to a pole and record the GPS coordinates of visible objects such as large distinctive rocks or coral. As the photo orthomosaic has such a high resolution (2.5cm pixel size), obvious submerged objects can be seen within the images, and can therefore be used as ground control points when georeferencing the mosaic in ArcGIS Pro.

A slight spatial offset was seen in the positioning of the photo orthomosaic and the digitized transect points, likely due to a combination of the difference in GPS signals at the time of each UAV flight, and the adjusted heading direction and GPS offset variables used in the telemetry processing steps, creating some innate error in positional accuracy. Although these offsets were within 1m, such discrepancies may be an issue when using georeferenced underwater imagery to train and validate classifications across the photo orthomosaic. A potential solution to this issue is discussed further below.

4.2.1.3 Benefits of spatially referenced photo orthomosaics and transects

Most estimates of benthic cover and other measures of reef substrata and associated biota have, in the past, been derived from randomly sampling the area of interest with replicate

sampling units (e.g. quadrats or belt or line transects) without spatial referencing at a scale finer than the start and end of transects or the general position of the overall site (Bouchon, 1981; Dean et al., 2015; Morrissey, 1981; Pichon & Morrissey, 1982). Estimates of, for example, percentage cover, are averaged or summed for each replicate sample unit (e.g. transect) and then the mean of all transects for the area, and an estimate of the differences among transects (e.g. standard error), provides a summary measure for the whole area (Bull, 1982).

However, point or line intercepts along a line or belt transect can provide important information on the spatial distribution of zones, gradients, and patches and also data on coral size, number of recruits and species associations (Bouchon, 1981; Bull, 1982; Dean, 2015; Morrissey, 1981). Without fine-scale georeferencing this information is subsumed into a single averaged value for each sample unit (e.g. transect) and then into a single mean for the area of interest. Sampling areas can be stratified into smaller areas according to categorical factors based on habitat, population density and other variables either of interest, or likely to be a source of potential confounding. In this study, for example, data were assigned to two types of habitats, the reef crest and reef flat, but the summary statistics for even these factors have a relatively low spatial resolution compared to the many spatially referenced point estimates made within transects.

With UAV FMV georeferencing of underwater video, this fine-scale information is not lost but is made available to be mapped and modelled using a range of spatial statistics and other modelling techniques. This study demonstrated several novel quantitative approaches to evaluating, modelling, and presenting complex spatial data for coral reef habitats and species. In terms of interpretation, the high-resolution, photo orthomosaic of the Vavanga reef flat provided a visually intuitive understanding of spatial patterns in reef benthos.

As the photo orthomosaic is georeferenced it can be directly compared with other spatial data and importantly, compared with future imagery of the same area. Change detection tools in ArcGIS Pro would allow pixels in the photo orthomosaic captured in this study to be compared to mosaics generated in future years to accurately measure changes in spatial distributions. This potential is enhanced by the ability to now identify differences in colour

composition on the photo orthomosaic as different substrata and biota are visible on fine-scale underwater video at the same locations.

While the human eye and brain are good at detecting patterns, they can also appear to detect patterns where none exists. While there were visible differences evident in substrata and biota across the reef flat from the crest to the shore, classification and regression trees were able to delineate where, in distance from the reef crest, the main differences in mean percentage cover occurred statistically. These were used to map zones of varying abundance across the reef flat for seagrass, sand, macroalgae (including *Sargassum*, *Padina* and *Turbinaria*), hard coral, coral rock, and coral rubble, and these predicted values corresponded well with the original data points overlayed.

4.2.1.4 Potential limitations of the sampling technique

The spatial resolution of individual georeferenced frames was fit for the purpose of mapping spatial patterns, zones and gradients in reef flat substrata and biota, and provided more detailed information on the reef flat and crest than could be provided by means and standard errors over whole habitats. This information is important, particularly when comparing this data with other reef flats. A potential issue is that the sampling techniques used here, while geospatially efficient, sampled in an approximately systematic way along cross-shore transects at haphazard distances along the coastline, with some random variation due to water access, the inability to follow a compass underwater, issues with snorkeling over the shallow breaking reef crest, and the effect of local currents or wind.

Statistical sampling assumes a random selection of sampling units to provide unbiased estimates of the mean and variance (Andrew & Mapstone, 2006). Means may be biased for example where systematic transects align or misalign with natural ridges or other regular features of greater or lower abundance and thus misrepresent the true population mean. This can be avoided if the researcher is aware of the correlation between landscape and transects.

However, in this study, one of the primary objectives was to quantify patterns in reef flat zonation along the gradient from the reef crest to the shore and at increasing distances from the river and village. For this, a more systematic sampling design was more likely to

consistently cover the entire area of interest and provide higher-resolution data for mapping. There were logistical challenges in trying to achieve random sampling in the shallow surf zones over the reef. This included the difficulty of covering extensive areas at a high resolution while dealing with constraints such as limited battery power and field time, all within varying tide and weather conditions.

For systematic sampling, it is important to note, that the smaller variance of the sample data and dependent standard errors, confidence limits and tests of significance are likely to be more liberal in detecting statistical significances (Type I error or false positive) than under a completely random sampling design (Andrew & Mapstone, 2006). The statistical tests should therefore be regarded cautiously and more in the spirit of hypothesis generation. However, for most of the tests in this study, the differences were large and evident from the sample data and maps alone.

It would be possible to estimate the reduced variance among haphazard or systematic sampling by randomly sub-sampling from the total data set or predicted model, and potentially also testing the efficiency of different numbers and sizes of sample units. This is a general issue in differences in sampling design between experimental statistical sampling and geospatial sampling that requires further research, as there are benefits from both.

4.2.2 Automated underwater image classification with ReefCloud.AI

To reduce the effort required to manually identify substrata and biota on underwater video, the ReefCloud.AI deep learning image recognition software was trialed on a subset of 260 images and found to be moderately successful in identifying broad categories of substrata and some species. However, this is a rapidly developing field and the more outputs that are used to train the software, the more accurate it potentially becomes (ReefCloud, 2024). An accuracy assessment of the ability of ReefCloud to classify substrata and biota at a main substrate and species level was initially completed for 100% of the images classified in ReefCloud. However, this resulted in some species and substrate types returning a 100% accuracy level even when minimal training points were evident. This led me to believe the use of the bulk upload where 50% of the images were uploaded with their predetermined

human classifications caused an error in the machine learning algorithm and an overestimation of ReefCloud AI accuracy.

Thus, the actual accuracy of the machine learning software was determined by assessing the last 20% of images that were left with no human classifications. Although the overall accuracy of the ReefCloud AI was 69% at the main substrata level (Table 7), the classification success rate when compared to human identification varied greatly, between 0% (algae) to 94% (seagrass). The substrata most reliably identified by ReefCloud.AI were seagrass (94%), sand (79%) and hard coral (69%).

When based on a species level, the overall accuracy of the ReefCloud AI decreased slightly to 63% (Table 6), and again, a large variation in individual accuracies was seen ranging from 0% (algae, *Halimeda, Acropora clathrata, A. millepora,* and *Porites annae*) to 94% (seagrass). The substrata or biota most reliably identified by ReefCloud.AI was seagrass (94%) and fine sand (70%).

When substrate types such as macroalgae or hard coral were split into individual species categories, classification accuracy was often much lower. These inaccuracies were most likely due to the lack of training data. For example, the classification accuracy of coral species ranged from 0% to 50%, however, from the total 260 images uploaded into ReefCloud, the number of training points available for these species ranged between 2-58, which is relatively low. As this method was only trialed on a small subset of images, the machine learning algorithm lacked sufficient training on many of the less abundant species and substrate types, leading to many misclassifications. The macroalgal species *Padina* yielded a very low accuracy of 15%, as it was commonly misclassified as fine sand. This was likely due to the very similar colouration of both substrate types, which would suggest more training is necessary to yield a higher classification accuracy in this class. Some of the misclassifications may have also occurred due to image quality issues. A few of the frames extracted from the underwater video were blurred due to camera movement, which would have made classification more difficult for the machine, compared to using the human eye along with adequate field and taxa knowledge. Thus, the use of a much larger dataset, where extra training is focused on less abundant categories, would likely yield much better

results. Ensuring all images uploaded into ReefCloud are of sufficient quality, and equally distanced from the substrata, would likely further increase the machine learning accuracy.

Depending on objectives and the level of detail required, the results from this study still suggest that deep learning algorithms like ReefCloud.AI are potentially useful tools, especially where many images are analysed from across large areas or from source imagery obtained through citizen science.

4.2.3 Object-based image analysis of the aerial drone photo orthomosaic

The drone photo orthomosaic of the reef combined with estimates of percentage cover from georeferenced underwater video frames potentially provides the most detailed and spatially precise description of reef flat habitats. The high resolution of the photo orthomosaic meant that the image could be segmented according to object-based spatial and spectral resolution, and segment size. The many georeferenced underwater point estimates of percentage cover also provided a very large dataset to train and ground truth in the classification of these segments.

However, the spatial complexity and interspersion of different substrata and biota at fine spatial scales, even when grouped as combinations of substrate types, resulted in a range of inaccuracies for classification predictions when compared to test data withheld from the classification model. Although the overall classification success (71%) and the percentage accuracies for the coral/coral rock mix and sand/algal mix were reasonably high, percentage accuracies for the dense seagrass, coral rock/algal mix, macroalgae and sparse seagrass categories were surprisingly low (Table 8).

This may have been due to the high amount of complexity and mixing of categories at fine spatial scales, the suitability of the classification algorithm used, or the limitations of RGB imagery. Tait et al. (2019) found slightly higher levels of classification accuracy when using the same support vector machine (SVM) classification algorithm, to classify 3-band (RGB) UAV imagery of intertidal and shallow subtidal macroalgae habitats. The UAV imagery was collected during the lowest tide series of the month; however, they highlighted that increasing water depth caused a dampening of spectral signals, which only allowed the detection of taxonomically broad submerged algal classes. As our data was collected during

moderate to high tide during the day (low tide occurred at midnight during this time of year), the water depth of >1m, as well as its rippling effect across the surface, would have likely caused much of the spectral confusion between classes. When combining the broad spectral ranges of the RGB bands and the narrow multispectral bands, misclassification between macroalgal classes was greatly reduced for Tait et al. (2019). Thus, it would be beneficial to trial the combination of RGB and multispectral cameras at extremely low tides, when collecting UAV imagery across shallow reef flats.

Additionally, the positional accuracy of the point estimates, which at the scale of the photo orthomosaic pixels, would only need to be slightly in error for boundary mismatches between the mosaic and underwater estimates to occur. Slight positional offsets were found in this study, as the digitized transect points that ran through the classified raster had an average offset distance of 0.89m and bearing of 138.03°, compared to their adjusted position. To ensure the classification can be trained with accurately positioned ground truth points, these offsets need to be minimised. Instead of digitizing the transect points in FMV, an alternative step could be to extract UAV images every three or so seconds along the transects. This could be done using the same FFMPEG script maker used to extract the GoPro frames along each transect. These images could then be inserted into the map as raster files, and auto georeferenced to the photo orthomosaic within ArcGIS Pro. The position of the underwater scooter could then be digitized along the transects using these georeferenced images. This would ensure high positional accuracy of the underwater video frames that could be used to train and validate the classification.

To improve the classification outcomes, potential solutions include trialing alternative classification algorithms of which there are several within ArcGIS Pro and other software including Trimble eCognition; generating photo orthomosaics from photos taken at extremely low tides; using multispectral drone cameras; varying the resolution of the mosaic and the maximum segment size; and trialing the analysis on a larger portion of the data.

4.3 Areas for further research and potential applications

Spatially enabling underwater video data permits a wide range of spatial statistics and models to be applied which has rarely been possible for underwater data. Examples included the analysis of spatial autocorrelation to define and map gradients and patches of different sizes and scales, determining connectivity among individuals, colonies, species and patches and the analysis of point pattern processes (De'ath & Fabricius, 2000; Kerrigan et al., 2010; McArdle & Blackwell, 1989).

Spatial autocorrelation compares the degree of similarity (or correlation) between points at increasing distances apart. McArdle and Blackwell (1989) for example, mapped a two-dimensional autocorrelogram and contours of the spatial distribution of New Zealand cockles (*Chione stutchburyi*). Legendre (1993) demonstrated how unexplained variance in experimental and survey results is often spatially correlated, indicating the presence of unknown influential variables, and that including space as a potential explanatory variable can improve the performance of Analysis of Variance for example. In classifying soft coral communities, De'ath and Fabricius (2000) found that including space as a variable (distance across and along the Great Barrier Reef) was significantly more effective in explaining patterns in species composition than distance to rivers, coast, or turbidity.

Given the taxonomic resolution of the data in this study and its spatial georeferencing, there is potential to use the methods described in Kerrigan et al. (2010) to map multivariate patterns in species composition on the fringing reef at Vavanga. While percentage cover for most individual genera and species at Vavanga and elsewhere is generally low, multivariate analyses of community composition are often more effective using presence/absence data. Using presence/absence, rather than abundance, can avoid more abundant biota and species dominating analyses and allow less abundant species and sites to help define communities and species assemblages (Kerrigan et al., 2010).

The synchronized UAV FMV and underwater data collected in this study data should be analysed in more detail using multivariate methods such as described in De'ath and Fabricius (2000) and Kerrigan et al. (2010). Multivariate classification and regression trees can reliably detect differences in community species composition in response to both continuous and categorical environmental explanatory variables (De'ath & Fabricius, 2000;

Kerrigan et al., 2010). In this study, CHAID classification and regression trees were applied to univariate response data for different substrata and biota separately, to delineate spatial zones in percentage cover across the reef flat. Multivariate analyses avoid issues with multiple tests inflating Type I errors (false positive results) and can be more powerful in detecting patterns from multiple variables. This approach could be extended to include combinations of other spatial and environmental explanatory variables such as distance to the river, levels of sedimentation, and inclusion in flood plumes.

Classification and regression trees offer numerous benefits, including the ability to handle extensive datasets and missing values. They are distribution-free and are capable of modelling complex interactions among categorical and interval predictor and response variables (De'ath & Fabricius, 2000, Kerrigan et al., 2010). Moreover, regression trees can identify data splits based on the information present in the dataset, rather than relying on preconceived categories. They can also model multivariate responses from multiple biota to uncover subtle changes in species assemblages and community composition. De'ath and Fabricius (2000) and Fabricius et al. (2023) used univariate and multivariate classification and regression trees to investigate differences in the abundance and species composition of soft corals and macroalgae as a function of distance to rivers, the coast, and turbidity.

Kerrigan et al. (2010) used two spatial, explanatory variables to create draft bioregions from point estimates of the occurrence of hard and soft coral, algae, fish, and sponge species. The spatial regression variables used to delineate bioregions with the most similar species composition were the proportional distances of sample points across the Great Barrier Reef (between 0 and 1) and along the north-west to south-east axis of the entire reef (0 at the northernmost reefs, 1 at the southernmost reefs). These spatially defined bioregions were used as the basis for expert workshops, consultation, and in 2004, increasing the area of no-take, marine reserve 'Marine National Park' and no-entry 'Preservation zones' on the Great Barrier Reef from 6-33% of the World Heritage Area (Day et al., 2002; Fernandes et al., 2005; Kerrigan et al., 2010).

These marine reserves were replicated within and across over 70 representative habitats and species communities to optimize biodiversity representation and meet reserve design principles including their size, shape, number, distance apart, connectivity, efficiency and

complementarity with other reserves and marine park users (Day et al., 2002; Fernandes et al., 2005).

The development of bioregions and finer scale classifications from underwater video synchronized with UAV FMV and other data would inform the development of more effective customary management, fisheries, aquaculture, networks of protected areas and marine spatial planning in the Solomons and elsewhere. Knowledge of the spatial distribution of marine biodiversity is key to planning for conservation, food security and climate change, and underwater video synchronized with UAV FMV can provide this at spatial resolutions most relevant to local communities.

Game et al. (2010) described how a conservation planning process was developed for the Choiseul Province, that combined community-driven conservation opportunities with a systematic and representation-based approach to prioritisation. The combination of community involvement in the form of participatory mapping (Game et al., 2010), with the addition of spatially defined ecological regions, would ensure that the protected areas identified within each bioregion encompassed a diverse range of ecosystems, species, and processes, providing a more comprehensive representation of the region's biodiversity.

The use of geospatially referenced transects from UAV FMV provides a less invasive alternative to traditional fixed transects (Albert et al., 2014; Bouchon, 1981; Brown et al., 2002), as this allows researchers to return to the same location and repeat the transects undertaken, for example, in this study, without the use of artificial markers such as pegs, stakes or fishing line.

Additionally, resampling similar transects at successive intervals provides more precise estimates of changes through time. This can occur because repeated measures analyses compare sites based on how each transect within each site changes through time relative to how other transects behave through time. Whereas, when new random transects are sampled at each time interval, changes in mean values through time are assessed based on the spatial variation among the transects. In spatially heterogeneous (patchy) environments, this variation can be high, resulting in low precision and low power to detect temporal changes. For example, the techniques trialed here could be seamlessly reapplied to the

same area in 10 years' time. Similar transects across the reef flat could be repeated based on the GPS coordinates collected in this study. This would provide a temporal approach to accurately detect changes in substrate cover, coral diversity, and species assemblages, as well as detect potential increases in coral bleaching and mortality over time.

As part of the 'Building Social and Ecological Resilience to Climate Change in Roviana, Solomon Islands' report, Albert et al. (2012) created habitat maps across the Vonavona-Roviana lagoon complex, using an object-based image analysis of high-resolution Quickbird satellite imagery. Additionally, they conducted a coral bleaching and disease assessment to better understand and predict potential coral disease outbreaks due to climate change and other impacts.

47 50m video transects were surveyed across the area, and coral genera along with diseases and syndromes were identified under 15 points within 20 frames for each transect. The general position of each site was recorded using GPS coordinates; however, no specific spatial referencing was conducted on individual transects. As these transects were not spatially referenced, the accuracy of detecting temporal changes in coral disease and bleaching due to climate change will likely be low if new random transects were to occur across the same area in future years. Therefore, it may be beneficial to apply the methodology trialed in this study to conduct assessments such as these in the future, as it can provide a more precise estimate of change through time.

When a satisfactory level of classification accuracy is achieved, there exists significant potential for deep learning algorithms like ReefCloud AI to substantially reduce the current manual labour required for classifying georeferenced underwater images extracted along transects. Although not completed in this study due to time constraints, ReefCloud's classifications can be linked back to the extracted images using their corresponding MissionID in ArcGIS Pro. Utilizing ReefCloud for classifying all images along the southern reef flat, or elsewhere, would result in a remarkable reduction in image analysis time.

Quilter (2023) explored the potential of employing deep-learning object detection models and FMV for tracking surfers in drone video. These methods could be further refined and applied to this study for tracking the snorkeler and underwater scooter and mapping their

transect paths within ArcGIS Pro. The incorporation of deep learning models has the potential to fully automate this process in future studies.

The potential application of the synchronised video approach is substantial given that organisations like the Australian Institute of Marine Science (AIMS) re-sample hundreds of marked benthic transects every year (Emslie et al., 2020; English et al., 1998). This information is used to regularly monitor the condition of reefs over thousands of kilometres and support management for protected areas, threatened species, fisheries, land use, coral bleaching, and other effects of climate change (Day et al., 2000; Emslie et al., 2020; Fernandes et al., 2009; Mellin et al., 2020).

The institute also conducts broader scale, manta tow surveys of these reefs by slowly towing an observer on snorkel behind a small boat. The diver propulsion vehicle used in this study provided a more precisely controlled survey platform and higher taxonomic resolution, while still covering a substantial, albeit smaller area. As the video captured by the methods can be analysed later by trained observers, there is the potential to train field and video observers and adapt these techniques to many reef areas throughout the Pacific and elsewhere.

Geospatially referenced transects provide an accurate time-efficient approach to coral reef monitoring that could be applied across many reef systems globally. For example, the spatially referenced data collected through UAV FMV could be used to help monitor the effects of logging on the health and composition of fringing coral reefs. Kolombangara Island may be of particular importance, as extensive logging has already occurred across the island since the early 2000s. Wenger et al. (2019) used prediction models to assess the effects of sediment runoff from current land use and logging activity on downstream coral reef conditions and fisheries, using Kolombangara Island as a case study.

The model found current land use resulted in declines in live and branching coral cover, and fish grazer abundance and biomass, alongside increased turf algae, as a response to sediment runoff from catchments and log ponds. Even with best management practices at low clearing extents, 32% of reefs would still experience increased sediment exposure.

When clearing extent was increased, these practices became ineffective, putting 89% of coral reef areas at risk compared to unmanaged logging (Wenger et al., 2019).

If logging were to start up again near the Vavanga catchment, repeated surveys of the spatially referenced underwater transects would help validate and ground-truth predictions on the effects of logging on Kolombangara's fringing reefs and help inform communities, government, and industry of ways to avoid or mitigate adverse effects.

4.4 Conclusion

This study investigated the ability of novel UAV FMV techniques to effectively quantify the dynamics of habitat zonation across the Vavanga southern reef flat on Kolombangara Island, Solomon Islands. Throughout a two-week field trip between 2nd – 16th December 2022, UAV photography, FMV and underwater video transects were collected across the reef flat using an underwater propulsion device. The resulting data was then combined to create georeferenced transects across the entire area using the ArcGIS Pro FMV Image Analyst extension. A total of 1,396 georeferenced underwater images along 14 transects were extracted, and on each image, the substrate or biota under each of the ten points was recorded manually in ArcGIS Pro. Additionally, high-resolution UAV imagery was utilised to create highly detailed, spatially accurate photo orthomosaics across the survey area. Months of analysis resulted in detailed subtidal maps displaying the distribution of substrate types at Vavanga, across multiple classification levels. A combination of summary statistics, simple linear regressions, and classification and regression trees revealed some interesting patterns and obvious differences in the distribution of reef flat and reef crest substrata and biota. The combination of synchronous UAV FMV and underwater imagery successfully achieved the anticipated outcomes of this project, yielding precise images, maps, and statistical models of the subtidal area.

The classifying ability of the image recognition software, ReefCloud.AI, was assessed using a subset of 260 georeferenced images. Although the overall accuracy of ReefCloud and individual accuracies across some broad categories of substrata and biota were moderately high, classification accuracies were still highly variable for many of the less common

categories. The use of a much larger dataset, with training focused on less abundant and inconspicuous substrata and biota would likely yield much better results.

Additionally, a sample from the high-resolution drone photo orthomosaic was analysed using object-based image segmentation and classification, with validation from georeferenced underwater imagery. Classification accuracies varied across the selected classes, likely due to the high amount of complexity and mixing of categories at such a fine spatial scale, water depth and movement across the surface, and possible limitations of RGB imagery. Trialing alternative classification algorithms, and the collection of multispectral imagery across the reef flat at an extremely low tide may result in increased accuracies across the classification.

UAV FMV paired with synchronized underwater video transects provided a spatially accurate, non-invasive, time-efficient alternative to traditional reef surveying techniques. This innovative approach allows for the application of many spatial statistics and models, providing insights into the intricate patterns and dynamics of coral reef ecosystems. This study has highlighted a broad range of potential applications and avenues for further research. Overall, this research has contributed to the development of effective subtidal surveying and mapping techniques that will enhance our ability to make informed decisions around ecosystem-based management and conservation and assist in the monitoring of coral reef health in response to continued anthropogenic pressures and climate change.

5 References

Aalbersberg, B., Avosa, M., James, R., Kaluwin, C., Lokani, P., Opu, J., Siwatibau, S., Tuiwawa, M., Waqa-Sakiti, H., & Tordoff, A. W. (2012). *Ecosystem Profile: East Melanesian Islands Biodiversity Hotspot*. University of the South Pacific [Professional and Technical Reports]. http://www.cepf.net/SiteCollectionDocuments/east_melanesian_islands/EMI_ecosystem_profile.pdf

Adams, A. J., Dahlgren, C. P., Kellison, G. T., Kendall, M. S., Layman, C. A., Ley, J. A., Nagelkerken, I., & Serafy, J. E. (2006). Nursery function of tropical back-reef systems. *Marine Ecology Progress Series*, *318*, 287–301. https://doi.org/10.3354/meps318287

Ahmad, W., & Neil, D. T. (1994). An evaluation of landsat thematic mapper (TM) digital data for discriminating coral reef zonation: Heron reef (GBR). *International Journal of Remote Sensing*, *15*(13), 2583–2597. https://doi.org/10.1080/01431169408954268

Ainsworth, T. D., Heron, S. F., Ortiz, J. C., Mumby, P. J., Grech, A., Ogawa, D., Eakin, C. M., & Leggat, W. (2016). Climate change disables coral bleaching protection on the Great Barrier Reef. *Science*, *352*(6283), 338–342. https://doi.org/10.1126/science.aac7125

Albert, S., Grinham, A., Bythell, J., Olds, A., Schwarz, A., Abernethy, K., Aranani, K., Sirikolo, M., Watoto, C., Duke, N., McKenzie, J., Roelfsema, C., Liggins, L., Brokovich, E., Pantose, O., Oeta, J., & Gibbes, B. (2012). *Building social and ecological resilience to climate change in Roviana, Solomon Islands*. The University of Queensland. http://epic.awi.de/35284/1/pasap-solomons.pdf

Albert, S., Grinham, A., Gibbes, B., Tibbetts, I., Udy, J. (2014). Indicators of coral reef ecosystem recovery following reduction in logging and implementation of community-based management schemes in the Solomon Islands. *Pacific Conservation Biology, 20*(1), 75–85. https://doi.org/10.1071/PC140075

Albert, S., Udy, J., & Tibbetts, I. R. (2008). Responses of algal communities to gradients in herbivore biomass and water quality in Marovo Lagoon, Solomon Islands. *Coral Reefs, 27*, 73–82. https://doi.org/10.1007/s00338-007-0292-0

Andrew, N. L., & Mapstone, B. D. (2006). Sampling and the description of spatial pattern in marine ecology. In H. Barnes & M. Barnes (Eds.), *Oceanography and Marine Biology: An annual review* (pp. 26–69). Aberdeen University Press. https://books.google.co.nz/books?hl=en&lr=&id=OKFt7CCF-jkC&oi=fnd&pg=PA26&dq=andrew+and+mapstone&ots=O_zdRe1Sj1&sig=Jl6NupoGhrbvv_MD8mekSTzMWHc&redir_esc=y#v=onepage&q=andrew%20and%20mapstone&f=false

Australian Institute of Marine Science (AIMS). (2022). *ReefCloud.AI* [Image recognition software]. https://reefcloud.ai/

Baker, R., & Sheaves, M. (2007). Shallow-water refuge paradigm: conflicting evidence from tethering experiments in a tropical estuary. *Marine Ecology Progress Series*, *349*, 13–22. https://doi.org/10.3354/meps07102

Bell, J. D., Kronen, M., Vunisea, A., Nash, W. J., Keeble, G., Demmke, A., Pontifex, S., & Andréfouët, S.

(2009). Planning the use of fish for food security in the Pacific. *Marine Policy*, *33*(1), 64–76. https://doi.org/10.1016/j.marpol.2008.04.002

Bellwood, D. R., Tebbett, S. B., Bellwood, O., Mihalitsis, M., Morais, R. A., Streit, R. P., & Fulton, C. J. (2018). The role of the reef flat in coral reef trophodynamics: past, present, and future. *Ecology and Evolution*, *8*(8), 4108–4119. https://doi.org/10.1002/ece3.3967

Bohnsack, J. A. (1979). Photographic quantitative sampling of hard-bottom benthic communities. *Bulletin of Marine Science*, *29*(2), 242–252.

Bouchon, C. (1981). Quantitative study of the scleractinian coral communities of a fringing reef of Reunion Island (Indian Ocean). *Marine Ecology Progress Series*, *4*, 273–288. https://doi.org/10.3354/meps004273

Brander, R. W., Kench, P. S., & Hart, D. (2004). Spatial and temporal variations in wave characteristics across a reef platform, Warraber Island, Torres Strait, Australia. *Marine Geology*, *207*(1–4), 169–184. https://doi.org/10.1016/j.margeo.2004.03.014

Brown, B. E., Clarke, K. R., & Warwick, R. M. (2002). Serial patterns of biodiversity change in corals across shallow reef flats in Ko Phuket, Thailand, due to the effects of local (sedimentation) and regional (climatic) perturbations. *Marine Biology, 141*, 21–29. https://doi.org/ 10.1007/s00227-002-0810-0

Bull, G. (1982). Scleractinian coral communities of two inshore high island fringing reefs at Magnetic Island, North Queensland. *Marine Ecology Progress Series*, *7*, 267–272. https://doi.org/10.3354/meps007267

Burke, L., Reytar, K., Spalding, M., & Perry, A. (2011). *Reefs at risk: Revisited.* World Resources Institute (WRI). https://bvearmb.do/handle/123456789/1787

Cabaitan, P. C., Licuanan, W. Y., & Gomez, E. D. (2007). Comparison between videographic and photographic methods in assessing coral reef benthic communities. *Science Diliman*, *19*(1), 7–13. https://www.researchgate.net/profile/Wilfredo-Licuanan/publication/228723612_Comparison_Between_Videographic_and_Photographic_Methods_in_Assessing_Coral_Reef_Bethnic_Communities/links/552507080cf2b123c5176af3/Comparison-Between-Videographic-and-Photographic-Methods-in-Assessing-Coral-Reef-Bethnic-Communities.pdf

Carleton, J. H., & Done, T. J. (1995). Quantitative video sampling of coral reef benthos: large-scale application. *Coral Reefs, 14,* 35–46.

Casella, E., Collin, A., Harris, D., Ferse, S., Bejarano, S., Parravicini, V., Hench, J. L., & Rovere, A. (2017). Mapping coral reefs using consumer-grade drones and structure from motion photogrammery techniques. *Coral reefs, 36,* 269–275. https://doi.org/ 10.1007/s00338-016-1522-0

Chirayath, V., & Earle, S. A. (2016). Drones that sea through waves - preliminary results from airborne fluid lensing for centimetre-scale aquatic conservation. *Aquatic Conservation: Marine and Freshwater Ecosystems, 26*(2), 237–250. https://doi.org/ 10.1002/aqc.2654

Chirayath, V., & Instrella, R. (2019). Fluid lensing and machine learning for centimeter-resolution airborne assessment of coral reefs in American Samoa. *Remote Sensing of Environment*, *235*, 111475. https://doi.org/10.1016/j.rse.2019.111475

Colombo-Pallotta, M. F., Rodríguez-Román, A., & Iglesias-Prieto, R. (2010). Calcification in bleached and unbleached Montastraea faveolata: evaluating the role of oxygen and glycerol. *Coral Reefs*, *29*(4), 899–907. https://doi.org/10.1007/s00338-010-0638-x

Colomina, I. & Molina, P. (2014). Unmanned aerial systems for photogrammetry and remote sensing: a review. *ISPRS Journal of Photgrammetry and Remote Sensing, 92*, 79–97. http://dx.doi.org/10.1016/j.isprsjprs.2014.02.013

Cresswell, A. K., Ryan, N. M., Heyward, A. J., Smith, A. N. H., Colquhoun, J., Case, M., Birt, M. J., Chinkin, M., Wyatt, M., Radford, B., Costello, P., & Gilmour, J. P. (2021). A quantitative comparison of towed-camera and diver-camera transects for monitoring coral reefs. *PeerJ*, *9*, 1–21. https://doi.org/10.7717/peerj.11090

Davis, J. P., Pitt, K. A., Olds, A. D., Harborne, A. R., & Connolly, R. M. (2017). Seagrass corridors and tidal state modify how fish use habitats on intertidal coral reef flats. *Marine Ecology Progress Series*, *581*, 135–147. https://doi.org/10.3354/meps12311

Day, J., Fernandes, L., Lewis, A., De'ath, G., Slegers, S., Barnett, B., Kerrigan, B., Breen, D., Innes, J., Oliver, J., Ward, T., & Lowe, D. (2000). The Representative Areas Program for protecting biodiversity in the Great Barrier Reef World Heritage Area. *Proceedings of the ninth international coral reef symposium*, 1–11. https://www.gbrmpa.gov.au/__data/assets/pdf_file/0020/6176/Final_ICRS_paper_Aug01.pdf

De'ath, G., & Fabricius, K. E. (2000). Classification and regression trees: a powerful yet simple technique for ecological data analysis. *Ecology, 81*(11), 3178–3192. https://www.jstor.org/stable/177409

De Guzman, A. B. (2019). Women in subsistence fisheries in the Philippines: the undervalued contribution of reef gleaning to food and nutrition security of coastal households. *Women in Fisheries Information Bulletin*, *29*, 34–40. https://spccfpstore1.blob.core.windows.net/digitallibrary-docs/files/03/03e783a46811f14656d4340dcc751775.pdf?sv=2015-12-11&sr=b&sig=kKb1Y8HJRVYULRwJ8y4Ms0f2TLi%2B5fPcncjYhW03rdo%3D&se=2019-10-05T13%3A46%3A15Z&sp=r&rscc=public%2C max-age%3D864000%2C ma

Dean, A. J., Steneck, R. S., Tager, D., & Pandolfi, J. M. (2015). Distribution, abundance and diversity of crustose coralline algae on the Great Barrier Reef. *Coral Reefs*, *34*(2), 581–594. https://doi.org/10.1007/s00338-015-1263-5

Deshmukh, B., Bahuguna, A., Nayak, S., Dhargalkar, V. K., Jagtap, T. G. (2005). Eco-geomorphological zonation of the Bangaram reef, Lakshadweep. *Journal of the Indian Society of Remote Sensing, 33*(1), 99–106. https://doi.org/10.1007/BF02989997

Done, T. J. (1982). Patterns in the distribution of coral communities across the central Great Barrier Reef. *Coral Reefs*, *1*(2), 95–107. https://doi.org/10.1007/BF00301691

Douglas, A. E. (2003). Coral bleaching - How and why? *Marine Pollution Bulletin*, *46*(4), 385–392. https://doi.org/10.1016/S0025-326X(03)00037-7

Duffy, J.P., Cunliffe, A.M., DeBell, L., Sandbrook, C., Wich, S.A., Shutler, J.D., Myers-Smith, I.H., Varela, M.R. & Anderson, K. (2018). Location, location, location: considerations when using lightweight drones in challenging environments. *Remote Sensing in Ecology and Conservation, 4*(1), pp.7–19. https://doi.org/10.1002/rse2.58

Emslie, M. J., Bray, P., Cheal, A. J., Johns, K. A., Osborne, K., Sinclair-Taylor, T., & Thompson, C. A. (2020). Decades of monitoring have informed the stewardship and ecological understanding of Australia's Great Barrier Reef. *Biological Conservation*, *252*, 108854. https://doi.org/10.1016/j.biocon.2020.108854

English, S., Wilkinson, C., & Baker, V. (Eds.) (1997). *Survey manual for tropical marine resources* (2nd ed.). Australian Institute of Marine Science.

Esri (n.d.). ArcGIS Pro: Introduction to Full Motion Video. https://pro.arcgis.com/en/pro-app/latest/help/analysis/image-analyst/introduction-to-full-motion-video-in-arcgis-pro.htm

Esri (n.d.). ArcGIS Pro: Train Support Vector Machine Classifier (Spatial Analyst). https://pro.arcgis.com/en/pro-app/latest/tool-reference/spatial-analyst/train-support-vector-machine-classifier.htm

Fabricius, K. E. (2011). Factors determining the resilience of coral reefs to eutrophication: a review and conceptual model. In Z. Dubinsky & N. Stambler (Eds.), C*oral reefs: An ecosystem in Transition* (pp.493–505). Springer. https://doi.org/10.1007/978-94-007-0114-4_28

Fabricius, K. E., Crossman, K., Jonker, M., Mongin, M., & Thompson, A. (2023). Macroalgal cover on coral reefs: spatial and environmental predictors, and decadal trends in the Great Barrier Reef. *PLoS ONE*, *18*, 1–21. https://doi.org/10.1371/journal.pone.0279699

Fabricius, K. E., De'ath, G., McCook, L., Turak, E., & Williams, D. M. (2005). Changes in algal, coral and fish assemblages along water quality gradients on the inshore Great Barrier Reef. *Marine Pollution Bulletin, 51,* 384–398. https://doi.org/ 10.1016/j.marpolbul.2004.10.041

Fabry, V. J., Seibel, B. A., Feely, R. A., & Orr, J. C. (2008). Impacts of ocean acidification on marine fauna and ecosystem processes. *ICES Journal of Marine Science, 65*, 414–432. https://doi.org/10.1093/icesjms/fsn048

Feely, R. A., Alin, S. R., Newton, J., Sabine, C. L., Warner, M., Devol, A., Krembs, C., & Maloy, C. (2010). The combined effects of ocean acidification, mixing, and respiration on pH and carbonate saturation in an urbanized estuary. *Estuarine, Coastal and Shelf Science*, *88*(4), 442–449. https://doi.org/10.1016/j.ecss.2010.05.004

Fernandes, L., Day, J., Kerrigan, B., Breen, D., De'ath, G., Mapstone, B., Coles, R., Done, T., Marsh, H., Poiner, I., Ward, T., Williams, D., & Kenchington, R. (2009). A process to design a network of marine no-take areas: Lessons from the Great Barrier Reef. *Ocean and Coastal Management*, *52*(8), 439–447. https://doi.org/10.1016/j.ocecoaman.2009.06.004

Fernandes, L., Day, J., Lewis, A., Slegers, S., Kerrigan, B., Breen, D., Cameron, D., Jago, B., Hall, J., Lowe, D., Innes, J., Tanzer, J., Chadwick, V., Thompson, L., Gorman, K., Simmons, M., Barnett, B., Sampson, K., De'Ath, G., Mapstone, B., … Stapleton, K. (2005). Establishing representative no-take areas in the Great Barrier Reef: large-scale implementation of theory on marine protected areas. *Conservation Biology, 19*(6), 1733–1744.

https://www.jstor.org/stable/3591195

Fong, P., & Paul, V. J. (2011). Coral reef algae. In Z. Dubinsky & N. Stambler (Eds.) *Coral reefs: An ecosystem in transition* (pp. 241–272). Springer. https://doi.org/10.1007/978-94-007-0114-4

Foster, S. D., Hosack, G. R., Hill, N. A., Barrett, N. S., & Lucieer, V. L. (2014). Choosing between strategies for designing surveys: autonomous underwater vehicles. *Methods in Ecology and Evolution*, *5*(3), 287–297. https://doi.org/10.1111/2041-210X.12156

Fulton, C. J., & Bellwood, D. R. (2005). Wave-induced water motion and the functional implications for coral reef fish assemblages. *Limnology and Oceanography, 50*(1), 255–264. https://www.jstor.org/stable/3597898

Game, E. T., Lipsett-Moore, G., Hamilton, R., Peterson, N., Kereseka, J., Atu, W., Watts, M., & Possingham, H. (2010). Informed opportunism for conservation planning in the Solomon Islands. *Conversation Letters, 4,* 38–46. https://doi.org/ 10.1111/j.1755-263X.2010.00140.x

Grech, A., & Coles, R. G. (2010). An ecosystem-scale predictive model of coastal seagrass distribution. *Aquatic Conservation: Marine and Freshwater Ecosystems, 20,* 437–444. https://doi.org/10.1002/aqc.1107

Green, A. L., & Mous, P. J. (2008). *Delineating the Coral Triangle , its ecoregions and functional seascapes* (Report No. 1/08). The Nature Conservancy, Coral Triangle Program. https://www.conservationgateway.org/Documents/Green%20and%20Mous%202008%20CT%20Delineation%20v5%200.pdf

Green, A., Lokani, P., Atu, W., Ramohia, P., Thomas, P., & Almany, J. (Eds.) (2006). *Solomon Islands marine assessment: Technical report of survey conducted May 13-June 17, 2004.* The Nature Conservancy. https://www.equatorinitiative.org/old/images/stories/2008winners/Arnavon_Committee/solomonislandsmarineassessmentreport-full.pdf

Green, E. P., Mumby, P. J., Edwards, A. J., & Clark, C. D. (1996). A review of remote sensing for the assessment and management of tropical coastal resources. *Coastal Management*, *24*(1), 1–40. https://doi.org/10.1080/08920759609362279

Harborne, A. R. (2013). The ecology, behaviour and physiology of fishes on coral reef flats, and the potential impacts of climate change. *Journal of Fish Biology*, *83*(3), 417–447.

https://doi.org/10.1111/jfb.12203

Hay, M. E., Colburn, T., & Downing, D. (1983). Spatial and temporal patterns in herbivory on a Caribbean fringing reef: the effects on plant distribution. *Oecologia, 58*(3), 299–308. https://www.jstor.org/stable/4217035

Hedley, J. D., Roelfsema, C., Brando, V., Giardino, C., Kutser, T., Phinn, S., Mumby, P. J., Barrilero, O., Laporte, J., & Koetz, B. (2018). Coral reef applications of Sentinel-2: Coverage, characteristics, bathymetry and benthic mapping with comparison to Landsat 8. *Remote Sensing of Environment, 216*, 598–614. https://doi.org/10.1016/j.rse.2018.07.014

Hedley, J. D., Roelfsema, C. M., Chollett, I., Harborne, A. R., Heron, S. F., Weeks, S. J., Skirving, W. J., Strong, A. E., Mark Eakin, C., Christensen, T. R. L., Ticzon, V., Bejarano, S., & Mumby, P. J. (2016). Remote sensing of coral reefs for monitoring and management: a review. *Remote Sensing*, *8*(2). https://doi.org/10.3390/rs8020118

Hill, R., & Ralph, P. J. (2007). Post-bleaching viability of expelled zooxanthellae from the scleractinian coral *Pocillopora damicornis*. *Marine Ecology Progress Series*, *352*, 137–144. https://doi.org/10.3354/meps07159

Hinchliffe, G. (2021). FMV Telemetry conversion (Version 3) [Python]. Unpublished.

Hinchliffe, G. (2022). Low-cost Unmanned Aerial Vehicle Full Motion Video for Marine and Ecological Survey. PhD manuscript in preparation.

Hoang, T. C., O'Leary, M. J., & Fotedar, R. K. (2016). Remote-sensed mapping of *Sargassum* spp. Distribution around Rottnest Island, Western Australia, using high-spatial resolution WorldView-2 satellite data. *Journal of Coastal Research*, *32*(6), 1310–1321. https://doi.org/10.2112/JCOASTRES-D-15-00077.1

Hodgson, A., Peel, D., & Kelly, N. (2017). Unmanned aerial vehicles for surveying marine fauna: assessing detection probability. *Ecological Applications, 27*(4), 1253–1267. https://www.jstor.org/stable/26294485

Hoegh-Guldberg, O., Hoegh-Guldberg, H., Veron, J.E.N., Green, A., Gomez, E. D., Lough, J., King, M., Ambariyanto, Hansen, L., Cinner, J., Dews, G., Russ, G., Schuttenberg, H. Z., Peñaflor, E.L., Eakin, C. M., Christensen, T. R. L., Abbey, M., Areki, F., Kosaka, R. A., Tewfik, A., & Oliver, J. (2009). *The Coral Triangle and climate change: Ecosystems, people and societies at risk.* WWF Australia.

http://eprints.undip.ac.id/1394/1/climate_change___coral_triangle_summary_report.pdf

Houk, P., & Van Woesik, R. (2006). Coral reef benthic video surveys facilitate long-term monitoring in the commonwealth of the Northern Mariana Islands: toward an optimal sampling strategy. *Pacific Science*, *60*(2), 177–189. https://doi.org/10.1353/psc.2006.0005

Jackson, J. B. C. (2008). Ecological extinction and evolution in the brave new ocean. *Proceedings of the National Academy of Sciences of the United States of America*, *105*(1), 11458–11465. https://doi.org/10.1073/pnas.0802812105

Kerrigan, B., Breen, D., De'ath, G., Day, J., Fernandes, L., Tobin, R., & Dobbs, K. (2010). Classifying the biodiversity of the Great Barrier Reef World Heritage Area. *Great Barrier Reef Marine Park Authority Research Publication*, *104*.

Kleiber, D., Harris, L. M., & Vincent, A. C. J. (2014). Improving fisheries estimates by including women's catch in the Central Philippines. *Canadian Journal of Fisheries and Aquatic Sciences*, *71*(5), 656–664. https://doi.org/10.1139/cjfas-2013-0177

Klumpp, D. W., & McKinnon, A. D. (1992). Community structure, biomass and productivity of epilithic algal communities on the Great Barrier Reef: dynamics at different spatial scales. *Marine Ecology Progress Series, 86*(1), 77–89. https://www.jstor.org/stable/24830272

Knowlton, N., Brainard, R. E., Fisher, R., Moews, M., Plaisance, L., & Caley, M. J. (2010). Coral reef biodiversity. In A. D. McIntyre (Ed.) *Life in the world's oceans: Diversity, distribution and abundance* (pp. 65–77). Blackwell Publishing. https://dio.org/0.1002/9781444325508

Knudby, A., & Nordlund, L. (2011). Remote sensing of seagrasses in a patchy multi-species environment. *International Journal of Remote Sensing, 32*(8), 2227–2244. https://doi.org/10.1080/01431161003692057

Lam, K., Shin, P. K. S., Bradbeer, R., Randall, D., Ku, K. K. K., Hodgson, P., & Cheung, S. G. (2006). A comparison of video and point intercept transect methods for monitoring subtropical coral communities. *Journal of Experimental Marine Biology and Ecology*, *333*(1), 115–128. https://doi.org/10.1016/j.jembe.2005.12.009

Legendre, P. (1993). Spatial autocorrelation: trouble or new paradigm? *Ecological Society of America*, *74*(6), 1659–1673. http://www.jstor.org/stable/1939924

Leujak, W., & Ormond, R. F. G. (2007). Comparative accuracy and efficiency of six coral community

survey methods. *Journal of Experimental Marine Biology and Ecology*, *351*(1–2), 168–187. https://doi.org/10.1016/j.jembe.2007.06.028

Lewis, P., Fotheringham, S., & Winstanley, A. (2011). Spatial video and GIS. *International Journal of Geographical Information Science, 25*(5), 697–716. https://doi.org/10.1080/13658816.2010.505196

Littler, M. M., & Littler, D. S. (1988). Structure and role of algae in tropical reef communities. In C. A. Lembi & J. R. Waaland (Eds.), *Algae and human affairs* (pp. 29–56). Cabridge University Press. https://books.google.co.nz/books?hl=en&lr=&id=E3tYyXFg130C&oi=fnd&pg=PP13&dq=algae+and+human+affairs&ots=kBM4YOy9bI&sig=nr4Lr5mB01LOJL2W2E5zLYevzlE&redir_esc=y#v=onepage&q=algae%20and%20human%20affairs&f=false

McArdle, B., & Blackwell, R. (1989). Measurement of density variability in the bivalve *Chione stutchburyi* using spatial autocorrelation. *Marine Ecology Progress Series*, *52*(1977), 245–252. https://doi.org/10.3354/meps052245

McMahon, K. W., Berumen, M. L., Mateo, I., Elsdon, T. S., & Thorrold, S. R. (2011). Carbon isotopes in otolith amino acids identify residency of juvenile snapper (Family: Lutjanidae) in coastal nurseries. *Coral Reefs, 30*, 1135–1145. https://doi.org/10.1007/s00338-011-0816-5

McManus, J.W., Nanola, C. L. Jr., Reyes, R. B. Jr., & Kesner, K. N. (1992). *Resource ecology of the Bolinao coral reef system*. ICLARM. https://books.google.co.nz/books?hl=en&lr=&id=jSwjxQn2aNEC&oi=fnd&pg=PR5&dq=Resource+ecology+of+the+Bolinao+coral+reef+system&ots=eXN71Z249N&sig=KCj2HL-TUaClHWpGsgXDFYIAbXA&redir_esc=y#v=onepage&q=Resource%20ecology%20of%20the%20Bolinao%20coral%20reef%20system&f=false

McNie, A. (2020). *Underwater video surveys of fringing coral reef adjacent to logging developments in the Solomon Islands* [Summer scholarship report]. Auckland University of Technology.

Mellin, C., Peterson, E. E., Puotinen, M., & Schaffelke, B. (2020). Representation and complementarity of the long-term coral monitoring on the Great Barrier Reef. *Ecological Applications*, *30*(6), 1–13. https://doi.org/10.1002/eap.2122

MISB: Motion Industry Standards Board. (2020). MISB ST 0601.17 UAS Datalink Local Set. NSG Standards Registry. https://nsgreg.nga.mil/doc/view?i=5093

Molea, T., & Vuki, V. (2008). Subsistence fishing and fish consumption patterns of the saltwater people of Lau Lagoon, Malaita, Solomon Islands: a case study of Funaafou and Niuleni Islanders. *SPC Women in Fisheries Information Bulletin, 18,* 30–35. https://d1wqtxts1xzle7.cloudfront.net/31797738/WIF18_30_Molea-libre.pdf?1392461903=&response-content-disposition=inline%3B+filename%3DWIF18_30_Molea.pdf&Expires=1707192240&Signature=Ued0bumASgmMK7yfF7uhwzEF-CL94C7ccZpZnS8y3ZepJyVtWzPXQc3k2ChYhSWb3uLkZz2c7p~SV6dtY3ki5tfeP3WOLNA4uz1NGztJptQvI9NtqgOuSnBJBe-a68NPijAGb1wW7DbTmz-KiqIesFhxVlnmhulw5Hgy7J2IBgdQ8Sy95W6jYtrqw9EarRSYB7x9p8B7Ev35JmyR9c0jSdb20BRwGC2l5Gs7NCL~E6trmp8NdflX5Q6g-z3JlqCVwb~bXImIlSqhqUsb4hZaTxixNNumL~EC43P1nt74uZIneduNr7doC6HibqcenemWrGpGwkN~-j6MiT-ENkQoNg__&Key-Pair-Id=APKAJLOHF5GGSLRBV4ZA

Morrison, M., & Carbines, G. (2006). Estimating the abundance and size structure of an estuarine population of the sparid *Pagrus auratus*, using a towed camera during nocturnal periods of inactivity, and comparisons with conventional sampling techniques. *Fisheries Research*, *82*(1–3), 150–161. https://doi.org/10.1016/j.fishres.2006.06.024

Morrissey, J. (1980). Community structure and zonation of macroalgae and hermatypic corals on a fringing reef flat of Magnetic Island (Queensland, Australia). *Aquatic Botany*, *8*, 91–139. https://doi.org/10.1016/0304-3770(80)90045-5

Mumby, P. J., Green, E. P., Edwards, A. J., & Clark, C. D. (1999). The cost-effectiveness of remote sensing for tropical coastal resources assessment and management. *Journal of Environmental Management*, *55*(3), 157–166. https://doi.org/10.1006/jema.1998.0255

Mumby, Peter J., Dahlgren, C. P., Harborne, A. R., Kappel, C. V., Micheli, F., Brumbaugh, D. R., Holmes, K. E., Mendes, J. M., Broad, K., Sanchirico, J. N., Buch, K., Box, S., Stoffle, R. W., & Gill, A. B. (2006). Fishing, trophic cascades, and the process of grazing on coral reefs. *Science*, *311*(5757), 98–101. https://doi.org/10.1126/science.1121129

Mumby, P. J., Skirving, W., Strong, A. E., Hardy, J. T., LeDrew, E. F., Hochberg, E. J., Stumpf, R. P., & David, L. T. (2004). Remote sensing of coral reefs and their physical environment. *Marine Pollution Bulletin, 48,* 219–228. https://doi.org/ 10.1016/j.marpolbul.2003.10.031

Nakajima, R., Nakayama, A., Yoshida, T., Kushairi, M. R. M., Othman, B. H. R., & Toda, T. (2010). An

evaluation of photo line-intercept transect (PLIT) method for coral reef monitoring. *Galaxea, Journal of Coral Reef Studies*, *12*(1), 37–44. https://doi.org/10.3755/galaxea.12.37

Newton, K., Côté, I. M., Pilling, G. M., Jennings, S., & Dulvy, N. K. (2007). Current and future sustainability of island coral reef fisheries. *Current Biology*, *17*(7), 655–658. https://doi.org/10.1016/j.cub.2007.02.054

Ott, B., & Auclair, A. N. (1977). Cluster-analytic definition of species ecological groups for a submerged barrier reef in Barbados, West Indies. *Internationale Revue der gesamten Hydrobiologie und Hydrographie, 62*(1), 41–51. https://doi.org/10.1002/iroh.1977.3510620103

Parsons, D. M., Shears, N. T., Babcock, R. C., & Haggitt, T. R. (2004). Fine-scale habitat change in a marine reserve, mapped using radio-acoustically positioned video transects. *Marine and Freshwater Research, 55*(3), 257–265. https://doi.org/10.1071/MF03190

Patterson, S. M. (2022). *Novel drone technology improves habitat mapping for a coastal octopus species* [Unpublished master's thesis]. Auckland University of Technology.

Phinn, S. R., Roelfsema, C. M., & Mumby, P. J. (2012). Multi-scale, object-based image analysis for mapping geomorphic and ecological zones on coral reefs. *International Journal of Remote Sensing*, *33*(12), 3768–3797. https://doi.org/10.1080/01431161.2011.633122

Pichon, M., & Morrissey, J. (1981). Benthic zonation and community structure of South Island Reef, Lizard Island (Great Barrier Reef). *Bulletin Of Marine Science*, *31*(3), 581–593.

QUT - Centre for Data Science (2024). Reef Cloud. https://research.qut.edu.au/qutcds/projects/reef-cloud/

Quilter, L. (2023). *Surfer tracking from drones using deep learning and full motion video: a novel GIS approach* [Unpublished master's thesis]. Auckland University of Technology.

Quinn, N., & Mataki, M. (1999). The subsistence fishery productivity and marine resource knowledge of resettled Polynesians from Tikopia Island, Solomon Islands. *Micronesica*, *31*(3), 95–107. https://www.researchgate.net/profile/Norman-Quinn/publication/237397974_The_Subsistence_Fishery_Productivity_and_Marine_Resource_Knowledge_of_Resettled_Polynesians_from_Tikopia_Island_Solomon_Islands/links/02e7e53760d4c83d44000000/The-Subsistence-Fishery-Productivity-and-Marine-Resource-Knowledge-of-Resettled-Polynesians-from-Tikopia-Island-Solomon-Islands.pdf

Rahav, O., Dubinsky, Z., Achituv, Y., & Flakowski, P. G. (1989). Ammonium metabolism in the zooxanthellate coral, *Stylophora pistillata*. *Proceedings of the Royal Society of London, 236*(1284), 325–337. https://www.jstor.org/stable/2410564

Reaka-Kudla, M. L. (1997). The global biodiversity of coral reefs: a comparison with rain forests. In M. L. Reaka-Kudla, D. E. Wilson, & E. O. Wilson (Eds.), *Biodiversity II: Understanding and protecting our biological resources* (pp. 83–108). Joseph Henry Press. https://books.google.co.nz/books?hl=en&lr=&id=-X5OAgAAQBAJ&oi=fnd&pg=PR1&dq=Biodiversity+II:+Understanding+and+Protecting+Our+Biological+Resources&ots=f4PolG_0bn&sig=NQTl1wLqIiBpbdvkb9H97-BIFP4&redir_esc=y#v=onepage&q=Biodiversity%20II%3A%20Understanding%20and%20Protecting%20Our%20Biological%20Resources&f=false

ReefCloud. (2024). *ReefCloud Manual: Part 2 Analyse Data: Validated AI results. https://docs.reefcloud.ai/train-and-validate-ai/validated-ai-results*

Reid, P. C., Fischer, A. C., Lewis-Brown, E., Meredith, M. P., Sparrow, M., Andersson, A. J., Antia, A., Bates, N. R., Bathmann, U., Beaugrand, G., Brix, H., Dye, S., Edwards, M., Furevik, T., Gangstø, R., Hátún, H., Hopcroft, R. R., Kendall, M., Kasten, S., … Washington, R. (2010). Impacts of the oceans on climate change. *Advances in Marine Biology,* 56, 1–150. https://doi.org/10.1016/S0065-2881(09)56001-4

Riegl, B., Bruckner, A., Coles, S. L., Renaud, P., & Dodge, R. E. (2009). Coral reefs: Threats and conservation in an era of global change. *Annals of the New York Academy of Sciences*, *1162*, 136–186. https://doi.org/10.1111/j.1749-6632.2009.04493.x

Roberts, C. M. (1995). Effects of fishing on the ecosystem structure of coral reefs. *Conservation Biology*, *9*(5), 988–995. https://doi.org/10.1046/j.1523-1739.1995.9051332.x-i1

Roelfsema, C., Kovacs, E., Ortiz, J. C., Wolff, N. H., Callaghan, D., Wettle, M., Ronan, M., Hamylton, S. M., Mumby, P. J., & Phinn, S. (2018). Coral reef habitat mapping: a combination of object-based image analysis and ecological modelling. *Remote Sensing of Environment*, *208*, 27–41. https://doi.org/10.1016/j.rse.2018.02.005

Schaffelke, B., Mellors, J., & Duke, N. C. (2005). Water quality in the Great Barrier Reef region: responses of mangrove, seagrass and macroalgal communities. *Marine Pollution Bulletin, 51*, 297–296. https://doi.org/10.1016/j.marpolbul.2004.10.025

Sheppard, C., Dixon, D. J., Gourlay, M., Sheppard, A., & Payet, R. (2005). Coral mortality increases wave energy reaching shores protected by reef flats: examples from the Seychelles. *Estuarine, Coastal and Shelf Science*, *64*(2–3), 223–234. https://doi.org/10.1016/j.ecss.2005.02.016

Silverman, J., Lazar, B., Cao, L., Caldeira, K., & Erez, J. (2009). Coral reefs may start dissolving when atmospheric CO2 doubles. *Geophysical Research Letters*, *36*(5), 1–5. https://doi.org/10.1029/2008GL036282

Spalding, M. D., & Brown, B. E. (2015). Warm-water coral reefs and climate change. *Science, 350*(6262), 769–771. https://doi.org/10.1126/science.aad034

Stanley, G. D., & Swart, P. K. (1995). Evolution of the coral-zooxanthellae symbiosis during the triassic: a geochemical approach. *Paleobiology 21*(2), 179–199. https://doi.org/10.1017/S0094837300013191

Tait, L., Bind, J., Charan-Dixon, H., Hawes, I., Pirker, J., & Schiel, D. (2019). Unmanned aerial vehicles (UAVs) for monitoring macroalgal biodiversity: comparison of RGB and multispectral imaging sensors for biodiversity assessments. *Remote Sensing*, *11*(19). https://doi.org/10.3390/rs11192332

Takeda, J. (2001). Fishing-gleaning activities on reef flats and reef margins in the coral ecosystem in Yap, Federated State of Micronesea. *Kagoshima University Research Center for the Pacific Islands, Occasional Papers, 34,* 117-127. http://cpi.kagoshima-u.ac.jp/publications/occasionalpapers/occasional/vol-34/34-14.pdf

Thomas, A., Mangubhai, S., Fox, M., Meo, S., Miller, K., Naisilisili, W., Veitayaki, J., & Waqairatu, S. (2021). Why they must be counted: significant contributions of Fijian women fishers to food security and livelihoods. *Ocean and Coastal Management*, *205*. https://doi.org/10.1016/j.ocecoaman.2021.105571

Tigulu, I. G., Ifuto'o, M. R., & Sheppard, S. (2018). *Ridges to Reef Conservation Plan - Ghizo and Kolombangara, Western Province, Solomon Islands*. WWF-Pacific Solomon Islands. https://wwfeu.awsassets.panda.org/downloads/r2r_amended_with_logos_finalprinting__2__4.pdf

Ventura, D., Bonifazi, A., Gravina, M. F., Belluscio, A., & Ardizzone, G. (2018). Mapping and classification of ecologically sensitive marine habitats using unmanned aerial vehicle (UAV) imagery and object-based image analysis (OBIA). *Remote Sensing, 10*, 1–23. https://doi.org/

10.3390/rs10091331

Veron, J. E. N. (1986). *Corals of Australia and the Indo-Pacific*. Angus & Robertson Publishers.

Weeratunge, N., Pemsl, D., Rodriguez, P., Li, C. O., Badjeck, M., Schwarz, A., Paul, C., Prange, J., & Kelling, I. (2011). *Planning the use of fish for food security in Solomon Islands*. Coral Triangle Support Partnership. https://hdl.handle.net/20.500.12348/1076

Weinberg, S. (1981). A comparison of coral reef survey methods. *Bijdragen Tot de Dierkunde*, *51*(2), 199–218. https://repository.naturalis.nl/pub/504554/BD1981051002004.pdf

Wenger, A. S., Harris, D., Weber, S., Vaghi, F., Nand, Y., Naisilisili, W., Hughes, A., Delevaux, J., Klein, C. J., Watson, J., Mumby, P. J., & Jupiter, S. D. (2020). Best-practice forestry management delivers diminishing returns for coral reefs with increased land-clearing. *Journal of Applied Ecology*, *57*(12), 2381–2392. https://doi.org/10.1111/1365-2664.13743

Whittaker, M. (2021). *Mapping subtidal seaweed using high resolution, synchronised UAV video in northern New Zealand* [Unpublished master's dissertation]. Auckland University of Technology.

Whittingham, E., Campbell, J., & Townsley, P. (2003). *Poverty and reefs*. IMM. https://www.issuelab.org/resources/17884/17884.pdf

Wismer, S., Hoey, A. S., & Bellwood, D. R. (2009). Cross-shelf benthic community structure on the Great Barrier Reef: Relationships between macroalgal cover and herbivore biomass. *Marine Ecology Progress Series*, *376*, 45–54. https://doi.org/10.3354/meps07790

Womersley, H. B. S., & Bailey, A. (1970). Marine Algae of the Solomon Islands. *Philosophical Transactions of the Royal Society of London. Series B, Biological Sciences, 259*(830), 257–352. https://www.jstor.org/stable/2416955

Xu, Y., Vaughn, N. R., Knapp, D. E., Martin, R. E., Balzotti, C., Li, J., Foo, S. A., & Asner, G. P. (2020). Coral bleaching detection in the hawaiian islands using spatio-temporal standardized bottom reflectance and planet dove satellites. *Remote Sensing*, *12*(19), 1–16. https://doi.org/10.3390/rs12193219

Yang, B., Hawthorne, T. L., Torres, H., & Feinman, M. (2019). Using object-oriented classification for coastal management in the east central coast of Florida: a quantitative comparison between UAV, satellite, and aerial data. *Drones*, *3*(3), 1–15. https://doi.org/10.3390/drones3030060

6 Appendix

6.1 Link to the Vavanga Reef ArcGIS Web Map

https://aut-gis.maps.arcgis.com/apps/mapviewer/index.html?webmap=8ebc666d469a4fe59e36451f4f810c7c

The web map displays a collection of substrata and biota distribution data layers including seagrass, *Padina, Turbinaria, Sargassum*, hard coral, *Acropora*, coral rock, and coral rubble. Other layers include the transect names, UAV flight paths, the segmented mosaic used for OBIA, the resulting OBIA, and the photo orthomosaics for the north and south reef flats. To view corresponding extracted GoPro frames, select any point along transect Flat 11, 12 or Crest 4, scroll down to the bottom of the attribute table and select 'View' on the Image_Link_Web field.

6.2 Additional maps of the percentage cover of substrata and biota.

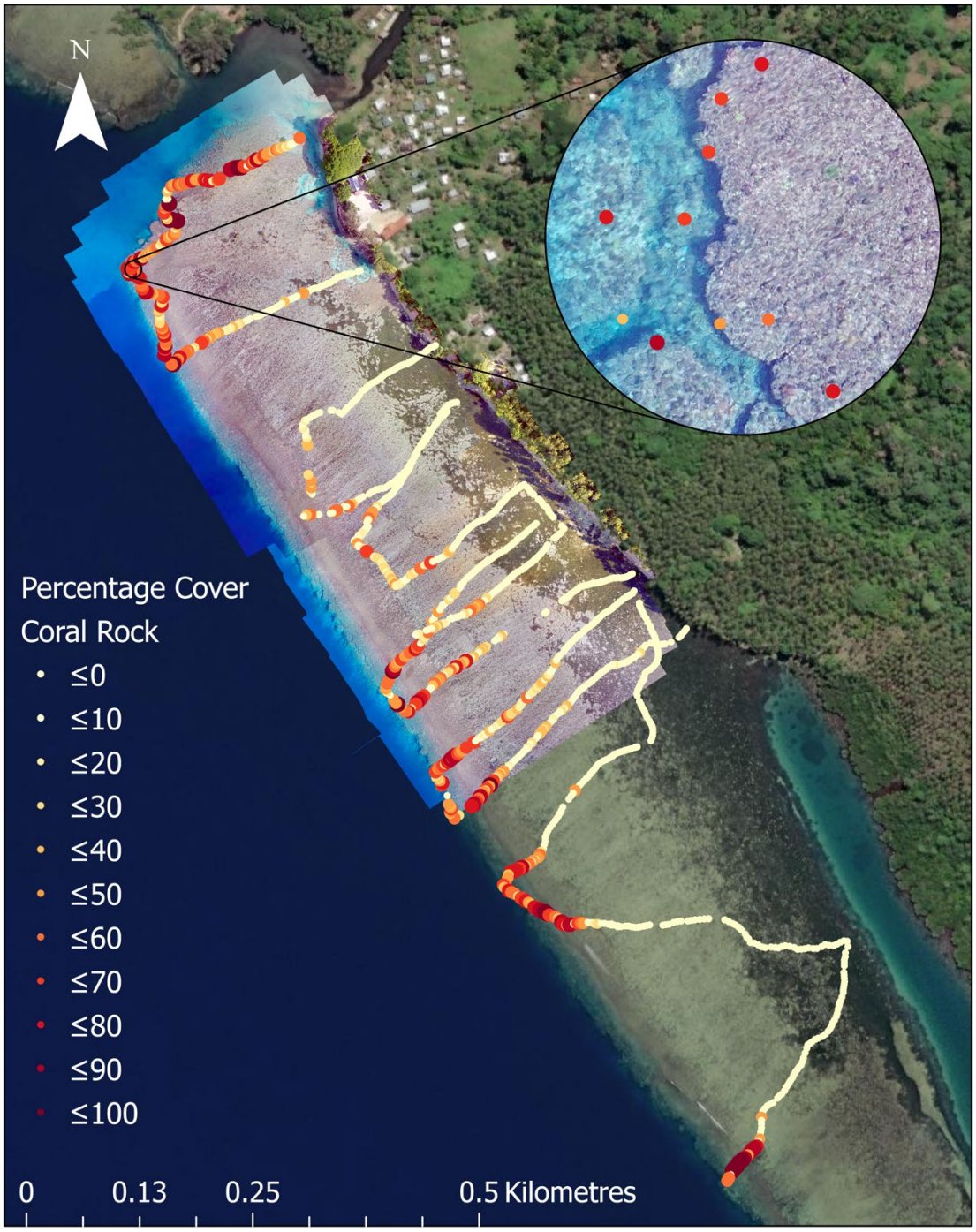

Figure 48. Distribution of consolidated coral rock across the southern reef. Percentage cover symbolized by colour; dark red (≤100%) to light yellow (≤0%) (Source: Esri, Maxar, Earthstar Geographics, and the GIS User Community).

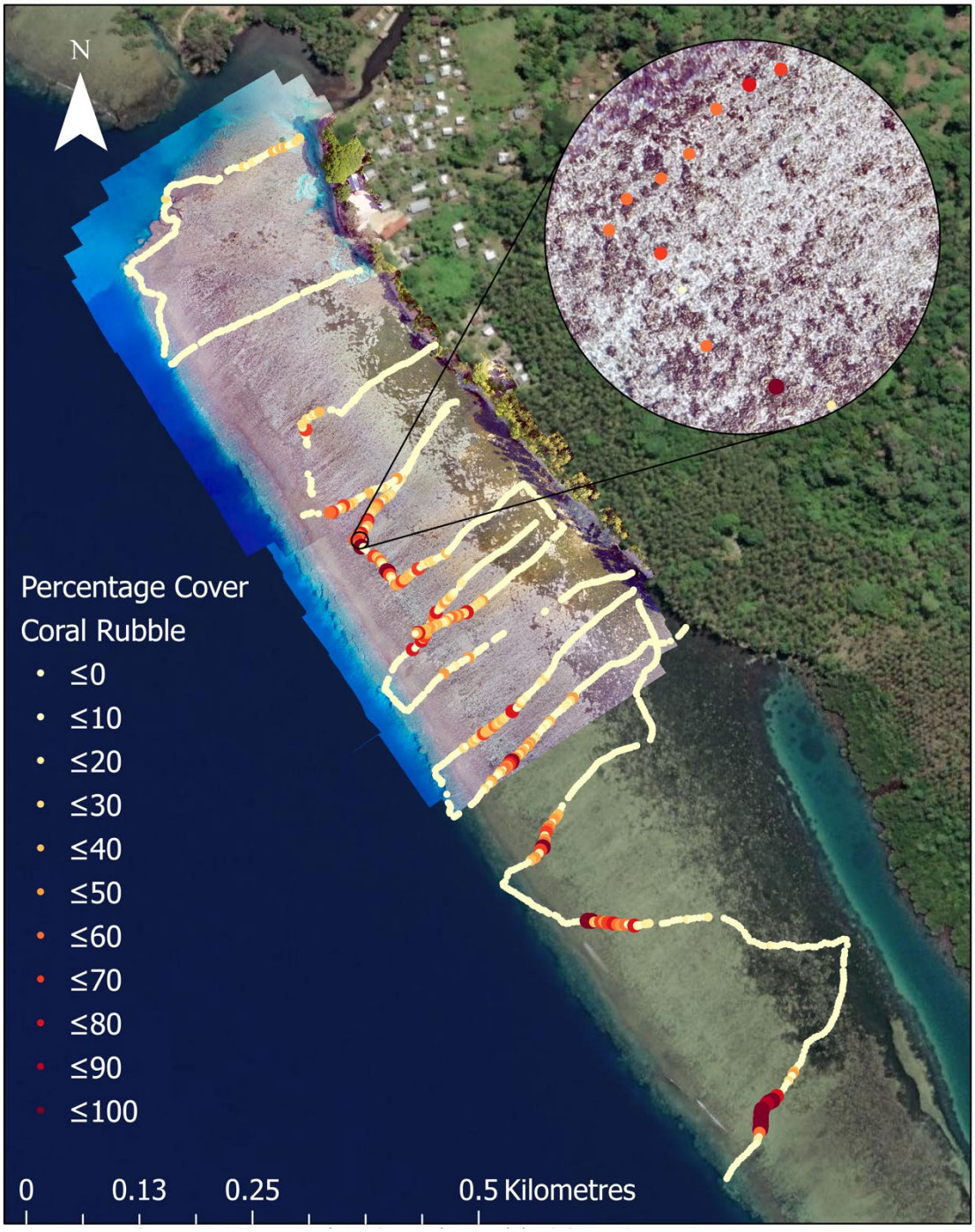

Figure 49. Distribution of coral rubble across the south reef. Percentage cover symbolized by colour; dark red (≤100%) to light yellow (≤0%) (Source: Esri, Maxar, Earthstar Geographics, and the GIS User Community).

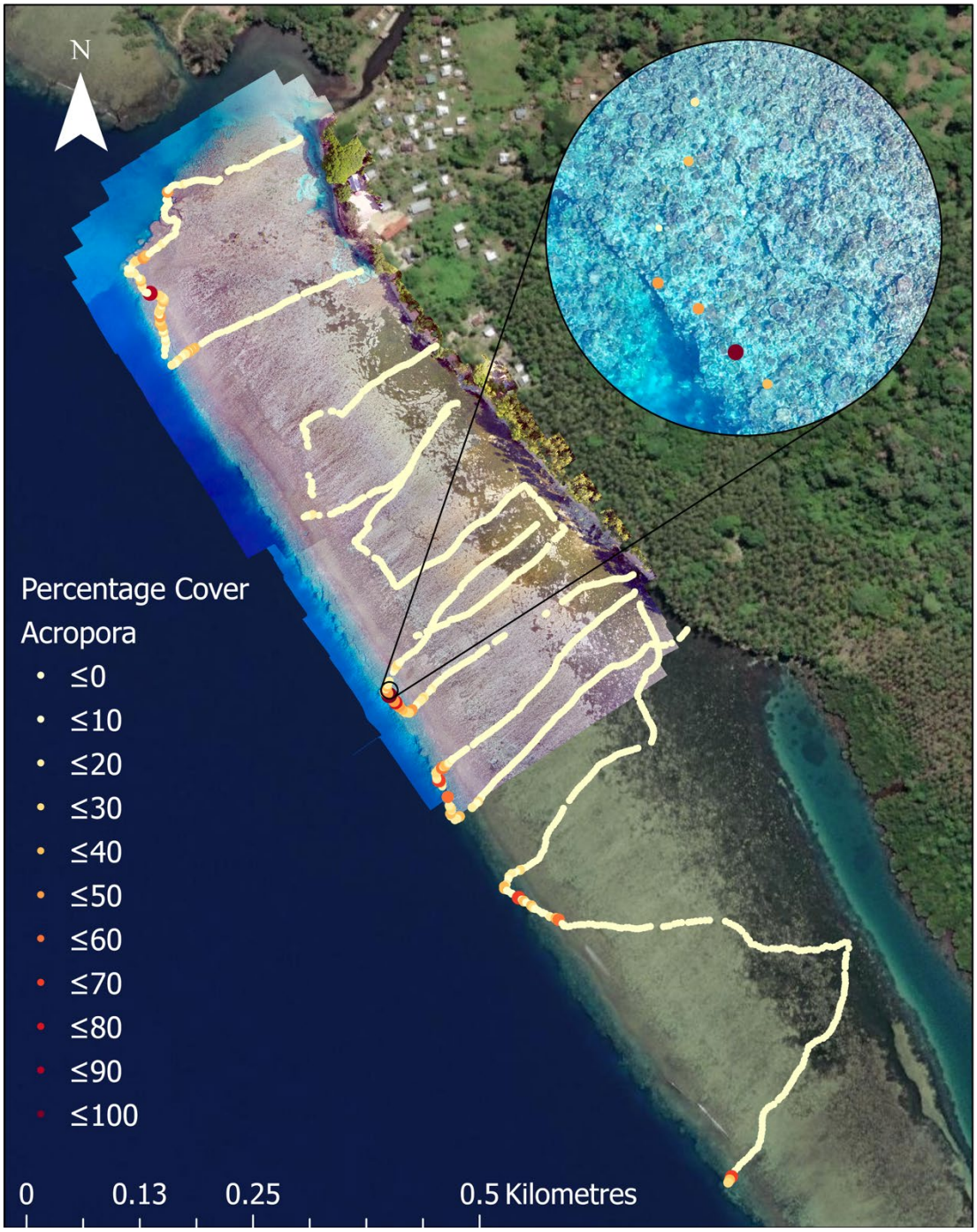

Figure 50. Distribution of all *Acropora* species across the south reef. Percentage cover symbolized by colour; dark red (≤100%) to light yellow (≤0%) (Source: Esri, Maxar, Earthstar Geographics, and the GIS User Community).

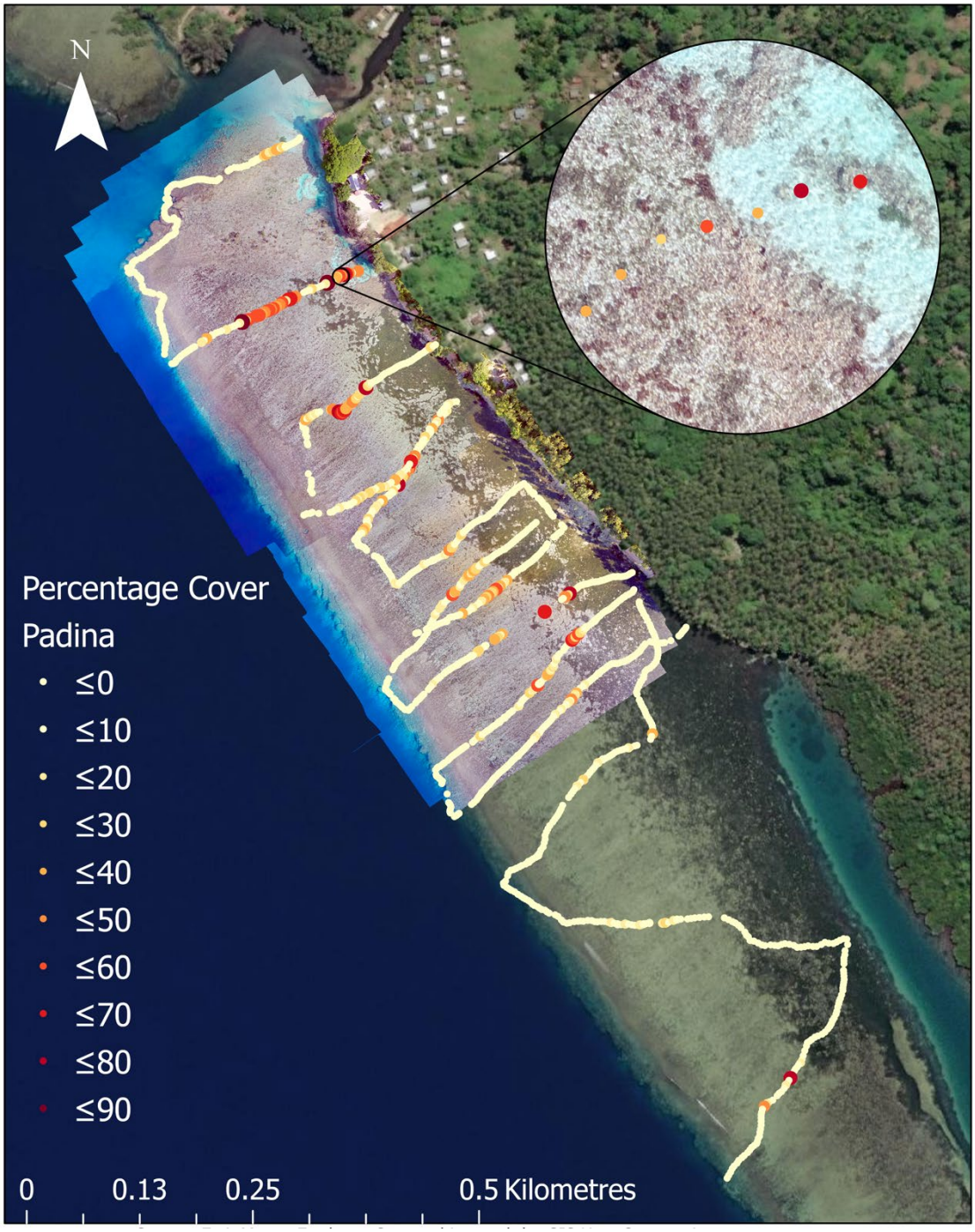

Figure 51. Distribution of the brown macroalgae genus *Padina* across the south reef. Percentage cover symbolized by colour; dark red (≤100%) to light yellow (≤0%) (Source: Esri, Maxar, Earthstar Geographics, and the GIS User Community).

6.3 Components of the CHAID classification and regression trees

In each tree, directly below the response variable (e.g. Seagrass), node 0 shows the mean percentage cover and standard deviation for the whole reef area, n – the number of data points and the number of points as a percentage of the whole data set.

Directly below node 0 in each tree is the independent explanatory variable (i.e. distance from the reef crest, Crest_ m) that explains the most variance in percentage cover. Below this, there is a Bonferroni corrected adjusted P-value (indicating the likelihood of getting differences this extreme under the assumption that the null hypothesis of no differences is true), F value and degrees of freedom. P values less than 0.05 indicated that differences in mean percentage cover among the nodes at the level below were unlikely to have arisen by chance alone.

Below this, in each tree, nodes 1 and onwards are defined by the explanatory variable (distance to the reef crest (m)), for the start and end distance of each statistically modelled zone (eg. <=76, 76-129, 129-163… for seagrass in Figure 29). Each node in the tree then shows mean percentage cover, standard deviation, n – the number of data points within each node, and the percentage of all data points found within each predicted zone at increasing distances from the reef crest. Additional layers of nodes subdividing the above nodes further are possible depending on their statistical and ecological significance, and multiple independent explanatory and response variables can be analysed.

6.4 Additional classification and regression trees and maps of predicted zones

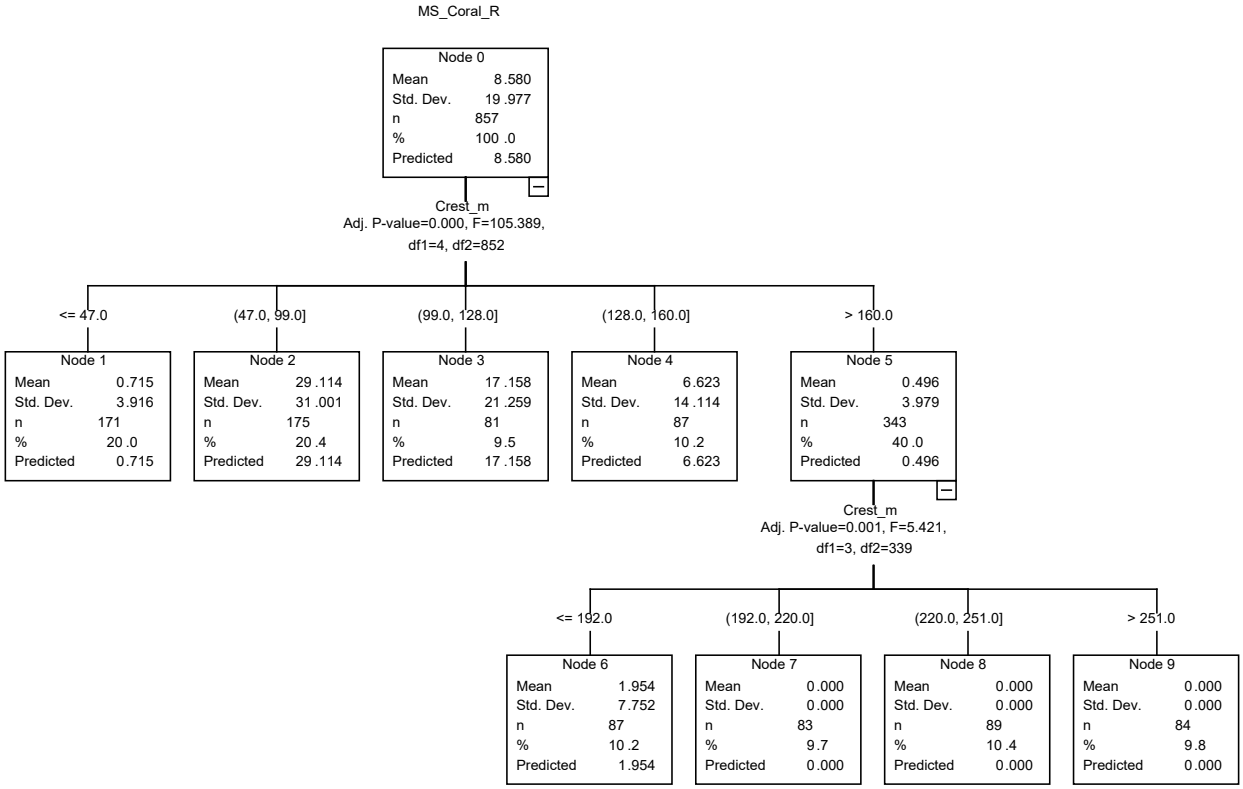

Figure 52. Predicted classification and regression zones of coral rubble species in response to distance from the reef crest.

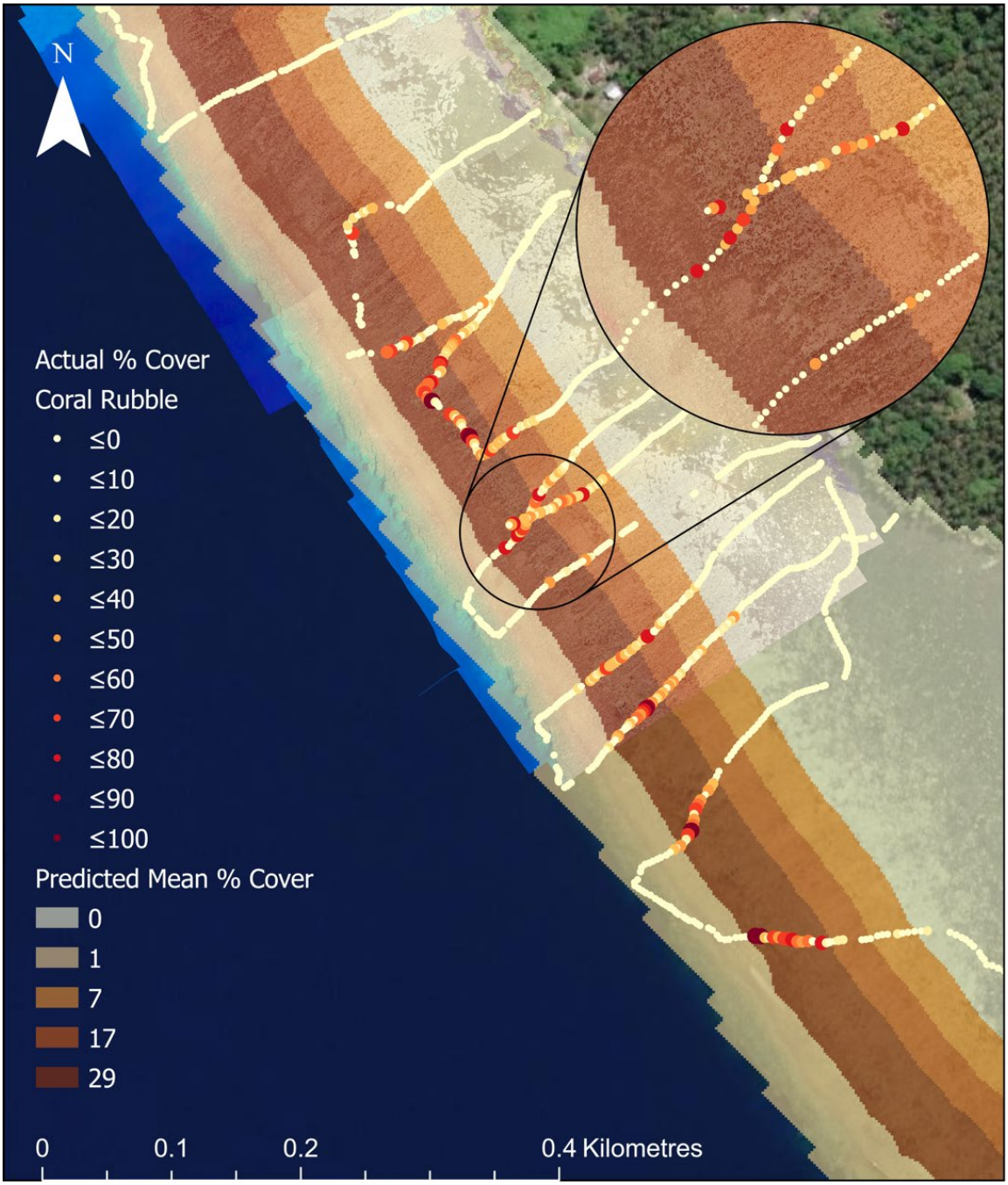

Figure 53. Predicted zones of mean percentage cover (and video survey point estimates) of coral rubble from classification and regression tree analysis. (Additional data sources: Esri, Maxar, Earthstar Geographics, and the GIS User Community).

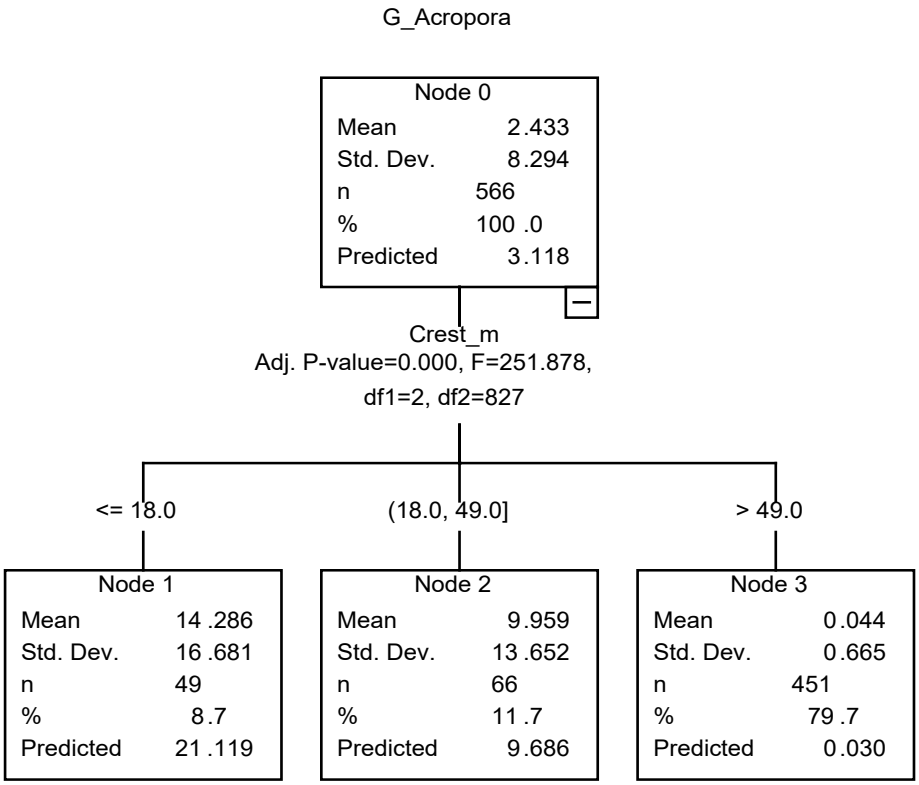

Figure 54. Predicted classification and regression zones of *Acropora* species in response to distance from the reef crest.

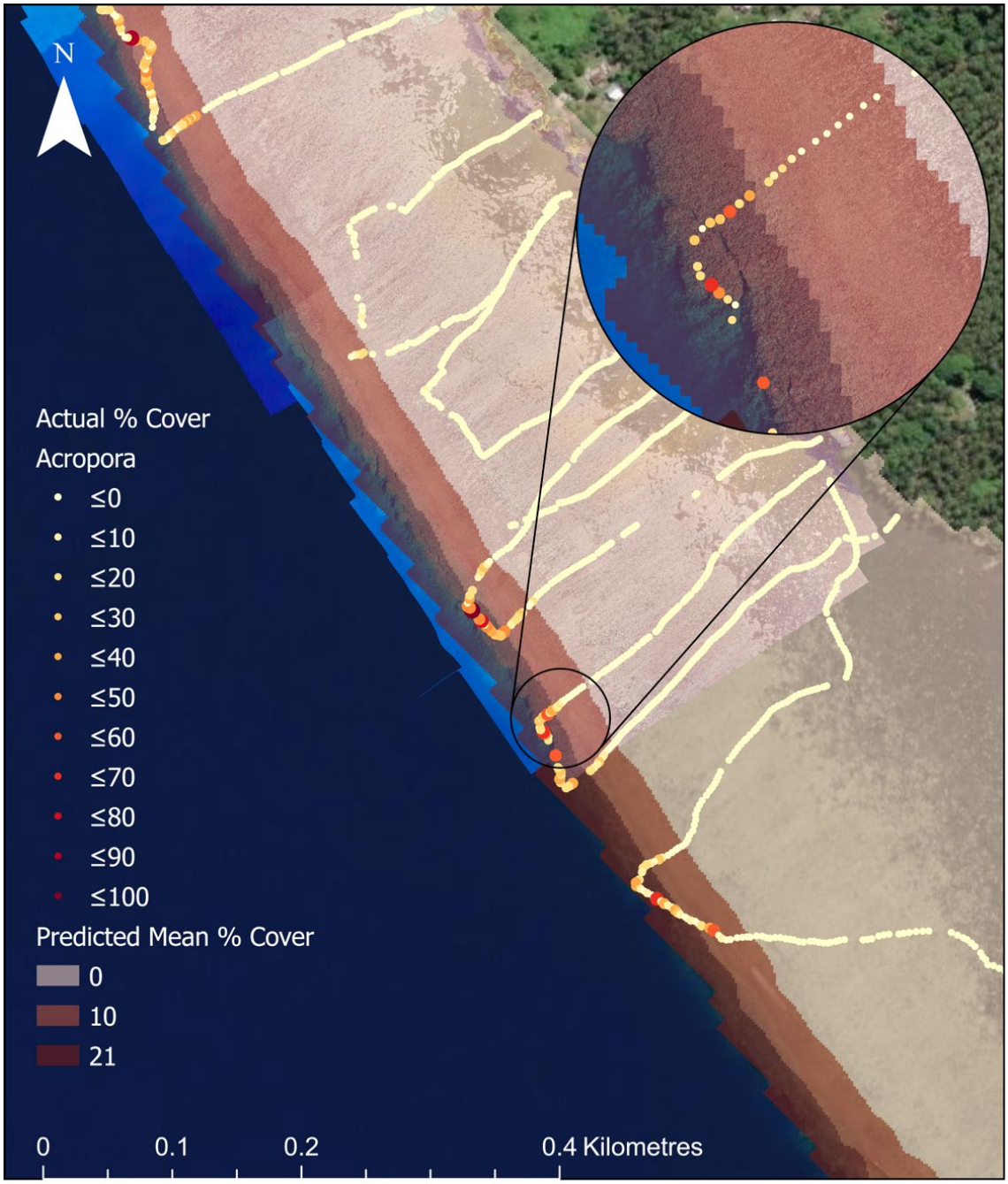

Figure 55. Predicted zones of mean percentage cover (and video survey point estimates) of *Acropora* species from classification and regression tree analysis. (Additional data sources: Esri, Maxar, Earthstar Geographics, and the GIS User Community).

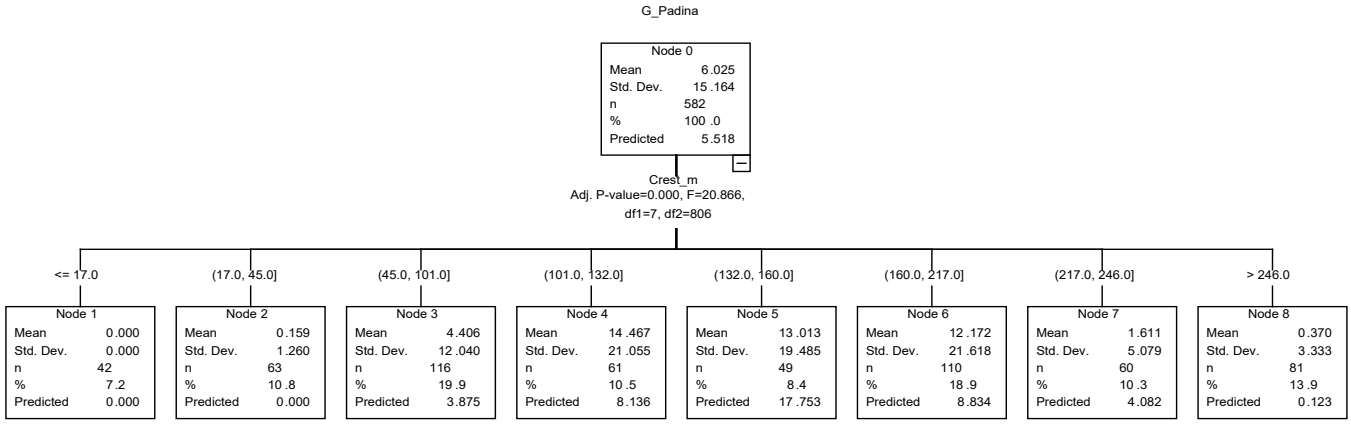

Figure 56. Predicted classification and regression zones of the macroalga *Padina* in response to distance from the reef crest.

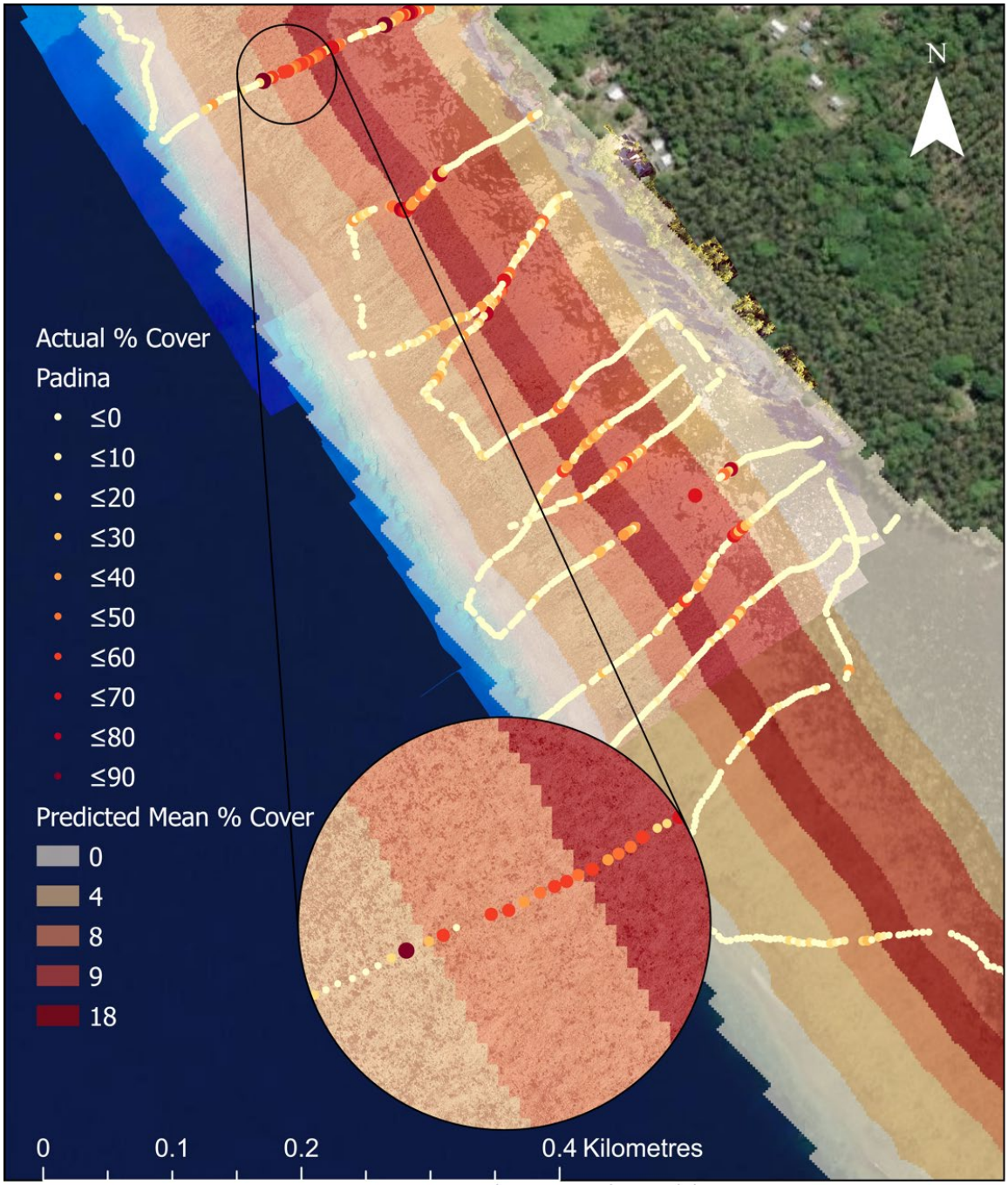

Figure 57. Predicted zones of mean percentage cover (and video survey point estimates) of the macroalga *Padina* from classification and regression tree analysis. (Additional data sources: Esri, Maxar, Earthstar Geographics, and the GIS User Community).

6.5 Additional results of the CHAID classification and regression trees

The mean percentage of coral rock was estimated as 50.4% (P< 0.001) within 19m of the reef crest; 49.8% (P< 0.001) between 19m and 49m; 23.4% (P< 0.001) between 49m and

82m; 13.0% (P< 0.001) between 82m and 105m; 7.6% between 105m and 163m; 1.0% (P< 0.001) between 163m and 194m; and 0.0% (P< 0.001) more than 194m from the reef crest.

The mean percentage cover of coral rubble was estimated as 0.7% (P< 0.001) within 47m of the reef crest; 29.1% (P< 0.001) between 47m and 99m; 17.2% (P< 0.001) between 99m and 128m; 6.6% (P< 0.001) between 128m and 160m; 2.0% between 160 and 192m; and 0.0% (P< 0.001) more than 192m from the reef crest.

The mean percentage cover of sand was estimated at 0.1% (P< 0.001) within 17m of the reef crest; 1.3% (P< 0.001) between 17m and 48m; 6.0% (P< 0.001) between 48m and 78m; 14.5% (P< 0.001) between 78m and 105m; 36.1% (P< 0.001) between 105m and 164m; 19.6% (P< 0.001) between 164m and 192m; 11.9% (P< 0.001) between 192m and 256m; and 4.2% (P< 0.001) more than 256m from the reef crest.

The mean percentage cover of macroalgae was estimated at 1.0% (P< 0.001) within 19m of the reef crest; 9.5% (P< 0.001) between 19m and 48m; 25.8% (P< 0.001) between 48m and 168m; 10.0% (P< 0.001) between 168m and 225m; 2.4% (P< 0.001) between 225m and 251m; and 0.1% (P< 0.001) more than 251m from the reef crest.

The mean percentage cover of algae of the genus *Padina* was estimated as 0.0% (P< 0.001) within 45m of the crest; 3.9% (P<0.001) between 45m and 101m; 8.1% (P< 0.001) between 101m and 132m; 17.8% (P< 0.001) between 132m and 160m; 8.8% (P< 0.001) between 160m and 217m; 4.1% (P< 0.001) between 217m and 246m; and 0.1% (P< 0.001) more than 246m from the reef crest.

The mean percentage cover of the alga *Turbinaria ornata* was estimated as 2.8% (P< 0.001) within 50m of the reef crest; 7.1% (P< 0.001) between 50m and 82m; 2.5% (P< 0.001) between 82m and 107m; 1.1% (P< 0.001) between 107m and 138m; and 0.0% (P< 0.001) more than 138m from the reef crest.

The mean percentage cover of the genus *Acropora* was estimated as 21.1% (P< 0.001) within 18m of the reef crest; 9.7% (P < 0.001) between 10m and 49m; and 0.0% (P< 0.001) more than 49m from the crest.

The mean percentage cover of genus *Montipora* was estimated at 6.6% (P< 0.001) within 51m of the reef crest; 2.5% (P< 0.001) between 51m and 82m; 0.6% (P< 0.001) between 82m and 135m; and 0.0% (P< 0.001) more than 135m from the crest.

6.6 Joining hierarchical classification of substrata and biota to GIS data

The final south reef points attribute table was exported out as an Excel spreadsheet using the table to excel tool. A new column was then created after each substrate proportion field and named Substrate.*#*. This field was populated with the species code and proportion using the formula '= Substrate_*#*&Substrate_*#*_Proportion', e.g., SeaTha 7.

All other columns were then deleted so we were left with the columns OBJECTID, Filename, MissionID, Transect, Image_Link, and Substrate.1 – Substrate.10. All empty cells were populated with 0. The Power Query Editor was then used to transform the data into long format. Once the table was opened in the Power Query Editor, the columns Substrate.1 – Substrate.10 were selected, and the unpivot columns tool was used. This shifted all the data into an 'attribute' column and a 'value' column. There were now 10 rows for each MissionID, where the attribute column was populated with Substrate.1 – Substrate.10, and the value column was populated with the species code and proportion. Any empty cells remained as 0 in the value column.

The table was then loaded back into Excel and all rows where value = 0 were deleted. The value column was then split into two columns: 'substrate' and 'points'. The substrate column was populated with the species code and the points column was populated with the proportion. The table was then imported into ArcGIS Pro. The add join tool was used to join the original classification table to the data, using the species codes as the input and output join fields. The table was exported back into Excel using the table to excel tool.

The PivotTable tool was then used to create pivot tables for each classification level, using the MissionID as the rows, the classification level as the columns, and the sum of points as the values. All classification tables were then pasted into a single Excel sheet and imported into ArcGIS. The join field tool was then used to join this table to the master south reef points data layer using the MissionID's as the input and output join fields. This now allowed

us to visualize the data across multiple classification levels, and map the distribution of singular species, genera, or family.

6.7 Computing confusion matrices to assess accuracy of ReefCloud

The first step was to export the point classifications from the Reefcloud interface. This produced an Excel sheet containing all the data associated with each classified point. The necessary data extracted from this sheet included the image path (used to link the classifications to their associated image using the MissionID), the human point annotation, and the machine point annotation. These fields were copied into a new Excel spreadsheet. To conduct the accuracy assessment on the points without a manual annotation, all points with a human annotation were removed. Using the MissionID, the original manual classifications were located in the main south points dataset and pasted into the Excel sheet. All points that were classified as Scuz (substrata or biota not identifiable) were removed for the accuracy assessment.

The confusion matrix requires a set of accuracy assessment points, that contain a classified (machine annotation) and ground truth (manual classification) field. Both fields require numeric input, therefore, the species and main substrata type code IDs were used. The steps to extract these unique IDs are as follows. Create two separate Excel sheet for the human and machine classifications, with the fields image_path and classification code. Each table was then uploaded into AcrGIS Pro, as well as a species table that included the species code, species name, species ID (1-193), substrate name, and substrate ID (1-28). The add join tool was used to join the species table to both the human and machine classification tables, using the species code as the input and output join field.

The human and machine classification tables were then exported back into Excel. Two new sheets were then created for the species and substrate accuracy assessments, with an ‘actual’ and ‘predicted’ field. The actual fields were populated with the human classified IDs, and the predicted fields were populated with the machine classified IDs. These accuracy assessment tables were then imported into ArcGIS.

The next step was to create accuracy assessment points in ArcGIS Pro, to be used in the confusion matrices. This was done using the create random points tool, which created a dataset of 401 points. A 'Classified' and 'Grndtruth' field was then added to the random points dataset.

For the species accuracy assessment, the add join tool was used to join the species table to the random points dataset, using the object ID as the input and output join fields. The calculate field tool was then used to populate the classified and grndtruth fields with the human and machine species IDs. The remaining fields were then removed from the dataset.

The compute confusion matrix tool was then run, using the random points as the input accuracy assessment points. The same steps were carried out for the substrate ID table. This process was then repeated to perform an accuracy assessment across the whole ReefCloud dataset.

6.8 List of substrata and species identified on transects

Abiotic
Water
Consolidated coral rock
Rubble
Coral rubble
Boulders
Silt on rock
Silty sand
Fine sand
Coarse sand

Sponge
Sponge spp.
Sponge yellow

Seagrass
Seagrass spp.
Thalassia hemprichii
Enhalus acoroides

Mangrove

Algae
Algae spp.

Caulerpa racemosa
Encrusting coralline algae
Filamentous algae
Halimeda spp.
Padina spp.
Sargassum echinocarpum
Turbinaria ornata

Hydroid
Millepora fire coral branching

Anemone
Stichodactyla gigantea

Hard coral
Dead coral
Partly bleached coral
Wholly bleached coral
Coral spp.
Acropora spp.
A. clathrata
A. corymbose
A. digitifera
A. florida
A. gemmifera
A. humilis
A. hyacinthus
A. intermedia (nobilis)
A. millepora
A. monticulosa
A. valida
Caulastrea furcata
Echinopora lamellosa
Favites spp.
F. abdita
Favia spp.
F. stelligera
Goniastrea spp.
G. aspera
G. edwardsi
G. retiformis
Leptoria phyrgia
Lobophyllia hemprichi
L. corymbosa
Montipora spp.
M. aequituberculata
M. confusa

M. digitata
Platygyra daedalea
Pocillopora damicornis
P. eydouxi
P. meandrina
P. verrucosa
Porites spp.
P. annae
P. cylindrica
P. massive
P. nigrescens
Symphyllia recta
Stylophora pistillata